

Air Induction Design for Restricted Race Engines

by

Constandi John Shami

Department of Mechanical Engineering and Materials Science
Duke University

Date: _____

Approved:

W. Neal Simmons, Supervisor

Edward J. Shaughnessy

Nico Hotz

Thesis submitted in partial fulfillment of
the requirements for the degree of
Master of Science in the Department of
Mechanical Engineering and Materials Science in the Graduate School
of Duke University

2014

ABSTRACT

Air Induction Design for Restricted Race Engines

by

Constandi John Shami

Department of Mechanical Engineering and Materials Science
Duke University

Date: _____

Approved:

W. Neal Simmons, Supervisor

Edward J. Shaughnessy

Nico Hotz

An abstract of a thesis submitted in partial
fulfillment of the requirements for the degree
of Master of Science in the Department of
Mechanical Engineering and Materials Science in the Graduate School of
Duke University

2014

Copyright by
Constandi John Shami
2014

Abstract

The air induction system is one of the most influential subsystems within the vehicle powertrain for both fuel efficiency and power generation, especially in restricted race engine applications. The primary focus of this investigation is to parameterize the air induction system into three components, namely the diffuser, plenum, and runners, and to determine the internal geometric parameters most dominant for power generation with the goal of designing an air induction system to generate maximum performance for a given restricted internal combustion engine. This was accomplished through theoretical calculations; engine simulation and modeling using GT-Power; computational fluid dynamics modeling using SolidWorks Flow Simulation; and finally building a prototype of the final configuration for experimentation on an engine dynamometer. It was determined through these simulations that a symmetric air induction design featuring a 6.0° diffuser angle, 0.54L plenum volume, and 5" runner lengths proved to sustain an evenly distributed 19% greater mass flow rate than the 2013 design, generating a 4.8% increase in power output and sustaining 95% of peak torque output for 1000RPM longer than the 2013 design. Experimentally, the dynamometer test sessions with normalized results for power and torque generation versus engine speed validated the trends predicted by the engine simulation and CFD analysis for an overall holistic investigation into air induction system design.

Dedication

This thesis is dedicated to my parents, John and Lisa Shami, for their support and faith in enabling me to be the man I am today. Their trust, guidance, and love have given me the confidence to take on the world with full force and a smile on my face, and for that, I am eternally grateful.

Contents

Abstract	iv
List of Tables	viii
List of Figures	ix
Acknowledgements	xv
1. Introduction of problem.....	1
2. Background.....	3
3. Methodology and parameter development	11
3.1 Theoretical calculation.....	16
3.2 Internal combustion engine simulation: GT-Power	19
3.2.1 GT-Power engine simulation results	23
3.2.1.1 Variation of diffuser length study: GT-Power	26
3.2.1.2 Variation of plenum volume study: GT-Power	32
3.2.1.3 Variation of runner length study: GT-Power.....	38
3.2.1.4 GT-Power final results discussion and overall analysis.....	46
3.3 Air induction design model development and computational fluid dynamics analysis.....	50
3.3.1 Development of transient boundary condition.....	58
3.3.2 Total pressure losses throughout air induction system	65
3.3.3 Volumetric and mass flow rate through air induction designs	80
3.3.4 Transient internal flow visualization.....	94
3.4 Prototype development and experimental testing	103

4. Conclusion	124
5. Suggestions for future work.....	126
Appendix A: Torque versus engine speed figures.....	128
References	136

List of Tables

Table 1: Engine Specifications for Honda CBR600 F4i.....	4
Table 2: Diffuser length study summary	31
Table 3: Plenum volume study summary.....	38
Table 4: Runner length study summary	46
Table 5: Mass accumulation study summary at 9000RPM.....	89

List of Figures

Figure 1: Otto thermodynamic cycle	5
Figure 2: Single-cylinder Otto cycle visualization.....	6
Figure 3: Four cylinder internal combustion engine.....	7
Figure 4: Example air induction system	8
Figure 5: Directional fluid flow through air induction system	10
Figure 6: Segmented air induction system	12
Figure 7: GT-Power map configuration.....	20
Figure 8: Comparison between dynamometer data and GT-Power simulation. GT-Power (Red), Dynamometer tests (Green, Blue, Brown)	21
Figure 9: Power versus engine speed for baseline air induction model.....	23
Figure 10: Torque versus engine speed for baseline air induction model	24
Figure 11: Duke FSAE 2013 air induction design – front view.....	25
Figure 12: Duke FSAE 2013 air induction design – side view	26
Figure 13: Power versus engine speed for 12.3° diffuser angle.....	27
Figure 14: Power versus engine speed for 9.2° diffuser angle.....	28
Figure 15: Power versus engine speed for 12.3° diffuser angle.....	29
Figure 16: Power versus engine speed 6.0° diffuser angle.....	30
Figure 17: Power versus engine speed for 1.08L plenum.....	33
Figure 18: Power versus engine speed for 0.54L plenum.....	34
Figure 19: Power versus engine speed for 1.08L plenum.....	36
Figure 20: Power versus engine speed for 2.17L plenum.....	36

Figure 21: Power versus engine speed for 6" runner length	40
Figure 22: Power versus engine speed for 5" runner length	40
Figure 23: Power versus engine speed for 6" runner length	42
Figure 24: Power versus engine speed for 8" runner length	43
Figure 25: Power versus engine speed for 2013 air induction design	48
Figure 26: Power versus engine speed for proposed 2014 air induction design.....	48
Figure 27: Air induction surface envelope definition	52
Figure 28: 2013 air induction system.....	54
Figure 29: Proposed 2014 asymmetric, large plenum air induction model	54
Figure 30: Proposed 2014 symmetric, small plenum air induction model	55
Figure 31: Proposed 2014 asymmetric air induction design installation – rear view.....	56
Figure 32: Proposed 2014 asymmetric air induction design installation – side view.....	56
Figure 33: Proposed 2014 symmetric air induction design installation – rear view.....	57
Figure 34: Proposed 2014 symmetric air induction design installation – side view.....	57
Figure 35: 2013 air induction design installation on competition vehicle.....	58
Figure 36: Transient boundary condition with respect to crankshaft angle	62
Figure 37: Minimum pressure at cylinder head for transient boundary condition development	64
Figure 38: Total pressure differential versus crankshaft angle at 9000RPM	67
Figure 39: Uniformity index versus crankshaft angle.....	71
Figure 40: Velocity distribution at runner exits for 2013 air induction design	74
Figure 41: Velocity distribution at runner exits for 2014 asymmetric air induction design	76

Figure 42: Velocity distribution at runner exits for 2014 symmetric air induction design	78
Figure 43: GT-Power results for average mass flow rate of 2013 air induction design.....	81
Figure 44: Volumetric flow rate versus crankshaft angle.....	82
Figure 45: Mass flow rate versus crankshaft angle	84
Figure 46: Mass flow rate distribution versus crankshaft angle for 2013 air induction design.....	86
Figure 47: Mass flow rate distribution versus crankshaft angle for 2014 asymmetric air induction design.....	87
Figure 48: Mass flow rate distribution versus crankshaft angle for 2014 symmetric air induction design.....	88
Figure 49: Average mass flow rate versus RPM for 2014 symmetric small plenum design	91
Figure 50: Mass flow rate versus engine speed for 2014 symmetric design.....	93
Figure 51: Velocity trajectory configuration. Notice the lack of full utilization of plenum volume, particularly at the sharp junction between the plenum and diffuser	95
Figure 52: Velocity trajectory configuration. Notice the uneven flow distribution and swirling throughout the plenum	95
Figure 53: Velocity trajectory configuration. Notice the unevenness of flow throughout the diffuser	96
Figure 54: Velocity trajectory configuration. Notice that the air induction volume is used for evenly distributing the air flow amongst the runner inlets while being able to supply the necessary runners when needed	97
Figure 55: Velocity trajectory configuration. Notice the excessive swirling of the air flow throughout the plenum	98

Figure 56: Velocity trajectory configuration. Notice the highly uneven flow distribution through the diffuser as it pushes towards the outer wall, and even has a small amount of back-flow from the plenum	98
Figure 57: Velocity trajectory configuration. Notice the even flow distribution in the diffuser.....	100
Figure 58: Velocity trajectory configuration. Notice how the plenum is completely filled and is able to efficiently distribute the flow to the necessary runners	101
Figure 59: Velocity trajectory configuration. Notice how the fluid velocity is maintained throughout the entire air induction system	101
Figure 60: Average Mach number versus engine speed flowing through the restrictor for the 2014 symmetric design.....	103
Figure 61: SolidWorks CAD model of 2014 symmetric air induction design	104
Figure 62: 3D printed halves of the 2014 air induction design.....	105
Figure 63: Assembled halves of 2014 air induction design prototype.....	106
Figure 64: Epoxy coating applied to 2014 air induction design prototype	106
Figure 65: Final prototype of 2014 symmetric air induction system	107
Figure 66: Engine dynamometer used for testing and tuning of powertrain components	108
Figure 67: Power versus engine speed dynamometer results for 2013 air induction design.....	109
Figure 68: 2014 final intake design installed on engine dynamometer	111
Figure 69: Power versus engine speed dynamometer results for 2014 air induction design.....	112
Figure 70: Power versus engine speed dynamometer results comparison for the 2013 and 2014 air induction designs	113
Figure 71: Power versus engine speed dynamometer testing for the 2014 design featuring different ECU tuning.....	116

Figure 72: Power versus engine speed for the 2014 design documenting the effect of engine tuning.....	117
Figure 73: Power versus engine speed dynamometer results comparison for the 2013 and tuned 2014 air induction designs.....	118
Figure 74: Torque versus engine speed dynamometer results comparison for the 2013 and tuned 2014 air induction designs	118
Figure 75: Engine speed histogram for a competition autocross event.....	120
Figure 76: Normalized power versus engine speed dynamometer results	121
Figure 77: Normalized torque versus engine speed dynamometer results	122
Figure 78: Torque versus engine speed for 12.3° diffuser angle	128
Figure 79: Torque versus engine speed for 9.2° diffuser angle	128
Figure 80: Torque versus engine speed for 6.0° diffuser angle	129
Figure 81: Torque versus engine speed for 0.54L plenum	129
Figure 82: Torque versus engine speed for 1.08L plenum	130
Figure 83: Torque versus engine speed for 2.17L plenum	130
Figure 84: Torque versus engine speed for 5" runner length.....	131
Figure 85: Torque versus engine speed for 6" runner length.....	131
Figure 86 Torque versus engine speed for 8" runner length.....	132
Figure 87: Torque versus engine speed for 2013 air induction design.....	132
Figure 88: Torque versus engine speed for optimized 2014 air induction design	133
Figure 89: Torque versus engine speed dynamometer results for 2013 air induction design.....	133
Figure 90: Torque versus engine speed dynamometer results for 2014 air induction design.....	134

Figure 91: Torque versus engine speed dynamometer results comparison for the 2013 and 2014 air induction designs	134
Figure 92: Torque versus engine speed dynamometer testing for the 2014 design featuring different ECU tuning.....	135
Figure 93: Torque versus engine speed for the 2014 design documenting the effect of engine tuning.....	135

Acknowledgements

There are many parties that I would like to acknowledge and thank for their support and patience:

To Dr. Neal Simmons – thank you for your dedication and support for not only my undertakings, but for the Duke Motorsports team and the Pratt School of Engineering.

To Dr. William Gardner – thank you for never fully trusting a conclusion I arrived at and pushing me to take my design to the next level.

To my parents and family – thank you for always asking how my project was going and allowing me to vent any frustration during our nightly phone calls.

To Adrienne Niederriter – thank you for your love and patience and always being by my side through the thick and thin.

To the faculty and staff of Hudson Hall – thank you for allowing me to interrupt your classes and important business matters to conduct the loud experiments that reverberated throughout the building.

To Duke University and the Pratt School of Engineering – thank you for providing me the opportunity to achieve my education and establish the foundation for my future endeavors, knowing that I will always be a Blue Devil.

1. Introduction of problem

The internal combustion engine found in modern automobiles today is one of the most critical elements of the vehicle's powertrain. From its creation in the late 19th century, the internal combustion engine focused on a 4-stroke thermodynamic cycle, named the Otto cycle, which has developed into one of the most widely used methods of power generation, especially for automobiles. The focus of this investigation is a specific application of a four stroke internal combustion engine, namely for restricted race engines found in motorsports. In this application, an internal combustion engine is developed for automobile racing, focused on providing maximum power output while also maintaining fuel efficiency; however, the caveat is that many of these race engines have a constraint imposed on them by a rules committee on either the total engine displacement, which is the total amount of fluid the cylinders of an engine displace, or a throttle restriction, which forces all of the air entering into the engine to pass through a single orifice of a specified dimension. The goal of these constraints is to limit maximum power output in order to not only make the race safer, but also inspire creativity in design to overcome these obstacles, which inherently sparks innovative technologies that trickle down to the everyday commercial automobile.

With respect to an automobile internal combustion engine, the air induction system is one of the most crucial components to not only fuel efficiency, but also power

generation. The air induction system includes the following elements beginning with atmospheric air: air cleaner/filter; throttle body; diffuser; plenum; runners; and engine cylinder head. The primary focus of this investigation will be on the diffuser, plenum, and runner design since the atmospheric conditions are defined, the air filter and throttle body are typically purchased, and the engine cylinder head is a part of the internal combustion engine developed for racing. While this study will be specifically applied to the Duke Motorsports Formula SAE team application for an open-wheeled racecar, the generalized approach will be applicable to any restricted, four cylinder race engine.

2. Background

To fully understand the project scope and its benefits for restricted race engines, it is first necessary to grasp the research in terms of its application. In general, restricted race engines are seen at every level of motorsports, from kart racing up to Formula-1. The motivation behind restricting race engines stems not only from the safety point of view, but also from the idea that the thrill of motorsports is in testing a driver's true racing capability instead of only the vehicle's engineering development. However, as a race team, any competitive advantage is pursued in order to gain an edge on the other teams, which is why much of the new innovative technologies for automobiles start in racing applications and trickle down to the commercial vehicle. For this investigation, the specific racing application will be the world's largest intercollegiate engineering competition, the Formula SAE (Society of Automotive Engineers) competition. The Duke University Motorsports team engineers, builds, and races an open-wheeled race car for competition at the annual Formula SAE competition at the Michigan International Speedway. The vehicle is powered by a naturally aspirated four cylinder, Honda CBR-600 F4i motor, which has a 20.0 mm diameter restrictor placed between the throttling device and the cylinder head as specified by the 2014 Formula SAE competition rules for gasoline fueled vehicles (SAE International, 2014). The details of the Honda engine used are shown in Table 1 below (Honda Motor Company, 2001).

Table 1: Engine Specifications for Honda CBR600 F4i

HONDA CBR 600 F4i Internal Combustion Engine Specifications	
Cylinder arrangement	4 cylinders in-line, inclined 31° from vertical
Bore and stroke	67.0 x 42.5 mm (2.64 x 1.67 in)
Displacement	599 cm ³ (36.5 cu-in)
Compression ratio	12.0 : 1
Valve train	Chain driven, DOHC (double over-head cam)
Intake valve	at 1 mm (0.04 in) lift
Exhaust valve	
	opens — 22° BTDC
	closes — 43° ABDC
	opens — 38° BBDC
	closes — 7° ATDC
Lubrication system	Forced pressure and wet sump
Oil pump type	Trochoid
Cooling system	Liquid cooled
Air filtration	Paper element
Engine dry weight	59 kg (130 lbs)
Firing order	1 - 2 - 4 - 3

Before delving into the specifics of the design, it is important to first understand the fundamentals behind the internal combustion engine, as well as the general layout of the air induction system that will be studied. As dictated by the rules, the only internal combustion engine permitted is a four stroke, Otto cycle engine. This engine is a spark-ignition engine that uses a rod-piston combination connected to a crankshaft to effectively turn an air/fuel mixture into usable energy through combustion. From a thermodynamic perspective, the Otto cycle is displayed in Figure 1, both as an idealized and actual cycle. Breaking the cycle into individual steps, the Otto cycle is as follows (Quattrochi, 2006):

1. **Intake stroke:** air/fuel mixture is drawn into engine (5→1)

2. **Compression stroke:** pressure and temperature increase (1→2)
3. Combustion (spark/ignition): ideally at constant volume (2→3)
4. **Power stroke:** gas expansion (3→4)
5. Valve exhaust: exhaust valve opens, gas escapes.
6. Removing of heat (4→1)
7. **Exhaust stroke:** piston pushes remaining gas out of chamber (1→5)

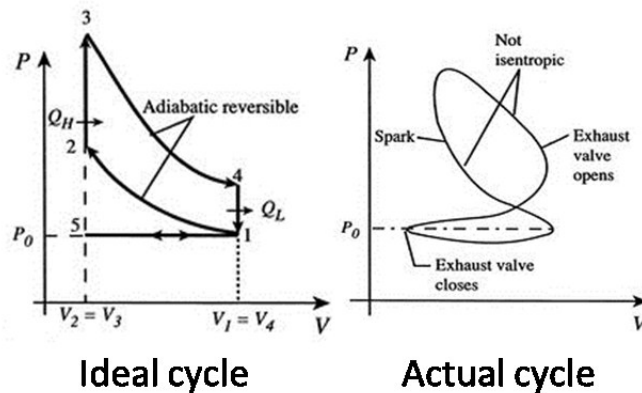


Figure 1: Otto thermodynamic cycle

Figure 2 shows the entire Otto cycle schematically for a four stroke internal combustion engine. The entire cycle takes two entire revolutions of the crank shaft, or 720° of rotation. It is also important to note that the intake valves and the exhaust valves per cylinder open only one time per cycle. The diagram in Figure 2 represents a single cylinder Otto cycle and does not account for any crankshaft rotation shift to compensate for additional cylinders in operation.

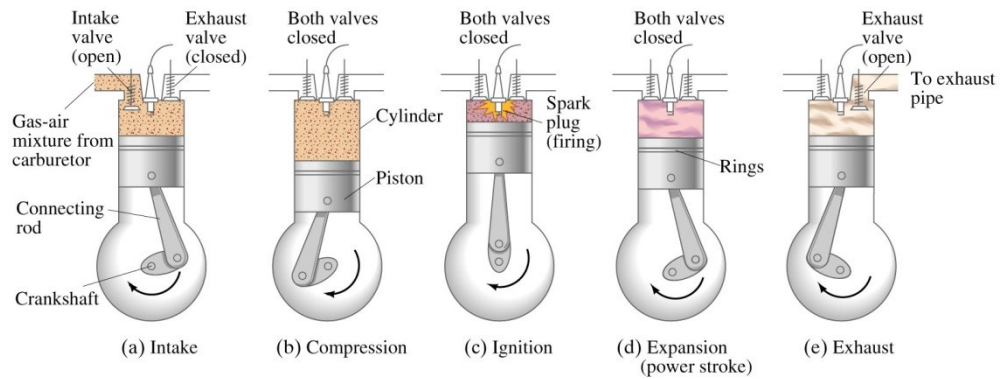


Figure 2: Single-cylinder Otto cycle visualization

The engine that will be studied in this investigation is a four cylinder engine. Due to the correspondence with the number of cylinders and the number of strokes in the cycle, each cylinder in a four cylinder engine is at a unique stroke in the Otto cycle. Figure 3 shows a typical four stroke, four cylinder engine (Kopeliovich, 2012). It is important to note that the outermost cylinders operate in unison geometrically, but within the Otto cycle, they are operating on different strokes, e.g. a 360° phase shift; the same applies for the inner two cylinders.

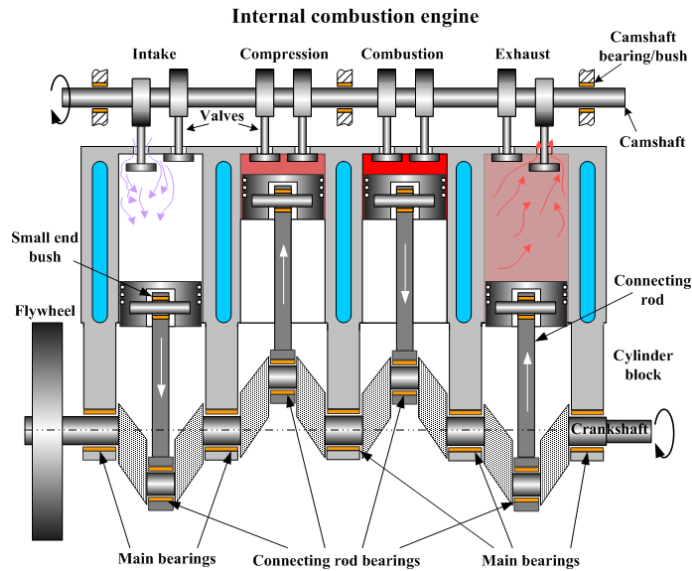


Figure 3: Four cylinder internal combustion engine

Given the description of the internal combustion engine operation, it would be expected that at any given moment in the Otto cycle, only one of the cylinders would have an opened intake valve and only one cylinder would have an opened exhaust valve, which would therefore mean that the air induction system would only be interacting with one cylinder at a time. However, this is not the case due to valve overlap caused by camshaft geometry. At any given instant in time within the cycle, there are in fact two intake valves that are open, with one opening and the other closing, which alludes to the fact that unsteady wave dynamics in the air induction system strongly influence the performance of naturally aspirated internal combustion engines (Harrison & Stanec, 2004). These details indicate that the subsonic and transonic fluid

dynamics relationship yield highly complex fluid interactions within the air induction system, especially when considering a fully theoretical solution.

Now that a general understanding of the four stroke, four cylinder engine has been established, it is now important to begin a general understanding of the air induction system. Figure 4 below represents a typical air induction system for the Duke Motorsports Formula SAE car with the main components labeled.

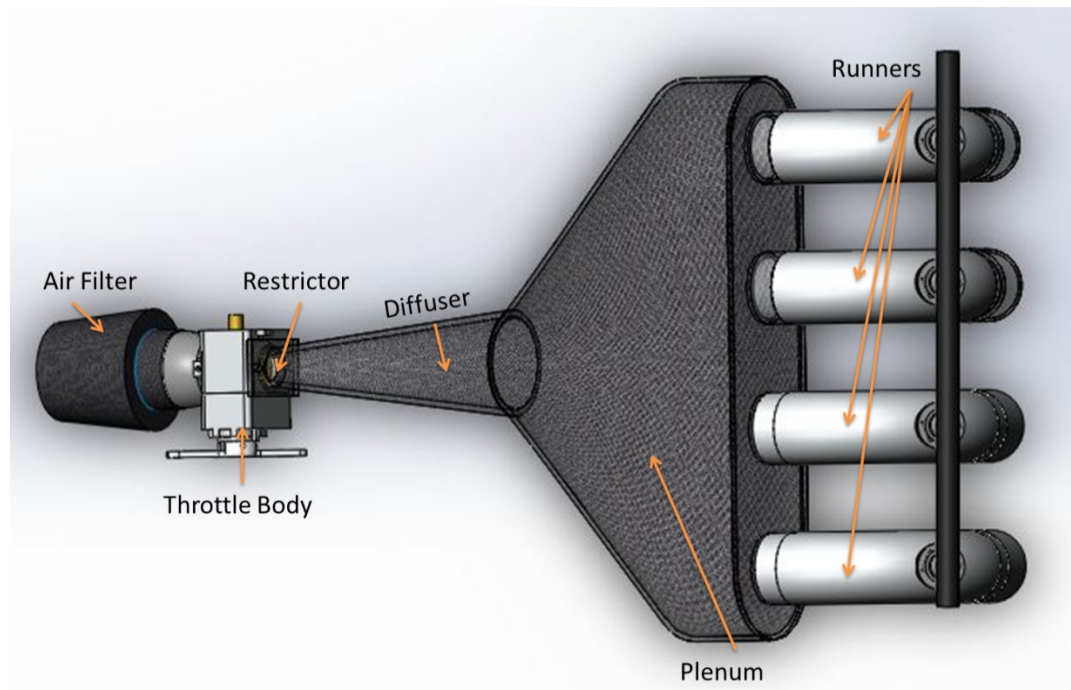


Figure 4: Example air induction system

Because this investigation involves the air induction system, the only part of the Otto cycle that needs to be considered is the intake stroke. The primary function of the

air induction system is to efficiently channel fresh air into the engine to provide a means for internal combustion (Davies, 1996). The intake stroke involves the piston drawing air into the cylinder by not only a partial vacuum caused by the downward motion of the piston, but also due to the scavenging effects from the exhaust gases leaving the cylinder as the exhaust valve closes. It is important to visualize a fluid element that is located outside of the intake and will enter the air induction system. The fluid field outside of the intake can be considered to be at atmospheric conditions, namely at atmospheric pressure and temperature. The partial vacuum caused by the intake stroke in the Otto cycle causes a differential pressure between the entrance of the air induction system and the combustion chamber. This differential pressure causes fluid motion into the intake.

The fluid element enters into the air induction system by first passing through the air filter. This is to ensure that the air is free from particulates that could potentially harm the internal components of the engine. The fluid element then enters the throttle body, which is a throttling device responsible for regulating the mass flow rate of air into the engine using a butterfly valve. Once passing through the throttle body, the fluid element enters into a converging/diverging nozzle, with the throat diameter that of the 20.0 mm restrictor dictated by the Formula SAE rules. The fluid element increases and decreases its velocity in the converging and diverging sections. The plenum is a large volume that attempts to equalize pressure across all four of the runners leading to the

cylinder head. Once the intake valve on the cylinder head opens, the fluid elements housed within the plenum are drawn into the given cylinder until the valve closes, at which point there is no additional fluid flow into the cylinder. Figure 5 shows the path of a fluid element through the air induction system.

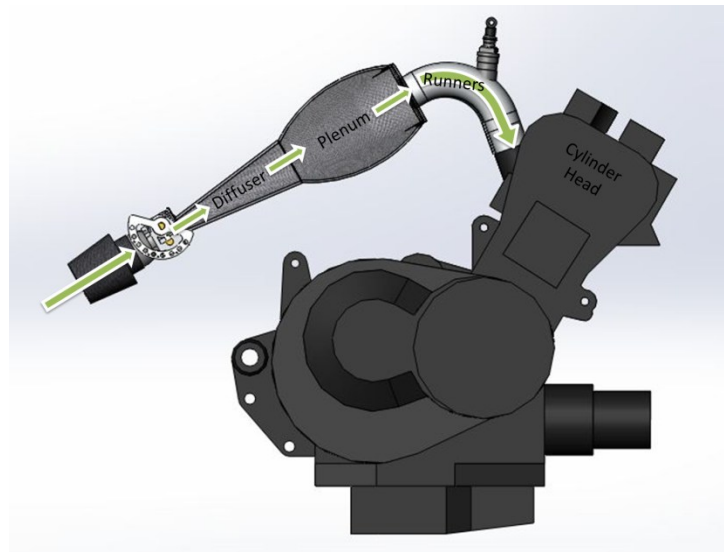


Figure 5: Directional fluid flow through air induction system

3. Methodology and parameter development

To reiterate, the goal of this investigation is to fully understand the different components of the air induction system for a restricted race engine and the role that each plays in maximizing power output. The intent of this investigation is to show that, with proper manipulation, modifications to the air induction system are capable of improving volumetric efficiency and prove to be an effective means of gaining specific power (Masi, Toffolo, & Antonello, 2010). Although this investigation will be directed specifically at the Duke Motorsports Formula SAE vehicle application on a Honda CBR600 F4i powertrain, it is important to realize that nearly all of these conclusions derived from this research can be applied to virtually any restricted, naturally aspirated race engine.

With respect to the different parameters of the air induction system that will be investigated, there are three fundamental components that will need to be studied: the diffuser, the plenum, and the runners. Figure 6 refers to a visual representation of these three components, but does not necessary represent what the final geometry or even orientation will be.

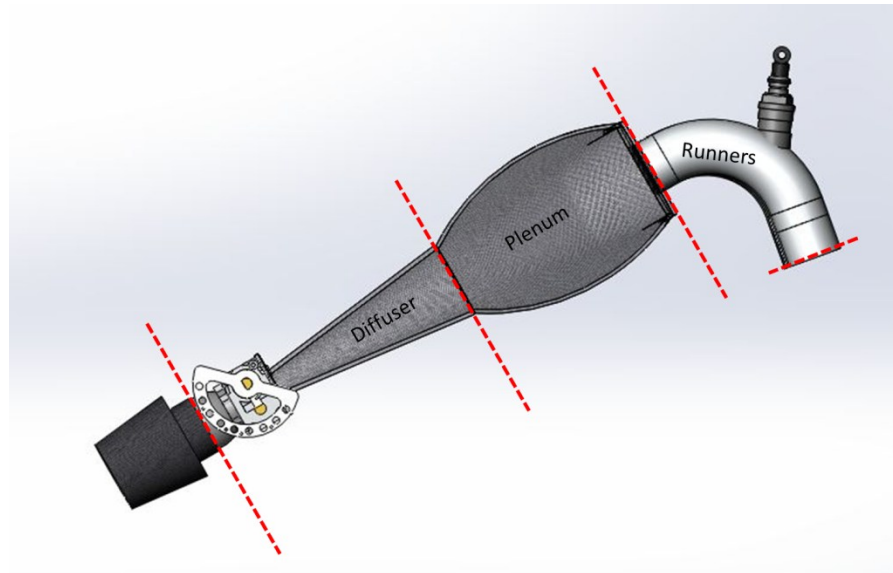


Figure 6: Segmented air induction system

The following provides a more thorough definition of each of the three components of the air induction system shown in Figure 6:

- I. Diffuser: The diffuser represents the trumpet-styled inlet tube that connects the throttle body and the plenum. It is comprised of a flange attachment to the throttle body with the inlet diameter matching that of the inner diameter of the throttle body. The inlet then converges to the restrictor diameter. After the restrictor, the airway then diverges until meeting the inner diameter required for attachment to the plenum.
- II. Plenum: The plenum is the large-volume container that lies in line with the diffuser and the runners. The purpose of the plenum is to evenly distribute the flow entering in from a single source (the diffuser) amongst the four separate

intake runners leading into the cylinder head. Another purpose of the plenum is to contain enough air to supply to the combustion chamber when needed without having too much as to reduce the throttle response resolution while driving (Ceviz, 2007).

- III. Runners: The runners are the tubes that connect the plenum to the engine cylinder head ports, and also house mounting bungs for the fuel injectors. Typically, the inner diameter of the runners matches the inner diameter of the intake port leading to the cylinder head. Maintaining a smooth radius of curvature ensures minimizing flow losses, and it is also necessary for the runners to sustain a relatively high flow velocity in order to properly mix the atomized fuel with the induction flow. The early stages of the intake process are typically governed by the instantaneous piston velocity and the open area under the valve; however, the effects of acoustic resonance soon dominate the induction process, which is heavily influenced by the length of the runners coupling the plenum to the cylinder head (Harrison & Dunkley, 2004).

The nature of the fluid flow properties throughout the air induction system is highly complex, which leads to many potential problems in attempting to derive a governing equation for optimizing system geometry. The induction flow throughout the system is highly unsteady, and during much of the operating engine speed range for the

race engine, the flow velocity through the restrictor approaches a maximum Mach number of 1, meaning sonic flow. Not only is the flow highly unsteady due to the motion of the intake valves, this rapid opening and closing results in a coupled acoustic wave action that is predominant throughout the runners. Due to the complex reflections and interferences of these compression and rarefaction waves coupled with flow velocity unsteadiness, the resulting flow field is virtually impossible to solve analytically (Harrison & Stanev, 2004).

In order to develop a robust approach for solving this complex problem, it is important to devise a plan for both theoretical and computational development and experimentation. Theoretical and computational development will begin with calculations using isentropic, compressible flow conditions to find a maximum mass flow rate through the restrictor. Once this mass flow is known, an approximate engine speed range at which this choked flow condition occurs can be found, which will then lead to further design decisions as to what target engine speed the air induction system will be tuned for. As a general rule of thumb, increasing the runner length leads to an increase in low engine speed torque generation while decreasing mid-range torque output; however, since there is no way to improve the torque for all engine speeds, it depends on the goals developed for a given air induction system to choose the best length for the specific application (Yang, Liao, & Liu, 2012). It is important to realize that

these theoretical calculations are based on many assumptions, many of which are not valid in a race engine on the track. Therefore, the conclusions drawn will be first used to gain insight into the flow properties that exist, and once understood, will be used to advance the design.

Once the theoretical calculations are completed, the computational development will begin. An industry standard software package developed by Gamma Technologies will be used to develop two dimensional engine simulation environments that enable any changes made to air induction system parameters to be documented by engine performance figures, specifically power versus engine speed and torque versus engine speed (Kmec, Kassebaum, & Noerenberg, 2009). This software package, called GT-Power, will also document fluid flow parameters, including flow velocities, fluid pressures, mass flow rates, and other important quantities crucial to comparing various geometric configurations for optimal performance (Gamma Technologies, 2006).

After compiling the GT-Power results, a broad two dimensional view of the air induction system will be established and a clear path towards design will be set forth. The next step in the computational development will be to design a three dimensional model of the air induction system that complies with competition rules and represents the conclusions developed using GT-Power; this will be accomplished by using SolidWorks for the CAD model development. From this CAD model, a computational

fluid dynamics (CFD) analysis will be performed on both the new air induction system design and the previous designs using SolidWorks Flow Simulation software package. This analysis will allow for a comparison between the GT-Power simulation and the CFD simulation, as well as provide evidence to support the design development towards an optimized air induction design for maximum engine performance.

Finally, a prototype of the air induction design will be built and tested on an engine dynamometer. Tests will be conducted to retrieve the power versus engine speed and torque versus engine speed figures for both the 2013 air induction design and the newly developed design in order to validate the theoretical and computational development.

3.1 Theoretical calculation

As previously stated, the theoretical calculations for this air induction system are highly complex, especially when considering the unsteady flow through the cylinder ports. However, one important calculation for any restricted race engine is to set an upper bound on the mass flow rate capable of travelling through the circular restrictor. While this calculation includes many assumptions, it does provide a comparative value for both the computational fluid dynamics results calculated later as well as the engine simulation results.

The main purpose of the restrictor is to limit the amount of power an engine with a given displacement can generate. Thinking of an internal combustion engine as an air pump, the amount of power that can be developed is bounded by how efficiently the engine can move the largest volume of air from the intake into the engine and out through the exhaust: the restrictor is, therefore, the limiting component to moving air into the engine, thereby bounding the volume of air that can be moved. In order to maximize power output, it is necessary to maximize mass flow and minimize losses through the restrictor. Using compressible fluid dynamics equations, assuming isentropic conditions, the following functional relationship is developed:

$$\dot{m}_{air} = \frac{A_{throat} P_{total}}{\sqrt{T_{total}}} \sqrt{\frac{\gamma}{R}} M \left(1 + \frac{\gamma - 1}{2} M^2 \right)^{\frac{-\gamma + 1}{2(\gamma - 1)}} \quad (3.1 - 1)$$

\dot{m}_{air} = mass flow rate of air

A_{throat} = cross-sectional area of throat

P_{total} = total pressure

T_{total} = total temperature

R = ideal gas constant

γ = specific heat ratio

M = Mach number

However, the maximum flow occurs at sonic flow at the throat, or when $M=1$. This condition is called choked flow, and the following equation is for the mass flow rate of air under this condition:

$$\dot{m}_{air} = \frac{A_{throat} P_{total}}{\sqrt{T_{total}}} \sqrt{\frac{\gamma}{R}} \left(\frac{\gamma + 1}{2} \right)^{\frac{-\gamma + 1}{2(\gamma - 1)}} \quad (3.1 - 2)$$

Under these ideal conditions considering a perfect gas and isentropic flow, the maximum mass flow rate that can be achieved is 74.3 g/s of air through a 20mm restriction. However, it is important to briefly touch upon the restrictions of this calculation. First, this calculation assumes that the flow reaches a Mach number equal to 1, which in reality is very difficult to achieve, especially under highly unsteady flow conditions and extremely short time intervals, as seen in a race engine. Another consideration that the calculation does not account for is the boundary layer thickness; since the restrictor diameter is only 20mm, the boundary layer undoubtedly interferes with the flow, especially in the transonic regime. Lastly, the surfaces involved in the converging-diverging nozzle have a surface roughness, which accounts for a nontrivial loss that is unaccounted for. While this upper bound is important to note and understand, especially for comparing the results found through the engine simulation software and CFD analysis to compressible fluid theory, it is a highly optimistic result and should be looked at as a target for design, not as a goal for this study.

3.2 Internal combustion engine simulation: GT-Power

In order to see what effect each aspect of the air induction system has on engine power output, it is useful to model the air induction system using an engine simulation package. The software package used in this investigation is Gamma Technologies Integrated Simulation Environment, which is a 2-D environment in which various objects can be assembled into a project map for a full simulation of not only flow properties, but most importantly of engine performance. Figure 7 shows the project layout compiled for this analysis. The project map first defines the atmospheric conditions, and then every path fluid moves through must be fully defined not only geometrically (2-D), but also in the fluid domain. Examples of this include defining the inlet and outlet diameters of the diffuser, length, surface roughness coefficients, wall temperature, and even a discretization length for the compiler. Once all fluid paths are fully defined, each of the four cylinders must be defined in order to properly simulate an operational internal combustion engine. The valvetrain must also be defined, including camshaft profiles, intake and exhaust valve sizes, and port geometry, as well as the firing order, compression ratio, and the entire cylinder geometry.

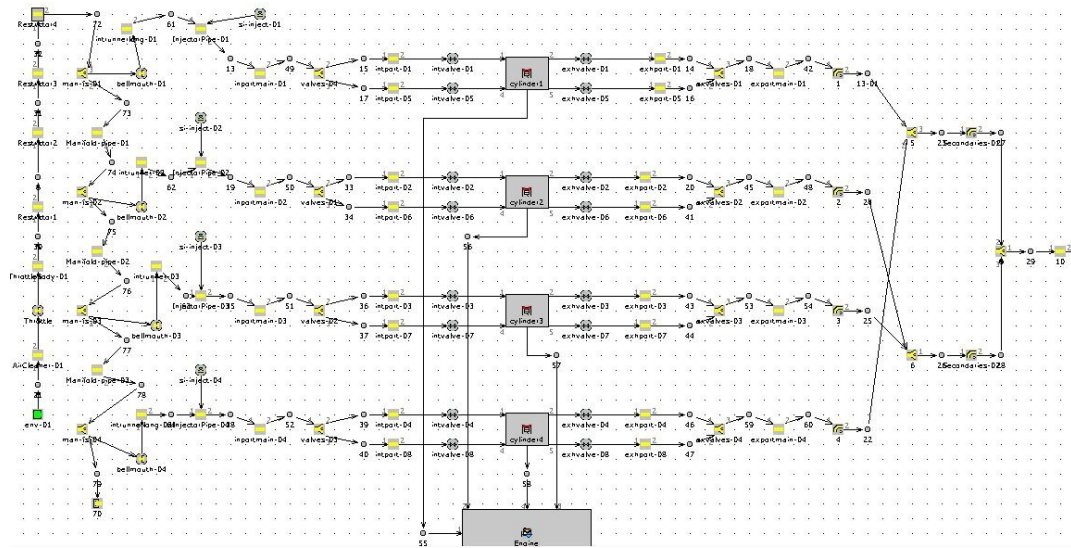


Figure 7: GT-Power map configuration

Once the GT-Power map configuration is finalized, the simulation is ready to be preprocessed and evaluated. The case setup for the simulation, which defines how the engine will be tested, evaluates the engine performance numbers, as well as all fluid property values throughout all fluid paths, at engine speed values ranging from 4000RPM to 11750RPM at increments of 250RPM, representing the typical range of operational engine speeds for the Honda F4i.

The GT-Power simulations provided a mechanism to not only quantify engine performance, but also do comparative studies on different properties of the air induction system. Manufacturing different air induction systems with varying properties proves to be largely time consuming task; however, with the engine modeling software, these

parameters can be easily changed in order to see the incremental change in power output.

It is first important to verify that the engine simulation results represent what the actual engine output is. In order to do this, an old vehicle model was placed in a GT-Power engine simulation and was compared to chassis dynamometer data from the same vehicle configuration. Figure 8 below shows the overlay of three separate tuning dynamometer pulls with the results from the GT-Power engine simulation.

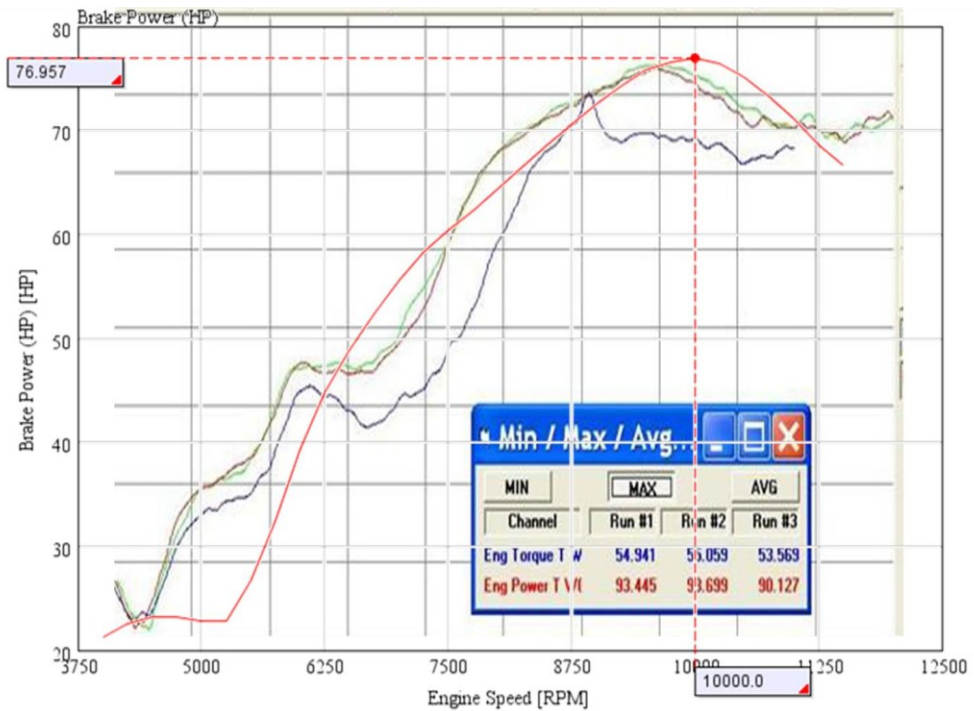


Figure 8: Comparison between dynamometer data and GT-Power simulation. GT-Power (Red), Dynamometer tests (Green, Blue, Brown)

Typically, chassis dynamometer figures are adjusted according to the atmospheric conditions present, usually following the SAE standard correction, and

some types of dynamometers are more accurate than others. However, these corrections are only shown in the scaling of the exact value shown while the trends seen in the horsepower and torque curves remain the same. For comparison, the GT-Power simulation results are lined up properly on the x-axis (engine speed) and then scaled to show how closely they align with the dynamometer curve shown.

Looking closely at the figure overlay, most of the discrepancies occur in the lower engine speed range (from ~4000-6500 RPM). Despite these deviations, both the dynamometer results and the GT-Power engine simulation results follow the same trends and do not significantly differ in any particular way. For the purposes of this investigation, the main concern is optimizing peak power output and maintaining the power as much as possible throughout the upper engine speed range; in essence, the majority of the analysis will be focused around the choked flow condition, which will be defined as an engine speed in the range of 7000-12000 RPM. When looking at the overlay, the curves corresponding with engine speed values ranging from 7000-12000RPM are generally accurate, with minimal differences between the actual dynamometer data and the GT-Power engine simulation data. Therefore, it is safe to conclude that the GT-Power simulation results are sufficient to show trends in power and torque output of this powertrain configuration.

3.2.1 GT-Power engine simulation results

Now that the engine simulation results have been shown to correlate well with actual engine performance, the next step is to run multiple studies to show the impact of altering parameters of the air induction system on engine performance. For comparison, the baseline control settings will be defined as a 5.6" long diffuser (defined as the length between the restrictor and the plenum); a plenum volume of 1.08L; and runner lengths of 5.91". Figure 9 shows the power output in horsepower versus engine speed for this air induction setup, and Figure 10 shows the torque output in N-m for the baseline air induction setup. It is important to note that max power output occurs at 9000 RPM (68.99 HP), and max torque occurs at 8000 RPM (56.75 N-m).

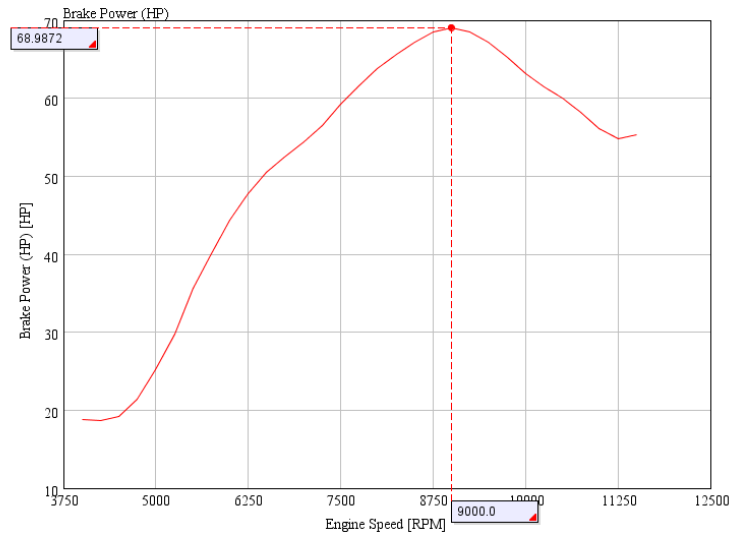


Figure 9: Power versus engine speed for baseline air induction model

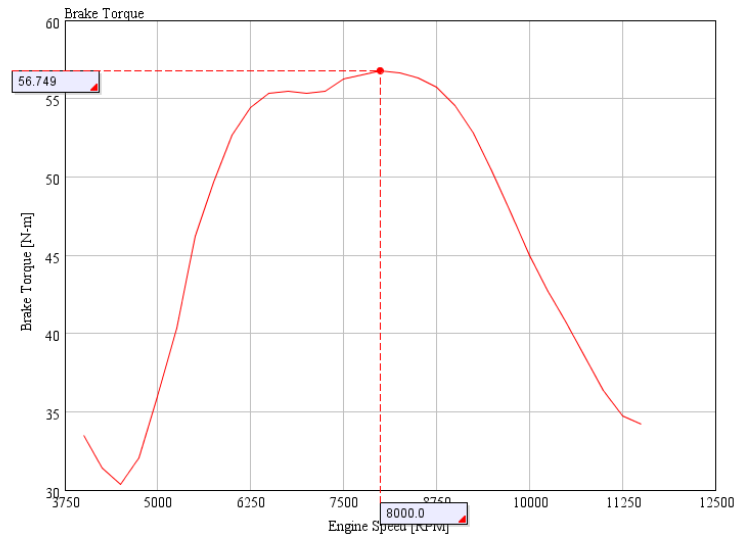


Figure 10: Torque versus engine speed for baseline air induction model

The comparisons that will be developed will be focused on the trends that certain geometric changes impose on two factors: 1) maximum output values for power and torque and 2) the engine speeds that these maximum engine performance values occur. The following sections will delve into the separate geometric sections, namely the diffuser, plenum, and runners, and their effects on power output. Figures 11 and 12 show the 2013 air induction system design with all of the parameters mentioned above, and this design produces the power and torque versus engine speed plots shown in Figures 9 and 10.



Figure 11: Duke FSAE 2013 air induction design – front view



Figure 12: Duke FSAE 2013 air induction design – side view

3.2.1.1 Variation of diffuser length study: GT-Power

The diffuser geometry is defined by a nominal length between the 20mm restrictor and the entrance to the plenum. However, because the entrance and exit diameters are known, the length of the diffuser governs the diffuser angle. With respect to diverging nozzles, one of the greatest flow related problems that limits efficiency and performance is flow separation, which is almost strictly governed by the diffuser angle. Using the 2013 design as the control, the calculated conical diffuser angle is 12.3° . According to literature and previous experiments regarding flow separation and diffuser angle, this value is in the upper range of what is a tolerable diffuser angle due to the onset of significant flow separation losses. By essentially defining the 2013 design as

the upper bound for diffuser angle, the minimum length of the diffuser is set at around 5.5". The effect of diffuser length, which inherently defines diffuser angle, will involve testing diffuser lengths of 192mm (~7.5") and 247mm (~9.5"), which correspond with diffuser angles of 9.2° and 6.0°, respectively.

The first comparison is between the 2013 design (12.3° diffuser angle) and the 7.5" long diffuser (9.2° diffuser angle). This comparison represents the shortest diffuser with a medium length diffuser, mostly corresponding with a more commonly accepted diffuser angle. Figures 13 and 14 below show the power versus engine speed plots for the 2013 diffuser and the medium length diffuser, with all other parameters kept constant. See Figures 78 and 79 in Appendix A for the torque output versus engine speed figures for these two configurations.

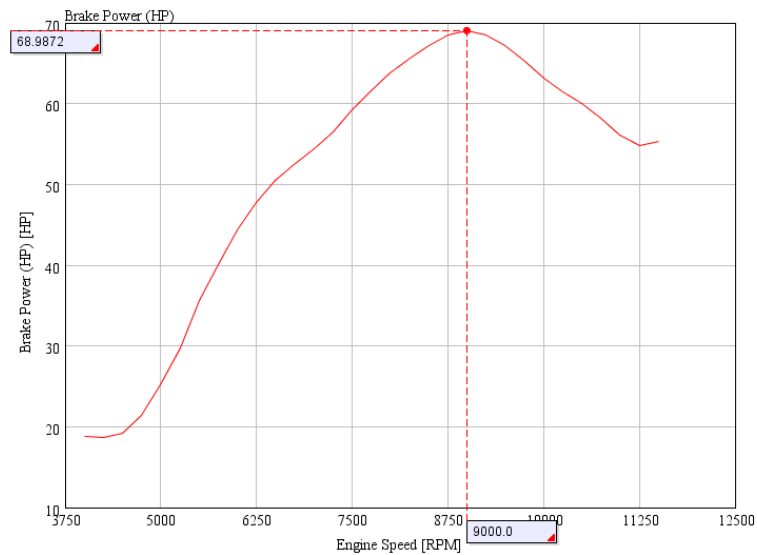


Figure 13: Power versus engine speed for 12.3° diffuser angle

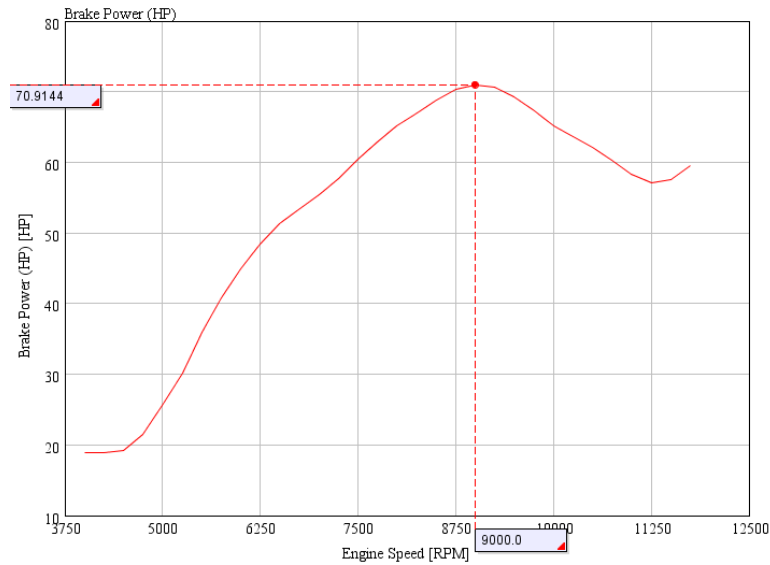


Figure 14: Power versus engine speed for 9.2° diffuser angle

The power versus engine speed figures shows the engine speed at which the maximum power output occurs does not shift, and the shape of the curve looks almost identical. However, the maximum power output increases with a smaller diffuser angle. The GT-Power engine simulation shows that the power output of the 12.3° diffuser peaks at 68.98 HP, whereas the 9.2° diffuser peaks at 70.91 HP, a 2.8% increase in power with no adverse effects throughout the rest of the engine speed range. In fact, if the figures are closely examined, it is clear that the entire power versus engine speed curve is shifted upward for the 9.2° diffuser, which means that the engine is producing more power at every engine speed due to the change in diffuser angle. This observation alludes to the fact that flow separation may be a limitation in the 2013 design, and to best mitigate this problem, a longer diffuser with a smaller diffuser angle is necessary.

The second comparison is between the 2013 design (12.3° diffuser angle) and the 9.5" long diffuser (6.0° diffuser angle). This represents the shortest and longest diffuser lengths that would be viable options for the air induction system design for the Formula SAE vehicle. Figures 15 and 16 below show the power versus engine speed figures for the 2013 diffuser length and the longest diffuser length, with all other parameters kept constant. See Figures 78 and 80 in Appendix A for the torque output versus engine speed figures for these two configurations.

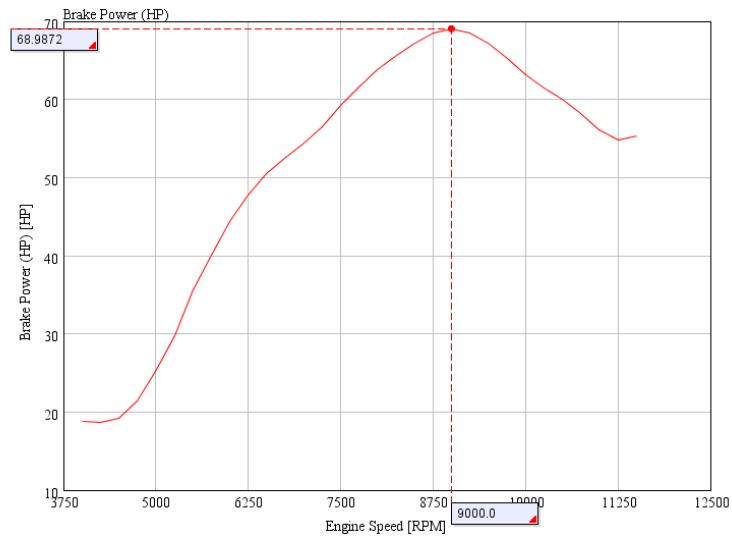


Figure 15: Power versus engine speed for 12.3° diffuser angle

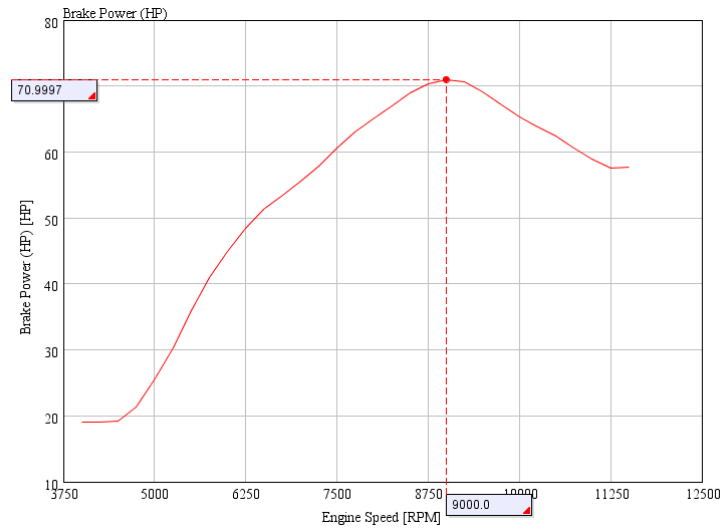


Figure 16: Power versus engine speed 6.0° diffuser angle

The power versus engine speed figures for these cases show the engine speed at which the maximum power output occurs does not shift, and the shape of the curve looks almost identical. However, the maximum power output increases with the smaller diffuser angle. The GT-Power engine simulation shows that the power output of the 12.3° diffuser peaks at 68.98 HP, whereas the 6.0° diffuser peaks at 70.99 HP, a 2.9% increase in power with no adverse effects throughout the rest of the engine speed range. In fact, if the figures are closely examined, it is clear that the entire power versus engine speed curve is also shifted upward for the 6.0° diffuser, which means that the engine is producing more power at every engine speed due to the change in diffuser angle. The same general trend that was observed with the 9.2° diffuser angle holds true for the 6.0° diffuser angle.

It is also important to compare the 9.2° diffuser angle with the 6.0° diffuser angle. It is clear that the maximum power output numbers are very close; the 9.2° diffuser peaks at 70.91 HP and 6.0° diffuser peaks at 70.99 HP, which is only a 0.12% increase in power. The peak torque values are also only slightly different, with the 9.2° diffuser producing 57.97N-m and the 6.0° diffuser producing 57.91N-m, both at 8000RPM, which is also a 0.11% decrease in peak torque going with the smaller diffuser angle. These two diffuser angles are producing very similar maximum power and torque figures, and according to the GT-Power engine simulation, are essentially the same. However, since this investigation is concerned with designing the best possible air induction system for maximum power output, the trend for the diffuser design is towards a smaller diffuser angle, corresponding with the longest length that is able to fit within a given engine configuration. Therefore, the overall conclusion regarding the diffuser length would be to increase its length in order to decrease the diffuser angle; this helps to decrease flow separation, which minimizes flow losses and increases power output. Table 2 below summarizes the results discussed above.

Table 2: Diffuser length study summary

Configuration	Parameter: Diffuser length/angle	Power (HP)	Peak Power Engine Speed (RPM)
Control length	5.5" (12.315°)	68.9872	9000
Medium length	7.5" (9.17173°)	70.9144	9000
Long length	9.5" (6.03477°)	70.9997	9000

3.2.1.2 Variation of plenum volume study: GT-Power

The plenum, as previously defined, is the volume that distributes the air flow from the diffuser amongst the four separate intake runners leading into the cylinder head. One of the main goals of the plenum is to contain enough air to supply to the combustion chamber when needed without having the volume be too large, and this investigation will determine the role that the plenum volume has on overall engine performance.

The 2013 air induction configuration (Refer to Figures 11 and 12) features a plenum with a volume of 1.08L. This plenum volume represents a mix between equalizing pressure and maintaining a relatively significant amount of fluid momentum, and was developed by the Duke Motorsports team for previous vehicle designs. This configuration will be compared to a plenum with a volume about half that of the original configuration (0.54L), and to a plenum with a volume about double that of the original configuration (2.17L).

The first comparison is between the 1.08L (2013) plenum and the 0.54L plenum. From a practical perspective, the half-volume plenum represents a design that strictly focuses on maintaining fluid momentum; the premise behind the volume is that fluid is accelerated to such high velocities and so rapidly that a plenum focused on maintaining the fluid momentum from the diffuser into the runners would be most effective. Figures

17 and 18 show the power versus engine speed plots for the 2013 plenum (1.08L) and the half-volume plenum (0.54L), respectively, with all other air induction properties kept constant. See Figures 81 and 82 in Appendix A for the torque output versus engine speed figures for these two configurations.

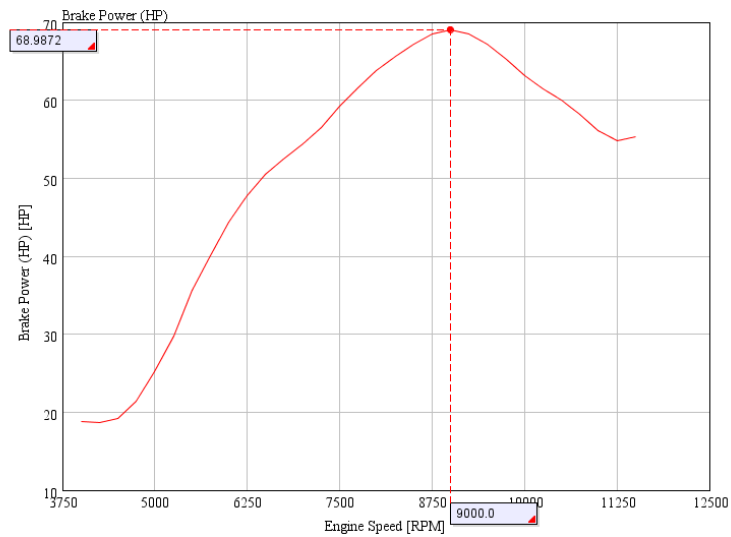


Figure 17: Power versus engine speed for 1.08L plenum

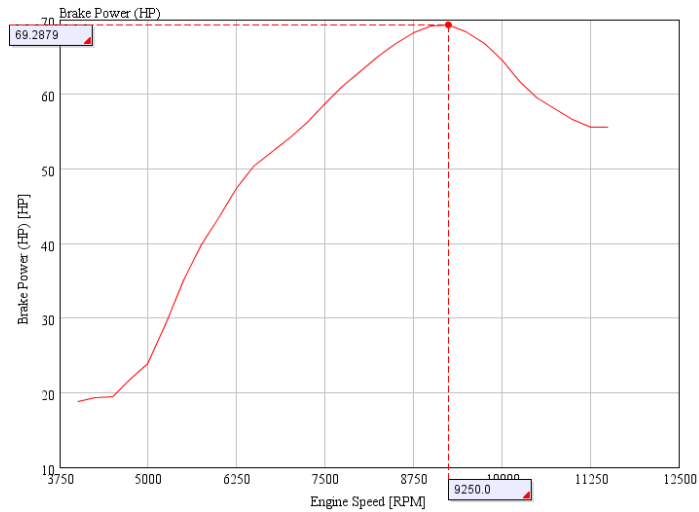


Figure 18: Power versus engine speed for 0.54L plenum

According to the power versus engine speed plots, the engine speed at which the maximum power output occurs shifts by 250RPM, with the 0.54L plenum producing peak power at 9250RPM versus the 1.08L plenum producing peak power at 9000RPM. This also corresponds with the torque versus engine speed plots shown in Appendix A; however, when examined closely, the torque versus engine speed figures show that the 0.54L plenum enables the internal combustion engine to produce more torque at higher engine speed values, which therefore shifts the power versus engine speed curve towards higher engine speed values. Also, the maximum power output increases slightly with the smaller plenum volume. The GT-Power engine simulation shows that the power output of the 1.08L plenum configuration peaks at 68.9872 HP, whereas the 0.54L plenum configuration peaks at 69.2879 HP, a 0.4% increase in power with no adverse effects throughout the rest of the engine speed range. It is important to realize

that the drastic decrease in plenum volume slightly shifts the torque versus engine speed curve to the right for the 0.54L plenum, which therefore shifts the power versus engine speed curve in the same direction. This observation alludes to the fact that maintaining fluid momentum slightly benefits maximum power output. From a holistic perspective, decreasing the plenum volume, even to half its original value, minimally changes power output, but shifts the power curve into the upper engine speed range.

The second comparison is between the 1.08L plenum and the 2.17L plenum. From a practical perspective, the double-volume plenum represents a design that focuses on equalizing pressure throughout the plenum and having a large enough volume for the pressure pulses coming from the individual cylinders through the runners to effectively fill the cylinder; the premise behind the volume is that fluid is able to approach a total pressure as close to atmospheric as possible in order to obtain the greatest pressure differential once the intake valve is opened. Figures 19 and 20 show the power versus engine speed plots for the 2013 plenum and the double-volume plenum, respectively, with all other air induction properties kept constant. See Figures 82 and 83 in Appendix A for the torque output versus engine speed figures for these two configurations.

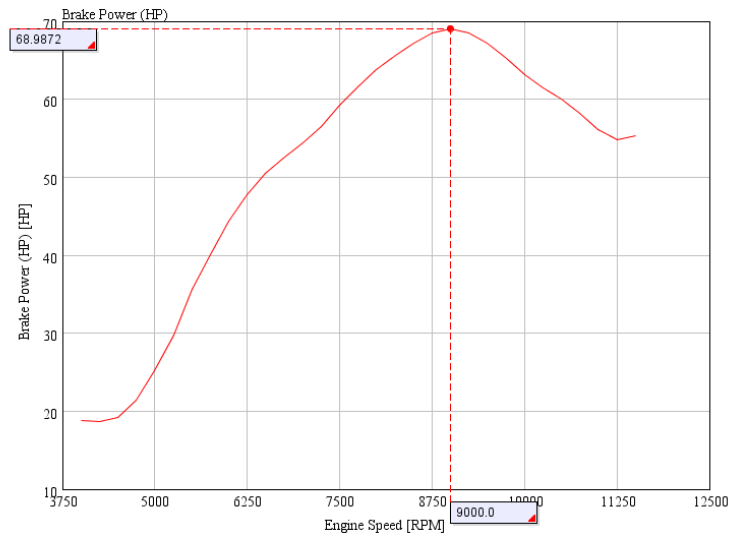


Figure 19: Power versus engine speed for 1.08L plenum

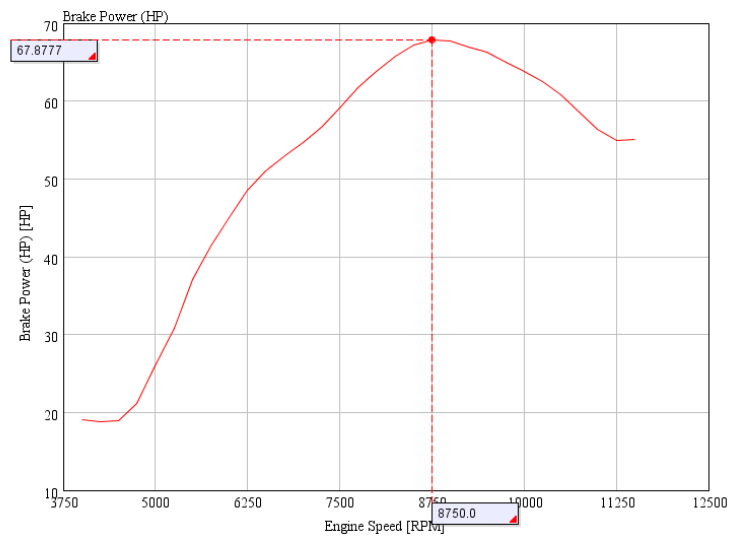


Figure 20: Power versus engine speed for 2.17L plenum

According to the power versus engine speed plots, the engine speed at which the maximum power output occurs shifts by 250RPM, with the 2.17L plenum producing

peak power at 8750RPM versus the 1.08L plenum producing peak power at 9000RPM. However, this does not correspond with the torque versus engine speed plots shown in Appendix A; when examined closely, the torque versus engine speed figures not only show that the 2.17L plenum produces slightly more torque 250RPM later than the 1.08L plenum (8250RPM versus 8000RPM, respectively), but also that the internal combustion engine produces more torque at lower engine speed values, which therefore shifts the power versus engine speed curve towards lower engine speed values. Also, the maximum power output slightly decreases with the larger plenum volume. The GT-Power engine simulation shows that the power output of the 1.08L plenum configuration peaks at 68.98 HP, whereas the 2.17L plenum peaks at 67.87 HP, a 1.6% decrease in power with no adverse effects throughout the rest of the engine speed range. It is important to realize that this drastic increase in plenum volume has minimal effects on power output, but does shift the power versus engine speed curve towards lower engine speeds. This observation alludes to the fact that equalizing pressure and having a large volume of air for induction slightly hurts maximum power output. From a holistic perspective, increasing the plenum volume, even to double its original value, minimally changes power output as was the case with the half-volume plenum, but shifts the power curve into the lower engine speed range.

Therefore, with respect to plenum volume, it appears as if there is a minimal effect on the maximum power output by changing the plenum volume, even if drastically, from this engine simulation analysis. The only notable change is the shift in the power versus engine speed curve into the upper or lower engine speed values; however, even this shift is relatively small. The overall conclusion, since this investigation is focusing on maximizing power output, especially in the upper engine speed range, would be to design the plenum with a smaller volume given the packaging constraints of the racecar. Table 3 below summarizes the results discussed above.

Table 3: Plenum volume study summary

Configuration	Parameter: Plenum volume	Power (HP)	Peak Power Engine Speed (RPM)
Control volume	1.0843L	68.9872	9000
Small volume	0.5422L	69.2879	9250
Large volume	2.1686L	68.8777	8750

3.2.1.3 Variation of runner length study: GT-Power

The runner geometry is defined by the length of the tube connecting the plenum with the cylinder head ports. The internal diameter of this tube is predetermined by the cylinder head port geometry, which is 1.375". As noted in the literature, typically the runner acts like a tube with resonant effects at certain engine speeds since the intake valve opens and closes at a prescribed frequency given the engine speed. In order to test these effects on maximum power output, the 2013 runner length, defined as 6", will be

tested against a runner length of 5" (short runner) and 8" (long runner). While these lengths may seem arbitrarily defined, these lengths represent the shortest and longest lengths that can be reasonably packaged given the vehicle setup and Formula SAE rules; also, these runner lengths will be able to show a general trend for peak power output for a given runner length.

The first comparison is between the 2013 design (6" runner length) and the 5" runner length. This comparison represents the shortest runner length compared with a medium length runner in order to derive the relationship between peak power and engine speed. Figures 21 and 22 below show the power versus engine speed plots for the 2013 runner length and the 5" runner length, with all other parameters kept constant. See Figures 84 and 85 in Appendix A for the torque output versus engine speed figures for these two configurations.

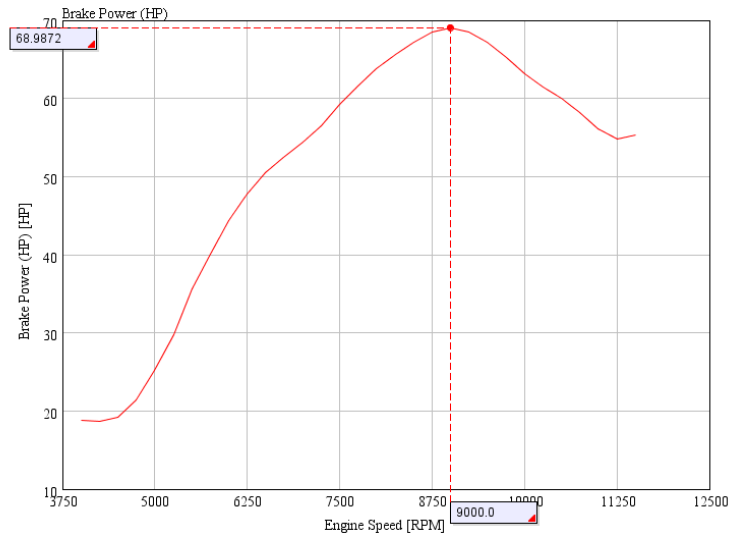


Figure 21: Power versus engine speed for 6" runner length

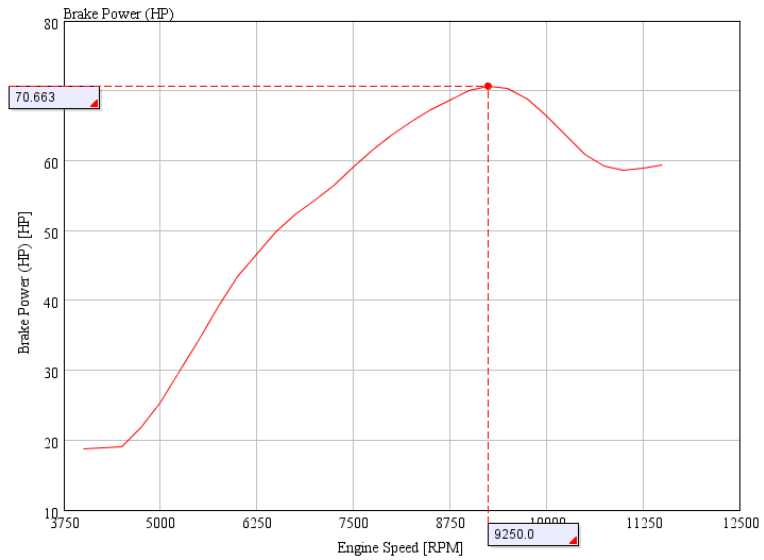


Figure 22: Power versus engine speed for 5" runner length

By examination of the power versus engine speed plots, the engine speed at which the maximum power output occurs shifts by 250RPM, with the 5" runner length

producing the maximum power at 9250RPM and the 6" runner length producing maximum power at 9000RPM. However, the peak torque versus engine speed plots show that the maximum torque output remains the same, at 8000RPM, as shown in Appendix A; the biggest difference in the torque versus engine speed curves for the 5" and 6" runner lengths is that the flat portion of the curve for the 5" runner length covers a broader range of engine speeds compared to the 6" runner length, even though the peak torque output for the 5" runner is slightly (0.062%) lower than the 6" runner length. A broader torque plateau corresponds with greater power output over a larger range of engine speeds, which is preferable in air induction design. According to the GT-Power engine simulation, the 6" runner length produces a peak power output of 68.98HP, whereas the 5" runner length produces a peak power output of 70.66HP, which is a 2.43% increase in power output with mostly positive power generation effects throughout the rest of the engine speed range. It is important to realize that this relatively small change in length shifted the engine speed at which the peak engine power occurs, as well as significantly modifying the range of maximum torque output; when closely examining the power versus engine speed plots, it is clear that the 5" runner length produces significantly more power from the 7500-11500RPM engine speed range when compared with the 6" runner length configuration.

The second comparison is between the 2013 design (6" runner length) and the 8" runner length. This comparison represents the longest runner length compared with a medium length runner in order to derive the relationship between peak power and engine speed. Figures 23 and 24 below show the power versus engine speed plots for the 2013 runner length and the 8" runner length, with all other parameters kept constant. See Figures 85 and 86 in Appendix A for the torque output versus engine speed figures for these two configurations.

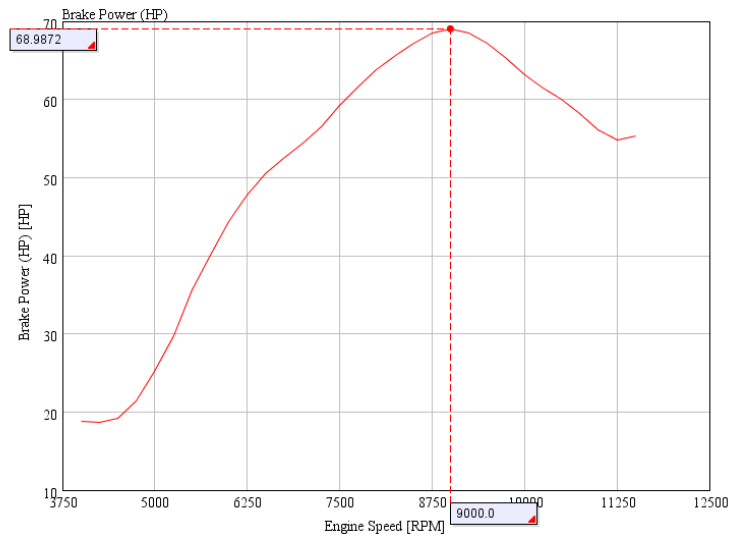


Figure 23: Power versus engine speed for 6" runner length

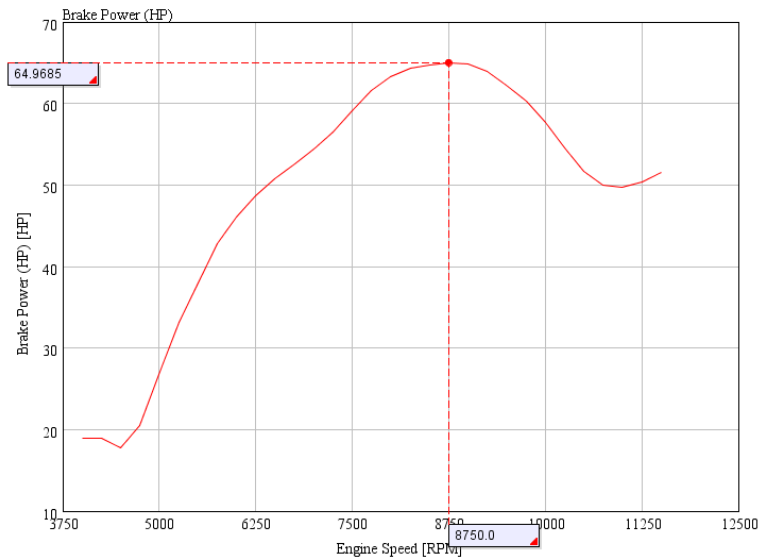


Figure 24: Power versus engine speed for 8" runner length

According to the power versus engine speed plots, the engine speed at which the maximum power output occurs shifts by 250RPM, with the 8" runner length producing its maximum power at 8750RPM and the 6" runner length producing maximum power at 9000RPM. This also corresponds with the peak torque versus engine speed plots, specifically that the maximum torque output for the 8" runner length occurs at 7750RPM and the 6" runner length peaks at 8000RPM, as shown in Appendix A. When closely examining these plots, it appears as though the entire torque curve has been pushed towards lower engine speeds and that the torque generated by the engine in the upper engine speed range drastically diminishes. The peak torque output for the 8" runner length is nearly the same as the peak torque output for the 6" runner length (0.32% decrease with the 8" runner length), but the major change is the shift of the entire curve.

According to the GT-Power engine simulation, the 6" runner length produces a peak power output of 68.98HP, whereas the 8" runner length produces a peak power output of 64.95HP, which is a 6.2% reduction in peak horsepower with a relative reduction in power output throughout all engine speeds. It is important to realize that this relatively small increase in runner length shifted the engine speed at which both peak power and peak torque output towards lower engine speeds and that the power output was significantly reduced throughout the entire range of engine speeds.

Therefore, with respect to runner length of the air induction system, the general trend is that more power generation, especially in the upper engine speed ranges, is related to shorter runner lengths. Having a shorter runner length does shift the engine speed at which maximum power peaks to the right (higher engine speed values), but not too drastically to where this could adversely affect the overall design. On the other hand, having a longer runner length shifts the engine speed at which maximum power peaks to the left (lower engine speed values), but also not too drastically to where this change could adversely affect the overall design of the air induction system. However, the biggest effect that the runner length has on the air induction design is on power generation, as well as maintaining a broader plateau of peak torque values. As shown in the torque versus engine speed plots, a shorter runner length maintains the torque plateau for a wider range of engine speeds, especially into the upper range for engine

speeds. Also, between the 5" runner length and the 8" runner length, there is a 5.7HP differential, with the 5" runner length producing 70.66HP and the 8" runner length producing 64.95HP; this is a 8.78% differential in peak power generation for a 3" difference in length. Referring back to the statement that the runner has an acoustic resonant property, it is clear that resonant frequency (engine speed) at which these peaks occur do change a total of 500RPM between the 5" and 8" runner lengths; however, the resonant properties do not explain the 8.78% differential in peak power generation between the two lengths. This result is believed to be primarily due to the ability of the shorter runner lengths to efficiently respond to the pressure drops from the intake valves opening and closing to direct the high velocity airflow into the proper cylinder at an increased pulse frequency (engine speed), without diverging too much air as to create backpressure within the air induction system. This observation can be qualitatively assessed by examining the torque versus engine speed plots in Appendix A for the 5" and 8" runner lengths, noting the breadth of engine speeds at which the torque plateau spans. The overall conclusion is that shorter runners provide not only the most power generation, but also provide a broader range of engine speeds at which elevated power output can be obtained.

Table 4: Runner length study summary

Configuration	Parameter: Runner length	Power (HP)	Peak Power Engine Speed (RPM)
Control length	5.945"	68.9872	9000
Short length	5.000"	70.663	9250
Long length	8.000"	64.9585	8750

3.2.1.4 GT-Power final results discussion and overall analysis

At this point in the analysis, many conclusions can be derived from the general trends shown in the parameterization of the air induction system into the diffuser, the plenum, and the runners. The diffuser analysis showed that minimizing the diffuser angle, which subsequently elongates its length, is preferred for improving power generation across all engine speeds due to a reduction in flow separation while not shifting the powerband with respect to engine speed. The plenum volume analysis showed that the volume has very little effect on engine performance and peak power location; however, when examining the figures closely, the preferred geometry for maximum power output is a small volume plenum, which maintains fluid momentum throughout the entire air induction system. The runner length analysis showed that the having a shorter runner length has a large positive effect on power generation, specifically in having a broader powerband, while slightly shifting the peak power generation engine speed higher.

Considering all of these geometric parameters, an ideal air induction geometry can be derived. Due to the relatively small effect of the plenum volume on maximum power generation when compared to the other parameters, there are two different design paths that can be taken for the air induction design. The first option is to have a long diffuser leading into a larger plenum in order to take advantage of the equalization of pressure, and then diverging flow into four short runners leading into the cylinder head. The second option is to have a long diffuser leading into a small plenum volume in order to take advantage of maintaining fluid momentum, and then diverging flow into four short runners leading into the cylinder head. While both design geometries will be considered for a final air induction design configuration, which involves rules compliance and packaging restrictions, the GT-Power analysis shows that the geometry with the smaller plenum volume produces the most peak power output. Figures 25 and 26 below show the power versus engine speed plots for the 2013 air induction design and the proposed 2014 air induction design, which involves a long diffuser length, small plenum volume, and short runner lengths. These parameters were chosen based on reasonable packaging restrictions, which will be discussed in greater detail in the following sections. See Figures 87 and 88 in Appendix A for the torque output versus engine speed figures for these two configurations.

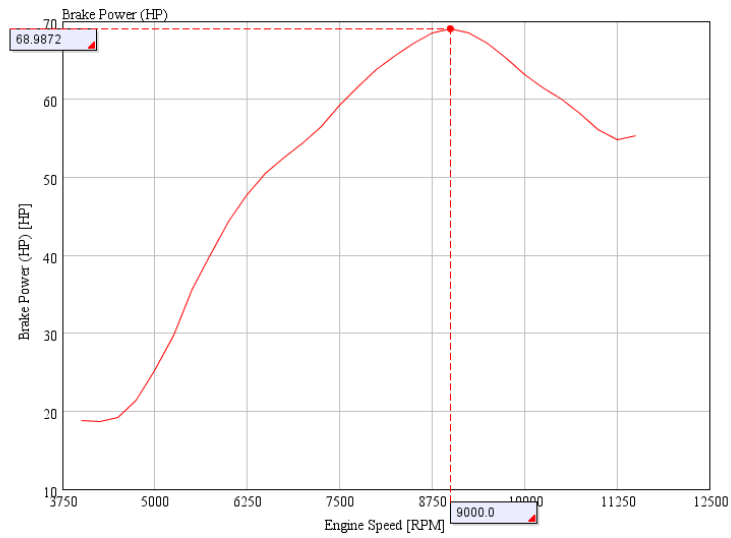


Figure 25: Power versus engine speed for 2013 air induction design

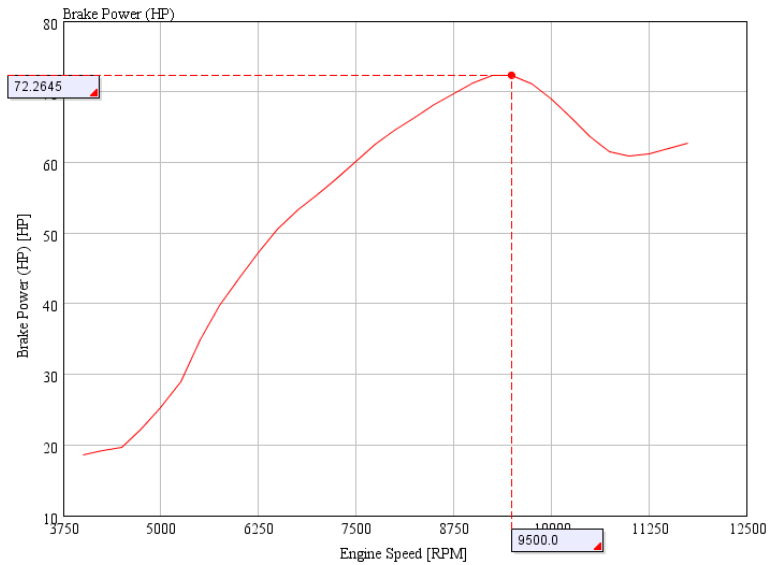


Figure 26: Power versus engine speed for proposed 2014 air induction design

According to the power versus engine speed plots, the engine speed at which the maximum power output occurs shifts a total of 500RPM higher with the optimized air

induction setup, which is expected due to the smaller plenum volume and shorter runner lengths, each contributing to a shift in 250RPM; the 2013 air induction design produces maximum power output at 9000RPM, whereas the optimized air induction design produces maximum power output at 9500RPM. However, an interesting observation between the two designs is that peak engine torque output, according to the plots shown in Appendix A, occurs at the same engine speed, nominally 8000RPM; while the peak torque output does not shift with respect to engine speed, when closely examining the figures, it becomes evident that the torque plateau elongates the powerband significantly into higher engine speeds, thereby producing more engine power output at higher engine speeds. The 2013 air induction design produces 68.98HP and 56.74N-M of engine output at the previously stated engine speeds, whereas the optimized air induction design produces 72.26HP and 57.45N-m of engine output at the previously stated engine speeds; this corresponds with a 4.75% increase in peak power output and 1.24% increase in peak torque output. According to the torque versus engine speed figures in Appendix A, the optimized air induction design maintains 90% of the peak torque output for 500RPMs longer than the 2013 design, but more importantly, the optimized design maintains 95% of the peak torque output for 1000RPMs longer than the 2013 design. This analysis of the powerband proves that the optimized design not only produces more engine output than the 2013 design, but that it also maintains these

elevated performance numbers for a broader range of engine speeds. From a design analysis perspective, the GT-Power optimization not only quantifies the performance benefits of this optimized air induction design, but also demonstrates that the parameterization of the air induction model proves to be a valid analysis methodology for showing general trends in design changes and their relative effects on total engine output.

3.3 Air induction design model development and computational fluid dynamics analysis

The GT-Power engine simulations have established an optimized air induction geometry that can be split into two viable design paths. However, geometric parameters are not the only consideration for designing the air induction system; one could argue that configuring the parameters in a smooth and efficient manner is almost more important than making sure the plenum volume is tuned to the volume specified in the engine simulations. This chapter aims to delve into the design development of the flow paths within the air induction system, focusing on computational fluid dynamics analysis.

First, it is important to discuss the conventional air induction designs typically seen in the Formula SAE collegiate competition. At the annual competition in May at the Michigan International Speedway, over 120 international teams bring the open-wheeled racecars that they have developed and built throughout the year to compete in the

world's largest intercollegiate engineering competition. The atmosphere at competition is extremely friendly and collaborative, which promotes discussion between teams, especially regarding design considerations. After talking with many teams and looking at their air induction design, the majority of teams have similar design characteristics. The diffuser geometries all featured a converging-diverging geometry in order to comply with the 20mm restrictor, and were relatively long in length, therefore representing a small diffuser angle. The runners are all the same diameter as the cylinder head ports, and for the most part, lie within the range of runner lengths tested. The biggest variation between the air induction designs is the plenum volume, which inherently dictates whether the design is symmetric or asymmetric.

Before delving further into the typical air induction design, it is important to discuss another restriction on air induction design imposed on the rules. The Formula SAE rules state that the entire air induction system must be contained within a surface envelope, as shown in Figure 27 below (SAE International, 2014).

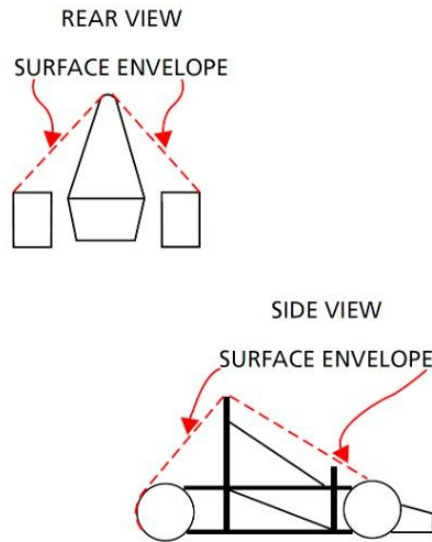


Figure 27: Air induction surface envelope definition

While this area seems to be relatively large, it is important to visualize the driver's compartment with an emphasis on the placement of the driver's head, the engine, aerodynamics kit, and other critical components for the racecar. For a symmetric design, the air induction system will be centered about the engine, which is generally centered in the vehicle laterally, but will either be positioned upward towards the top of the frame, or downwards to the back of the frame. This is a relatively small window for the entire geometry to fit, especially considering the geometric specifications derived from the GT-Power analysis. However, when considering the possibility of having a larger volume plenum with minimal effects, the configurations become much more feasible due to the fact that an asymmetric design is possible.

This general trend is shown in the conventional designs of many Formula SAE air induction designs. A larger plenum is typically used, either in a symmetric design to help an even flow distribution by having the air flow enter and exit the plenum at different plane angles, or in an asymmetric design, with the air entering almost perpendicular to the runner outlets to the cylinder head. Understanding the geometric considerations and the general flow trajectories, it is clear that a small plenum volume would not work well in an asymmetric design, as the point of a small plenum volume is to maintain fluid momentum; if the entrance into the plenum is not symmetric about the exits to the runners from the plenum, the asymmetric design featuring a small plenum volume would favor fluid motion into certain cylinders and inhibit flow into others. On the contrary, a larger plenum volume would more easily be able to equalize pressure across all runner inlets, thereby making a larger plenum volume more suitable for an asymmetric design.

Therefore, three designs will be analyzed using computational fluid dynamics methods: the 2013 air induction design; an asymmetric, large plenum air induction design with a small diffuser angle and short length runners; and a symmetric, small plenum air induction design with a small diffuser angle and short length runners. Figures 28, 29, and 30 depict the models developed for these designs that meet all requirements dictated by the rules.



Figure 28: 2013 air induction system

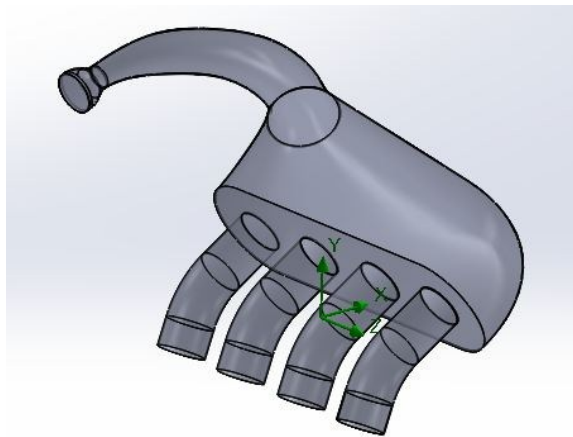


Figure 29: Proposed 2014 asymmetric, large plenum air induction model

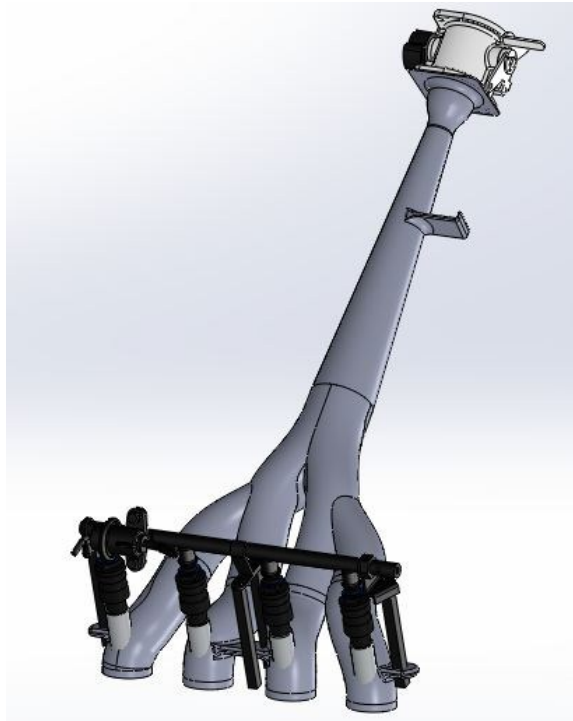


Figure 30: Proposed 2014 symmetric, small plenum air induction model

For validation purposes, both proposed 2014 air induction designs were placed in the full CAD model for the Duke Motorsports race car in order to ensure that the entire model fits well within the surface envelope. Figures 31 and 32 show the rear and side views of the 2014 asymmetric design installed on the race car, and Figures 33 and 34 show the rear and side views of the 2014 symmetric design installed on the race car. The 2013 air induction design is currently installed on the race car and has competed in the 2013 Formula SAE Michigan competition, and Figure 35 shows it installed on the 2013 competition vehicle.

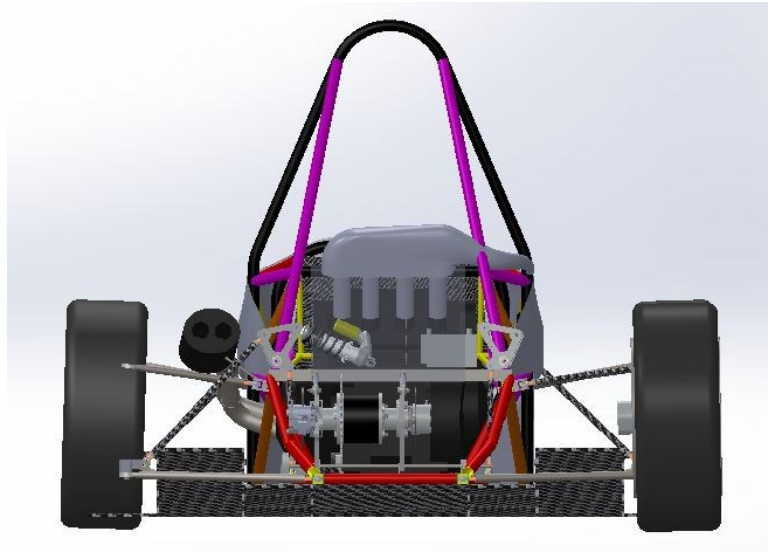


Figure 31: Proposed 2014 asymmetric air induction design installation – rear view

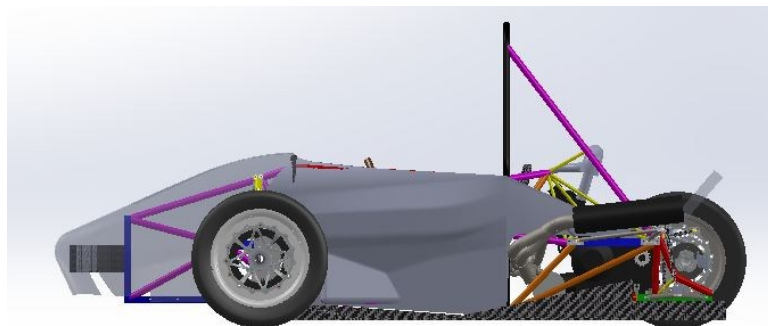


Figure 32: Proposed 2014 asymmetric air induction design installation – side view

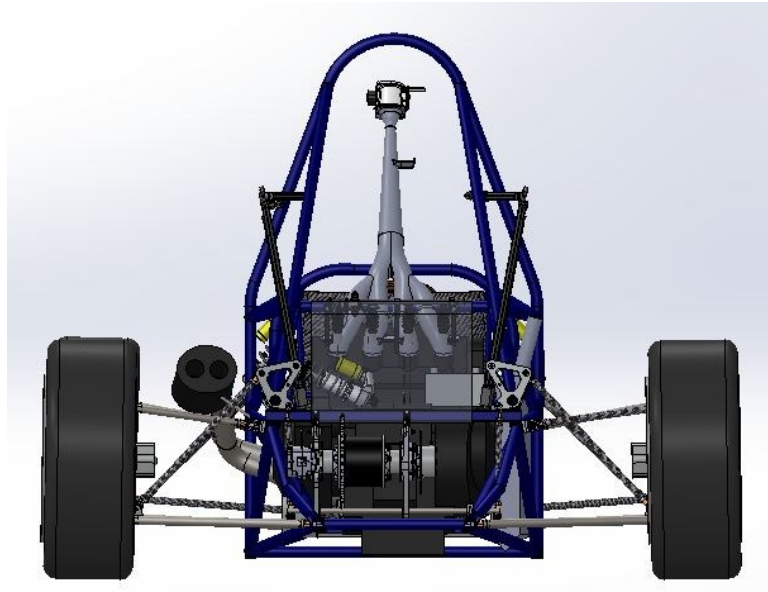


Figure 33: Proposed 2014 symmetric air induction design installation – rear view

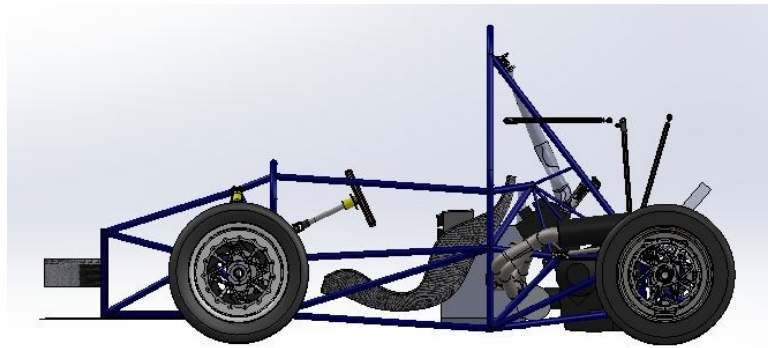


Figure 34: Proposed 2014 symmetric air induction design installation – side view



Figure 35: 2013 air induction design installation on competition vehicle

3.3.1 Development of transient boundary condition

The 2013 air induction system has a 5.6" long diffuser; a plenum volume of 1.08L; and runner lengths of 5.91". This design was focused on providing more power and torque output at lower engine speeds, which is evident in the engine output numbers: max power output occurs at 9000 RPM (68.99 HP), and max torque occurs at 8000 RPM (56.75 N-m). This design proved to be successful, especially when compared with goals set forth by the design. However, it was clear that there was more potential for refinement with the design, which has been shown through the GT-Power analysis.

In order to fully understand the 2013 air induction system design, computation fluid dynamics software was used to simulate the air flow from the environment

through the system. However, typical CFD analysis is done as a steady-state analysis, which is typically shown experimentally through a flow bench test; a constant vacuum is applied to all runner exit ports, and through port pressure measurements, the experimental results show whether equal mass flow is reaching each cylinder. Previous CFD analysis has been conducted in this manner, where constant boundary conditions are applied to each runner outlet. However, the fluid motion throughout the air induction system is not a steady-state scenario and is highly dynamic, as the intake valves are opening and closing at elevated frequencies corresponding with the engine speed. Therefore, it is necessary to derive a time-varying boundary condition which develops a fluid environment similar to that of the internal combustion engine of interest.

The CFD package used for this analysis is SolidWorks Flow Simulation software, which integrates the CAD software seamlessly with the CFD software. The SolidWorks Flow Simulation software allowed for a time varying boundary condition, which was applied to the runner outlets to effectively simulate the intake valves opening and closing. The development of the boundary conditions was simulated using the camshaft profile to know the movement of the intake valve and was then approximated as a sine function. The camshaft profile is known for both the intake and exhaust camshafts as a function of crankshaft angle; for every two revolutions of the crankshaft, the camshaft

completes one revolution. Within that one revolution of the camshaft, each set of intake valves corresponding with each of the four cylinders opens one time; in other words, for every two revolutions of the crankshaft, the internal combustion engine completes one intake cycle. However, the complicated aspect of this model involves the camshaft overlap, meaning that there are crankshaft angles where there are two sets of intake valves open; one set is opening and the other set is closing. Therefore, it is important to not only consider the opening and closing of valves for a given cylinder, but how this also happens in conjunction with the opening and closing of other intake valves throughout the engine. Figure 36 below shows how pressure changes at each of the runner outlets with respect to crankshaft angle over two full intake cycles, or four revolutions of the crankshaft. The pressure representing a closed intake valve is atmospheric pressure, or approximately 14.7psi, and the sinusoidal drop in pressure corresponds with the vacuum caused by the piston drawing air in through an opening or closing intake valve. The overlap in the curves represents a scenario as previously described, where the mass flow is being divided between multiple ports; this is the heart of the transient analysis performed and is important to develop in order to fully understand the fluid flow throughout the air induction system. Once the engine speed is defined, the crankshaft angles can then be transformed into a time based on a defined engine speed, and a pressure versus time table can be derived for input into the

SolidWorks Flow Simulation software. The chosen engine speed for CFD analysis is 9000RPM, which represents an engine speed corresponding with maximum or near maximum power output and is also nearly at the choked flow condition throughout the air induction system. Overall, this transient analysis occurs over 0.0267s, which alludes to how time dependent the air induction system, especially for a race engine that sweeps through the entire range of engine speeds in seconds.

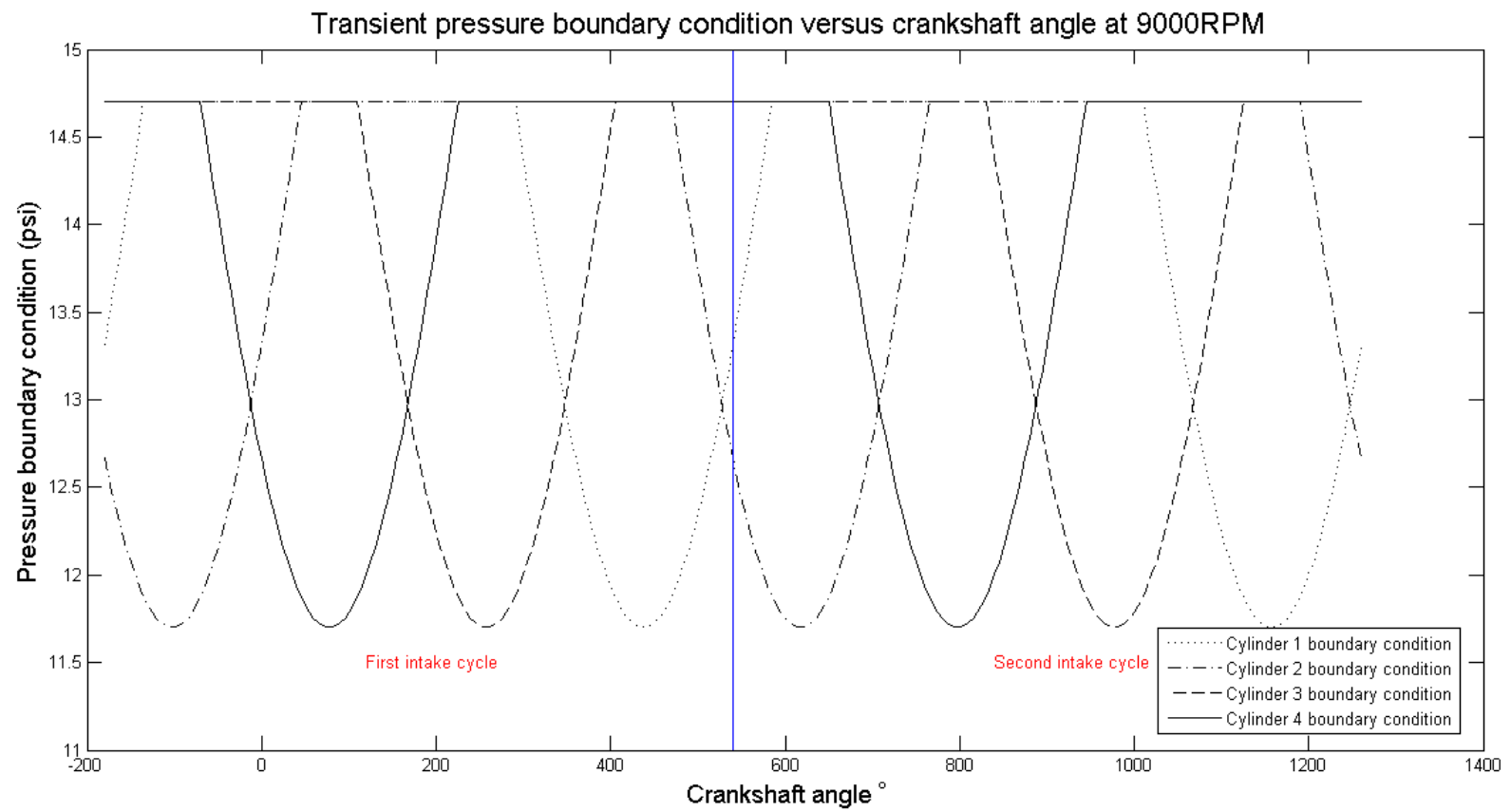


Figure 36: Transient boundary condition with respect to crankshaft angle

For the transient boundary condition, it was necessary to define the minimum pressure at the cylinder head to fully define the sine functions. This value was taken from the GT-Power analysis, which can be shown in Figure 37. The pressure at the cylinder head at 9000RPM is not the lowest pressure seen throughout the engine speed range, but it is a good estimate of an average pressure seen throughout the upper engine speed range and corresponds with the choked flow condition well. The pressure value of 0.81bar, or about 11.75psi, is the maximum amplitude of the transient boundary condition, as shown in the previous figure. As the intake valves are opening or closing, the pressure seen at the intake port is ramping up or down from this maximum vacuum created by the piston motion, which properly simulates the dynamic fluid motion inside the air induction system.

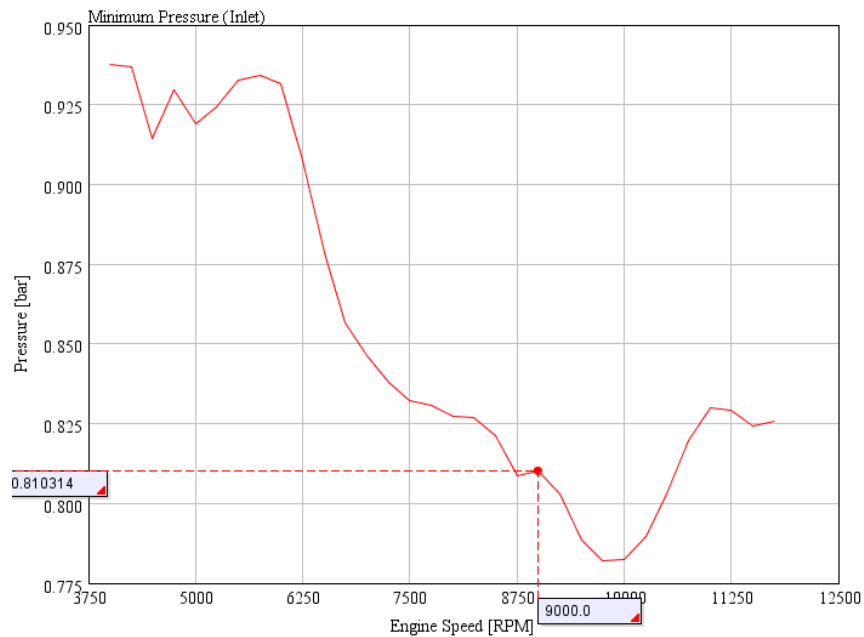


Figure 37: Minimum pressure at cylinder head for transient boundary condition development

As for the inlet boundary condition, atmospheric conditions were used to simulate wide open throttle, or in other words, enabling maximum mass flow rate of air for full engine power at the stated engine speed of 9000RPM. The analysis involved compiling the results of more than 400 iterations over a physical time interval of 0.0267 seconds, corresponding with two full intake cycles, or four full revolutions of the crankshaft at 9000RPM. The analysis was performed on all three air induction geometries, maintaining identical boundary conditions for each geometric configuration. The analysis was focused on not only quantifying the specific fluid properties corresponding with engine performance, specifically mass/volumetric flow and total

pressure losses throughout the air induction system, but was also meant to provide a visual representation of fluid motion for an instant in time. The following subsections delve into each of these aspects of the CFD analysis. The data was extracted from the Flow Simulation CFD as a function of time, and in converting it to a crankshaft angle at 9000RPM, resolution of the data was lost. Therefore, the data as a function of crankshaft angle appears to be a step function. To mitigate this problem, a smoothing curve was applied, and after comparing the modified data as a function of crankshaft angle and the original data as a function of time, the smoothing curve accurately represents the Flow Simulation results.

3.3.2 Total pressure losses throughout air induction system

An important aspect of the air induction system involves pressure losses throughout the system due to fluid motion (Ceviz, 2007). In order to quantify these losses, the total pressure was evaluated and spatially averaged across all runner outlets for each crankshaft angle, which was then compared to the atmospheric pressure condition to calculate a pressure loss through the system. The total pressure is defined as the sum of the static pressure, dynamic pressure, and pressure due to gravity, which will be neglected for this analysis; therefore, the stagnation pressure of the fluid is evaluated and compared at the inlet and outlets to the air induction system. Ideally, the fluid motion through the air induction system would not cause a pressure loss, but

because of high fluid velocities, fluid viscosity, and rough surface interfaces between the fluid and the walls, there will always be a quantifiable pressure loss. However, a design goal regarding the total pressure is to minimize any pressure losses throughout the air induction system to diminish the negative effects of flow losses on engine performance.

This total pressure differential was evaluated for all three geometric configurations and compared, which is shown below in Figure 38. It is important to note that the CFD results do not accurately describe the fluid environment at the beginning of the simulation, and as shown with later results, the internal flow is not entirely developed until the second intake cycle. Taking this into consideration, the largest pressure loss seen is approximately 0.45psi, or about a 3% loss in total pressure. Relatively speaking, this is a small, yet quantifiable, pressure loss, especially when considering the highly transient fluid motion with large fluid velocities through a 20mm orifice.

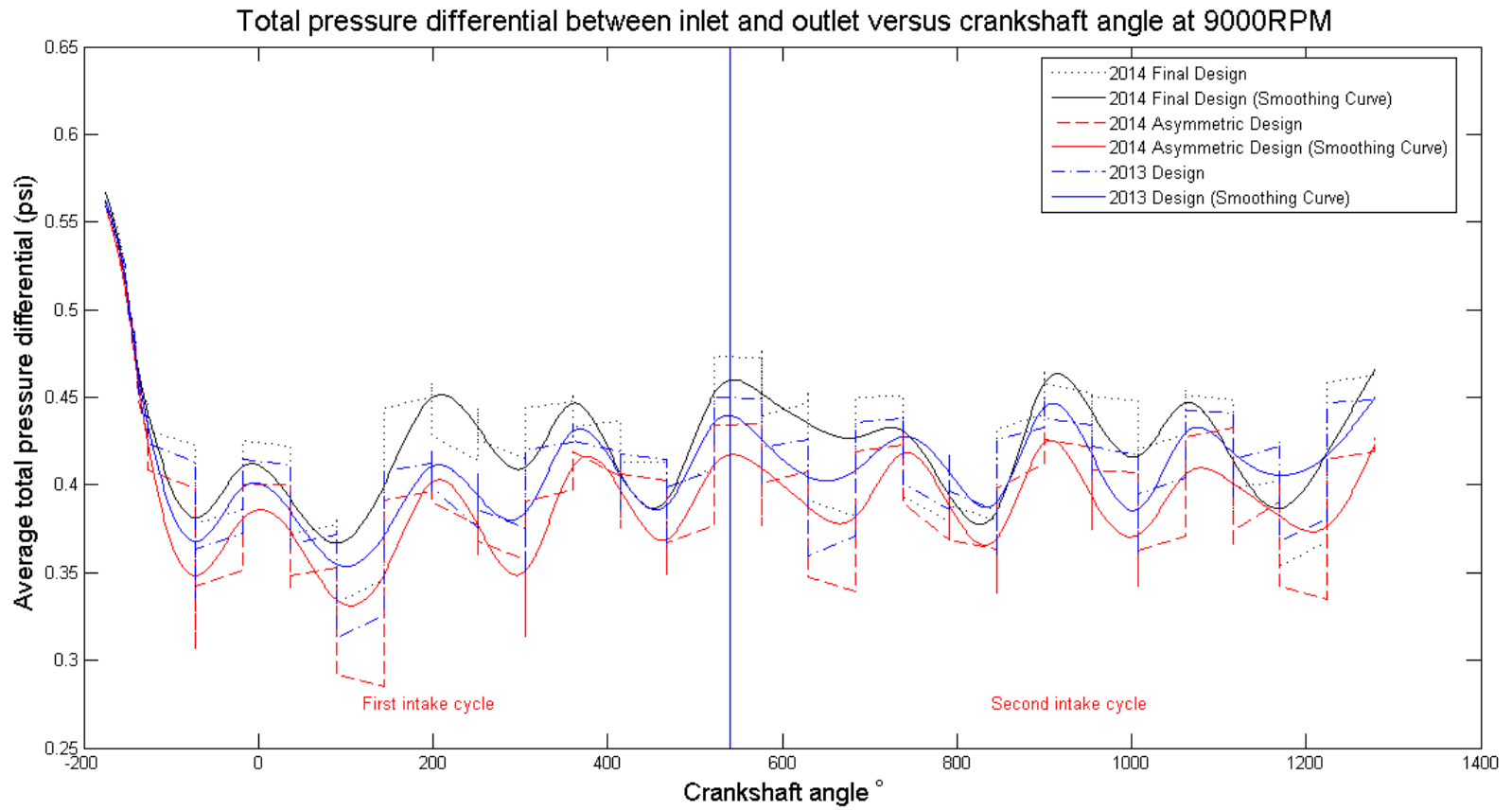


Figure 38: Total pressure differential versus crankshaft angle at 9000RPM

Looking at Figure 38, it is clear that there are fluctuations in the total pressure differentials at different crankshaft angles for an engine speed of 9000RPM, but when considering the highly unsteady flow field and the opening/closing of the intake valves, these variations are representative of the boundary conditions acting on the fluid environment. Looking strictly at the second intake cycle, the geometry with the smallest average total pressure loss is the 2014 asymmetric, large plenum air induction design with an average pressure loss of approximately 0.4psi over one intake cycle; the geometry with the largest average total pressure loss is the 2014 symmetric, small plenum air induction design with an average pressure loss of approximately 0.44psi over one intake cycle. For comparison, the 2013 air induction design features an average pressure loss of approximately 0.42psi over one intake cycle. While the physical difference in total pressure is ± 0.02 psi, this represents a 5% change in the total pressure differential.

From a geometric perspective, the trend in total pressure differential makes sense due to the differences in plenum volume. The only geometric parameter difference between the 2014 symmetric and asymmetric designs, besides the fact that the layout is symmetric or asymmetric, is the plenum volume; the symmetric design, which had the largest difference in total pressure with 0.44psi, features a 0.54L plenum, whereas the asymmetric design, which had the smallest difference in total pressure with 0.4psi,

features a 2.17L plenum. Increasing the plenum volume severely reduces fluid velocity through the volume, thereby reducing the effect of viscosity and skin friction. Decreasing the plenum volume has the opposite consequence because the goal of using a small plenum volume is to maintain fluid momentum, sustaining higher fluid velocities which increase the effect of viscosity and skin friction. These properties are inherent to the air induction design, and while there is a $\pm 5\%$ change in total pressure differential, the net effect is relatively small with a change in total pressure of ± 0.02 psi. Also, a key component that will be examined later involves the mass flow rate throughout the air induction system, which contributes to the overall pressure drop; it is important to view the total pressure drop in terms of the mass flow rate sustained and not strictly by itself for comparison purposes.

Another consideration that is directly related to the pressure losses affiliated with fluid motion through the air induction system is an industry standard quantity called the uniformity index, γ , which is defined by the equation below:

$$\gamma = 1 - \int_A \frac{\sqrt{(\bar{u} - u)^2}}{2A\bar{u}} dA \quad (3.3.2 - 1)$$

\bar{u} = average flow velocity

u = actual flow velocity

A = cross-sectional area of interest

The uniformity index is a measure of how uniform the flow through a given area section is, specifically with the velocity flow field; the closer the uniformity index is to 1, the more uniform the velocity distribution is across the particular area (Fridolin, 2013). The cross-section of interest included the runner outlets exiting the air induction system and entering into the cylinder head. The uniformity index was evaluated for each model and is shown as a function of crankshaft angle in Figure 39 below. Note once again that the simulation is developed after the first intake cycle, and therefore the second intake cycle data will be used to draw conclusions.

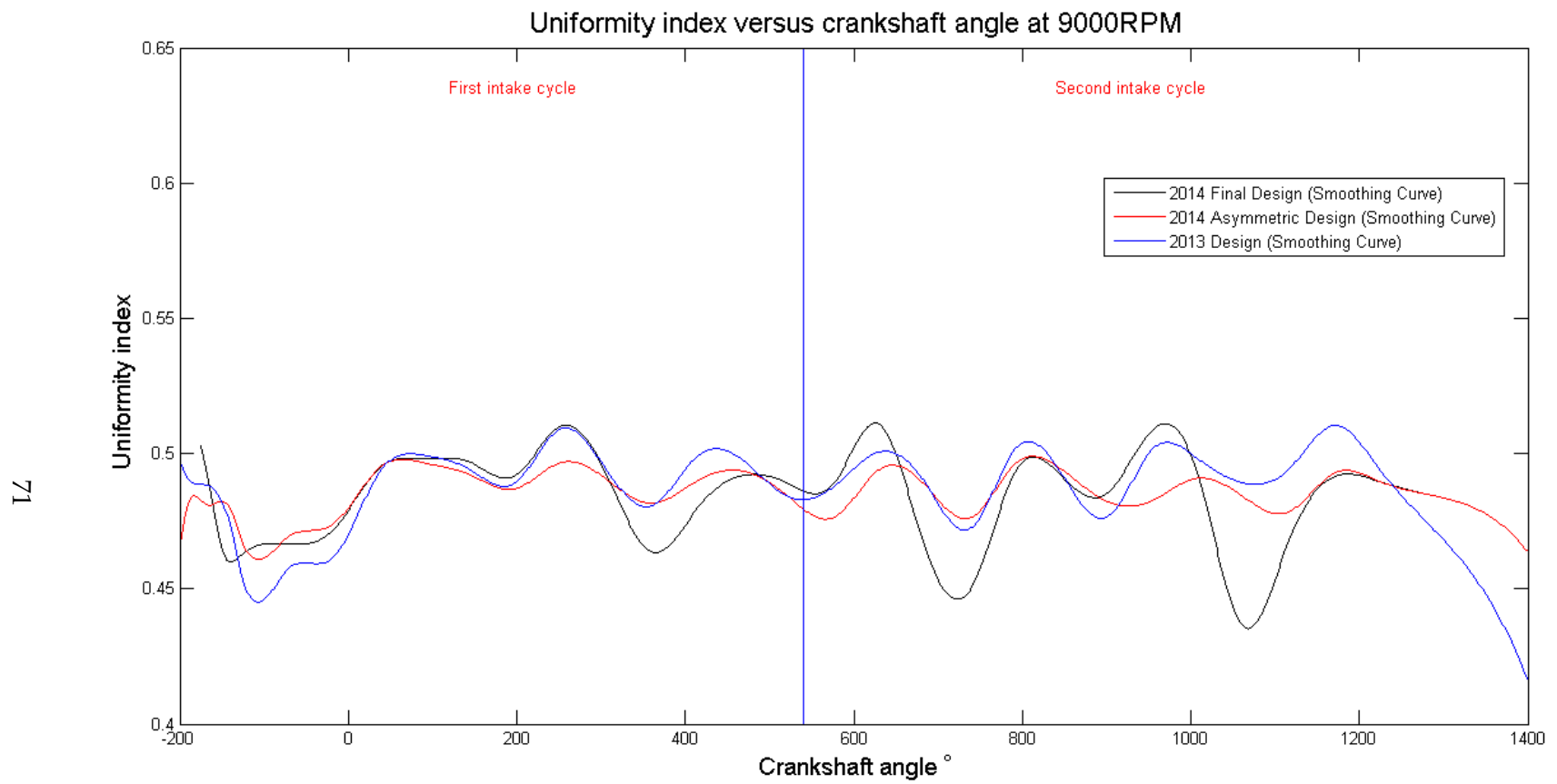


Figure 39: Uniformity index versus crankshaft angle

The results of the CFD analysis regarding uniformity index show that this quantity also varies with crankshaft angle, but in fact moves opposite with crankshaft angle when compared with the total pressure differential; as total pressure differential increases, the uniformity index generally decreases, and the opposite generally holds true. The values for the uniformity index range from approximately 0.51 to 0.44, having a span of 0.07. These values make sense physically due to the fact that not only is the fluid environment highly unsteady, but the flow is turbulent through the runner outlet, yielding a uniformity index less than 1 and near the range of values that were shown computationally.

Another way of looking at the uniformity index versus crankshaft angle figure is to mentally approximate it as a sine function with period corresponding to the transient fluid properties across geometries, but having an amplitude corresponding to a given geometric configuration. When comparing the uniformity index across the different geometries, the 2014 symmetric, small plenum volume design has the largest span of indices, ranging from 0.51 to 0.44; in other words, the 2014 symmetric, small plenum volume design has the largest amplitude. The 2014 asymmetric, large plenum volume design has the smallest span of indices, disregarding the ramp down effects towards the end of the second intake cycle. These values range from 0.475 to 0.49, which corresponds with the smallest amplitude. The 2013 air induction design lies in between these two

extremes, but more closely follows the trend of the 2014 asymmetric design for overall amplitude. These results yield the same conclusions derived from the total pressure differential trends shown previously. Because the 2014 symmetric design focuses on maintaining fluid momentum, the fluid flow exiting the air induction system into the cylinder head is at a higher velocity. This elevated fluid velocity contributes to the viscous effects, increasing the total pressure differential, while simultaneously increasing the difference in velocity distribution across all runner outlets due to turbulence. On the other hand, because the 2014 asymmetric design focuses on maintaining an even pressure distribution by slowing the fluid down, the fluid flow exiting the air induction system into the cylinder head is at a lower velocity. This slightly diminished fluid velocity reduces the viscous effects, which decreases the total pressure differential, while also decreasing the difference in velocity distribution across all runner outlets due to marginally reduced turbulence.

To better understand this evaluation, a surface plot was made to show the velocity distribution across all four runner outlets, which inherently shows the uniformity index. Beginning with the highest average uniformity index, Figure 40 shows the velocity distribution across each of the four runners for the 2013 air induction design during the second intake cycle.

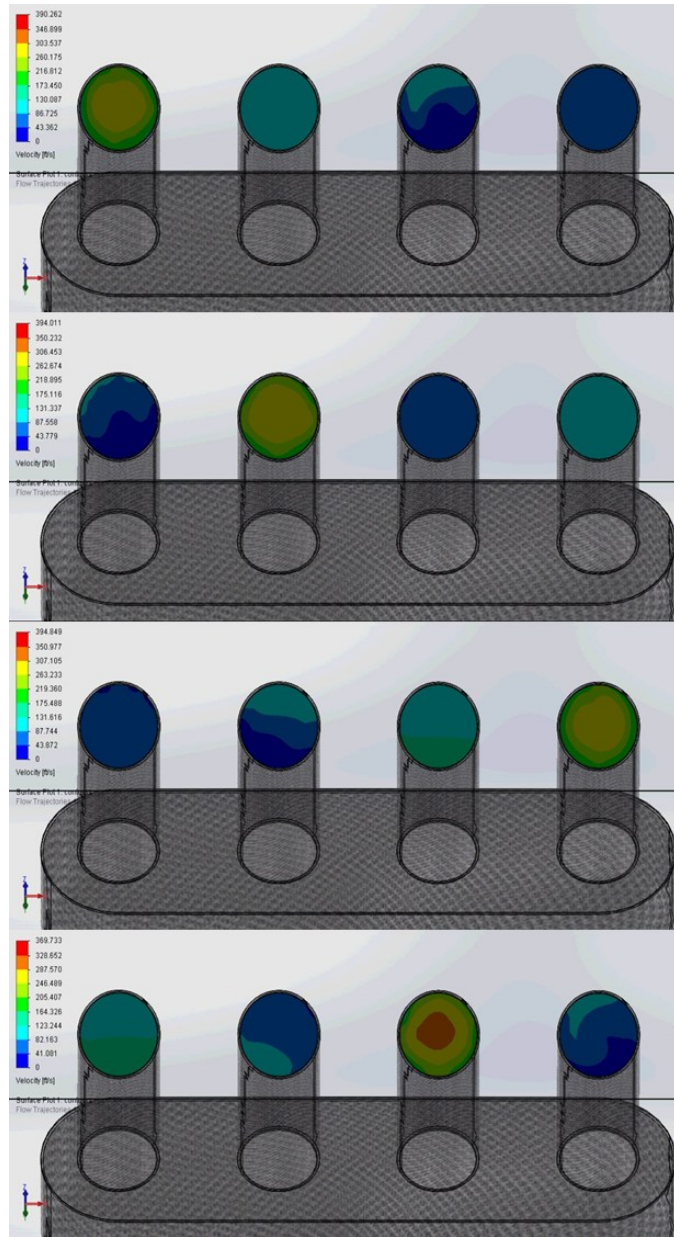


Figure 40: Velocity distribution at runner exits for 2013 air induction design

It is clear that the velocity distribution in the 2013 air induction design is nearly concentric about the runner center, which results in a higher uniformity index. Also, the main reason why this design has the best and most consistent uniformity index is because of how evenly the velocity is distributed across the runner exit cross-sectional area. Looking at the figure, for three of the four runner exits, the cross-sectional area is almost entirely yellow in color, which means that nearly all of the fluid is flowing at a constant velocity. Looking at Equation 3.3.2-1, if the average flow velocity is almost equal to that of nearly all other points in the flow cross section, the second term decreases in size and the overall uniformity index increases towards 1. The one discrepancy is with cylinder three, where the center of the runner sees a significantly higher velocity than the outer wall. Despite this factor bringing the overall uniformity index down, the 2013 design proves to have the most uniform flow corresponding with slower fluid velocities.

The second best uniformity index is seen in the 2014 asymmetric air induction design with the large plenum volume. Figure 41 shows the velocity distribution for this design across each of the four runner outlets during the second intake cycle.

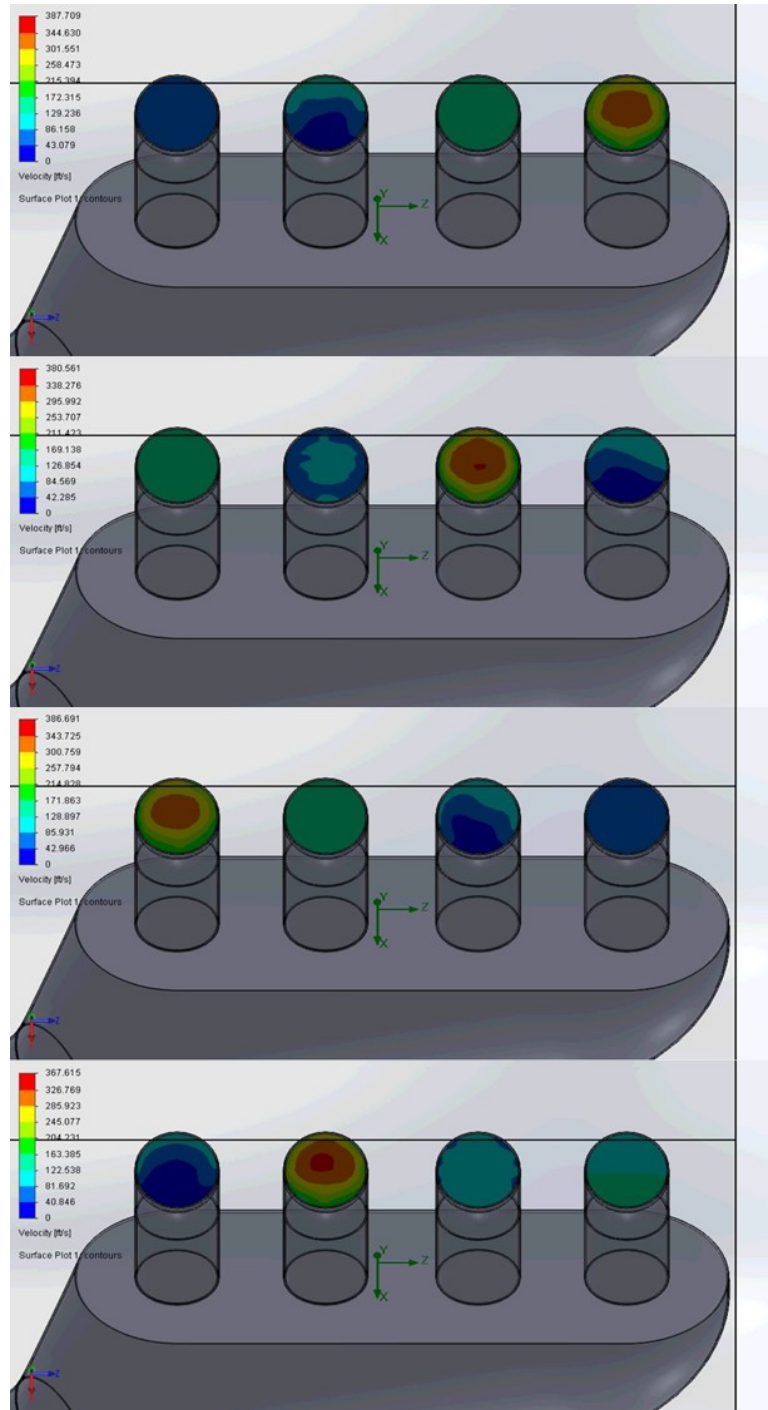


Figure 41: Velocity distribution at runner exits for 2014 asymmetric air induction design

It is clear that the velocity distribution in the 2014 asymmetric air induction design is nearly concentric about the runner diameter, which results in a higher uniformity index. However, it is also clear that the center of the runner outlet has a much larger fluid velocity than that seen at the outer wall. When referring back to Equation 3.3.2-1, it becomes clear that, even though all four cylinders behave very similarly and have concentric velocity distributions, because the average velocity is generally much different than the velocity at any other point in the runner outlet, the uniformity index decreases.

The 2014 symmetric air induction design has the largest fluctuation in uniformity index, having both the best and worst value throughout the second intake cycle. Figure 42 shows the velocity distribution for this design across the four runner outlets during the second intake cycle.

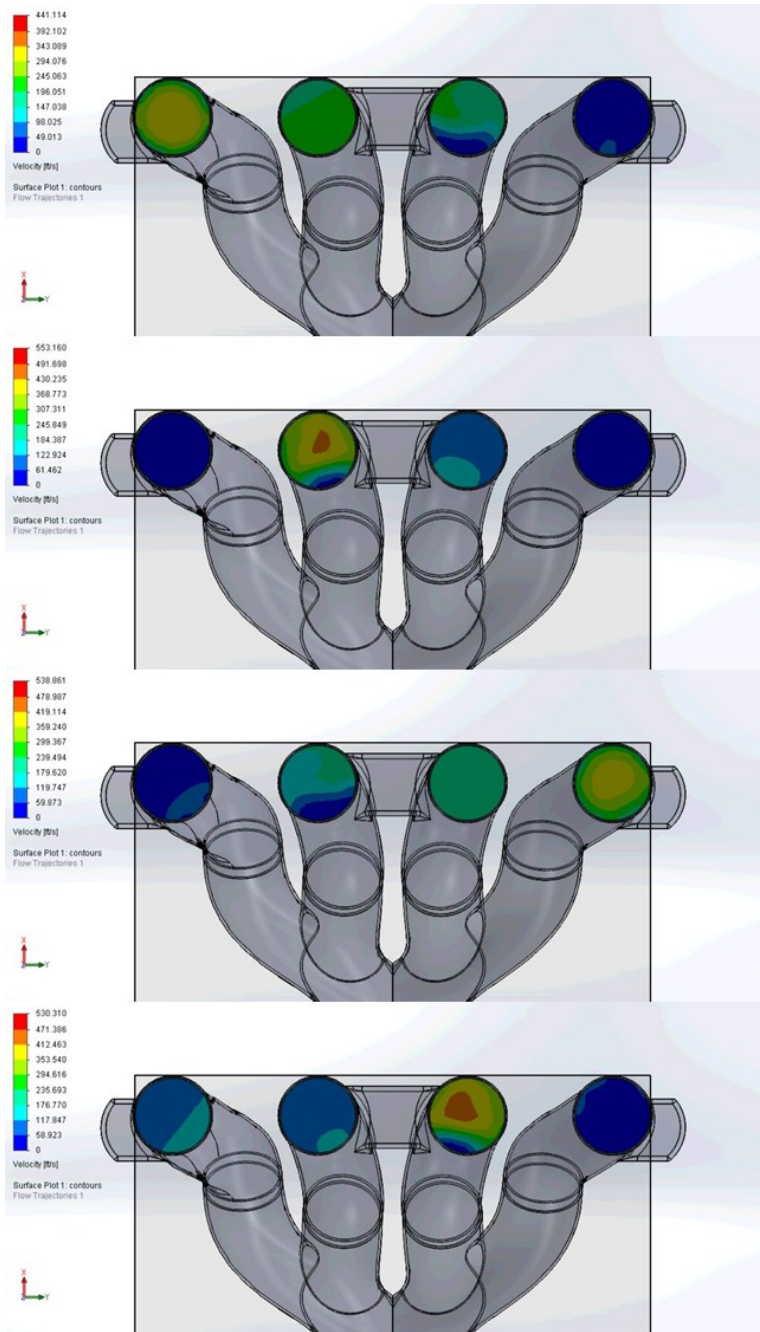


Figure 42: Velocity distribution at runner exits for 2014 symmetric air induction design

The 2014 symmetric air induction design shows a rather complicated velocity distribution at the runner outlets, as the outer two and inner two runner outlets have different fluid velocity distribution characteristics. It is clear that the outer two runner outlets have a highly uniform and concentric velocity distribution, with nearly all of the fluid traveling at a constant velocity. However, the inner two runner outlets show an offset velocity distribution towards the fuel injector mounts, as well as having a larger velocity gradient throughout the runner outlet area. These two scenarios represent both extremes seen in the uniformity index plot shown previously. While these two extremes balance each out for an average uniformity index, the more important question is to determine what effect the uniformity index has on overall performance. The velocity distributions give a little bit of insight as to what the volumetric and mass flow rates of the individual designs will be, and even though some of the designs feature non-uniform velocity distributions, because the velocities are elevated, an almost equivalent volumetric and mass flow rate can be expected through each of the runner outlets. This assertion will be explored in the next section featuring the volumetric and mass flow rates throughout the air induction system. Overall, there is about a 2% change from the best performing design to worst performing design for uniformity index, which has a relatively small impact on overall performance; the true measure of air induction performance lies in how large of a mass flow rate the design can sustain.

3.3.3 Volumetric and mass flow rate through air induction designs

With respect to the air induction system, the most crucial element to its overall performance is the mass flow rate through the system when prescribing pressure boundary conditions. The design goal for any air induction system is to be able to supply the internal combustion engine with as much air as possible, especially with respect to restricted race engines. The restriction effectively limits the mass flow throughout the entire system, but if the air induction system is not capable of sustaining this flow, the system is not properly designed.

The premise behind the analysis is to define a set of inlet pressure boundary conditions and outlet pressure boundary conditions to fully define the system and therefore solve for the mass flow rate the model is capable of providing at a given engine speed. According to the GT-Power results, the 2013 air induction design is capable of providing 52.74g/s of air flow at 9000RPM, as shown in Figure 43, which corresponds with the peak mass flow rate throughout the entire engine speed range. This is primarily why all CFD analysis was performed at 9000RPM in order to ensure that an even comparison could be made.

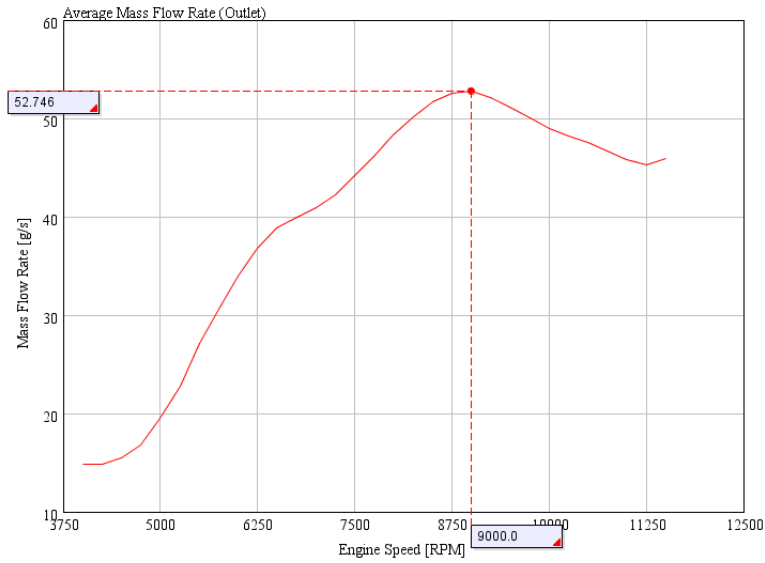


Figure 43: GT-Power results for average mass flow rate of 2013 air induction design

Compiling the CFD results and running the time varying boundary condition, the volumetric flow rate versus crank angle for each model was calculated and is shown in Figure 44. The results, as shown for the other CFD analyses figures, vary with crankshaft angle, which is to be expected due to the highly unsteady fluid environment present in the air induction system. Also, it is important to note that the CFD simulation needed one full intake cycle in order to ramp up to effectively converge on a solution, and therefore only results from the second intake cycle will be evaluated. It is clear from the figure that the 2014 symmetric, small plenum design sustains the most negative volumetric flow rate, meaning the largest amount of fluid volume leaving the system. The 2013 design performs the worst, as shown by the upper curve in the figure.

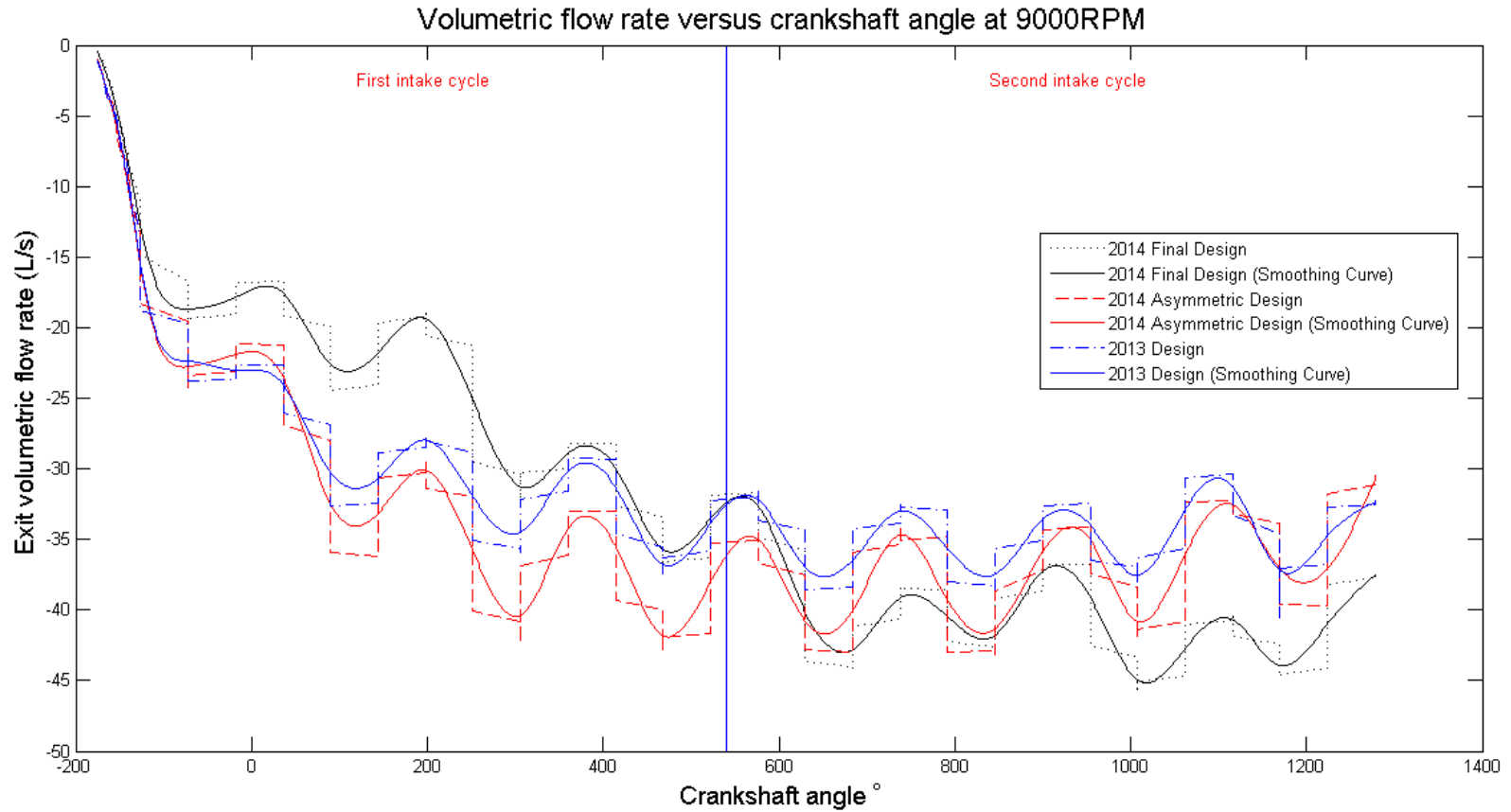


Figure 44: Volumetric flow rate versus crankshaft angle

However, due to the complexity of the transient analysis, it is difficult to discern the true performance of the air induction design based on the volumetric flow rate versus crankshaft angle. Therefore, the mass flow rate versus crankshaft angle was also solved for, and is shown below in Figure 45. It is clear that, while the volumetric flow rate significantly changes with crankshaft angle, the mass flow rate remains at a relatively constant value with respect to crankshaft angle once the CFD model is able to converge on a solution in the second intake cycle. This figure clearly shows the distinction in mass flow rate performance for the three different designs. According to the figure, the 2013 air induction design sustains approximately 37g/s of air flow at 9000RPM; the 2014 asymmetric large plenum design sustains approximately 38g/s of air flow at 9000RPM; and the 2014 symmetric small plenum design sustains approximately 44g/s of air flow at 9000RPM. The 2014 symmetric design sustains a mass flow rate 19% greater than the 2013 design and 16% greater than the 2014 asymmetric design.

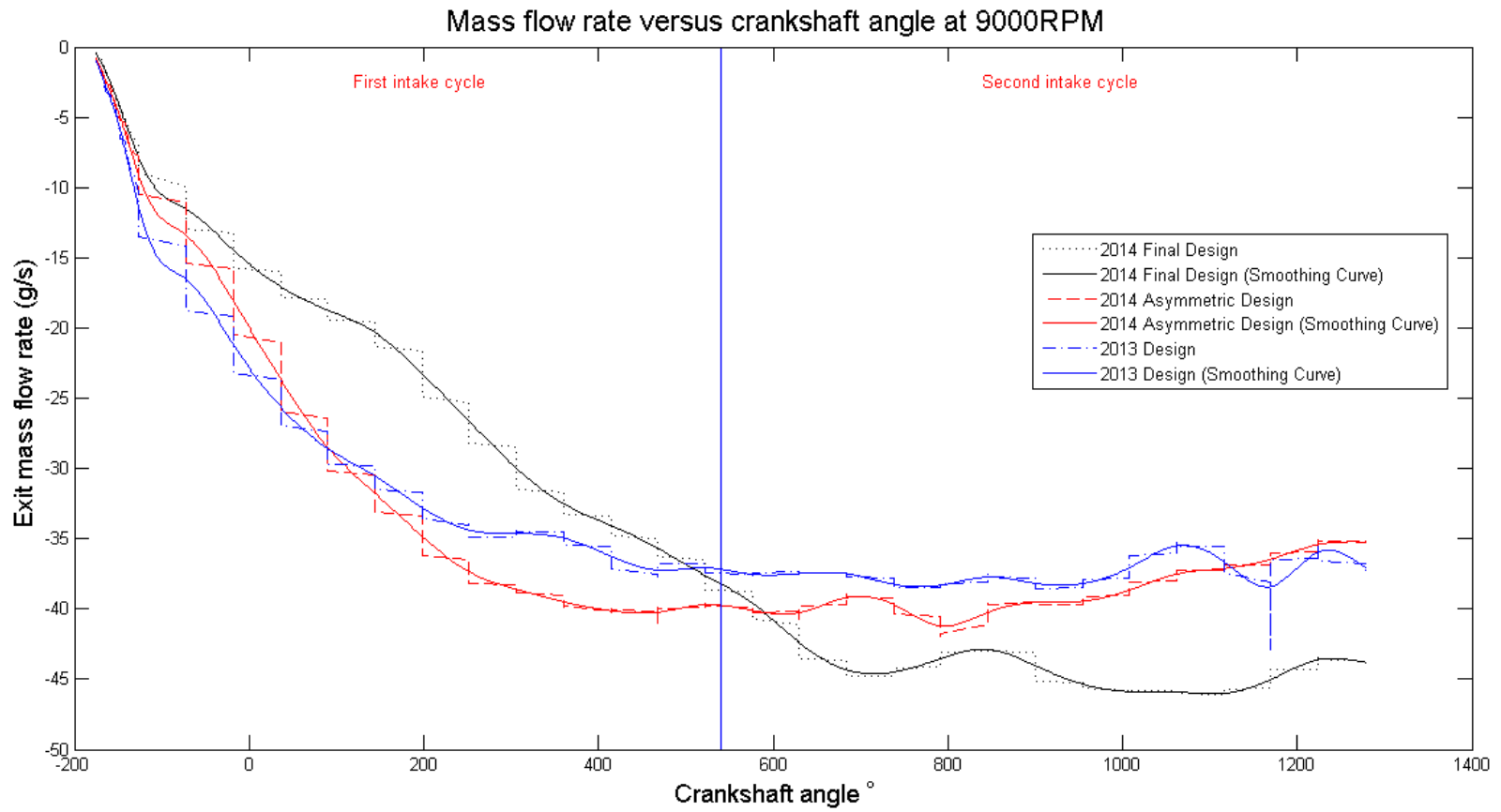


Figure 45: Mass flow rate versus crankshaft angle

According to the CFD analysis, the 2014 symmetric small plenum design sustains a 19% higher mass flow rate than the 2013 design, and also sustains a 16% higher mass flow rate than the 2014 asymmetric large plenum design. A larger sustained mass flow rate directly corresponds to a greater engine performance in terms of power and torque production from the internal combustion engine. Therefore, using the CAD geometry designed in SolidWorks and performing a CFD analysis on it using time varying boundary conditions, the best design for power generation is clearly the 2014 symmetric small plenum volume design.

While having a higher sustained mass flow rate through the air induction system is extremely important for power generation, having it equally distributed amongst the runners leading into the cylinder head is important for engine tuning and design efficiency. In order to examine this characteristic, the mass flow rate exiting through each runner outlet was solved for as a function of crankshaft angle and then normalized with the peak mass flow rate seen during the second intake cycle. The key to understanding these plots is to focus on the second intake cycle and on the mass flow rate distributions per cylinder. It is important to note that these plots are not meant to compare the actual mass flow rates of one design to the next; they are strictly meant to show the distribution of the mass flow rate exiting the air induction system between each of the four cylinders.

Figure 46 shows the mass flow distribution for the 2013 air induction design. Focusing on the second intake cycle, it is clear that all of the mass flow peaks are nearly at the same level, meaning that each cylinder experiences virtually the same peak mass flow rate. However, with respect to air induction performance, it is more important to solve for the total amount of air entering each cylinder per intake cycle.

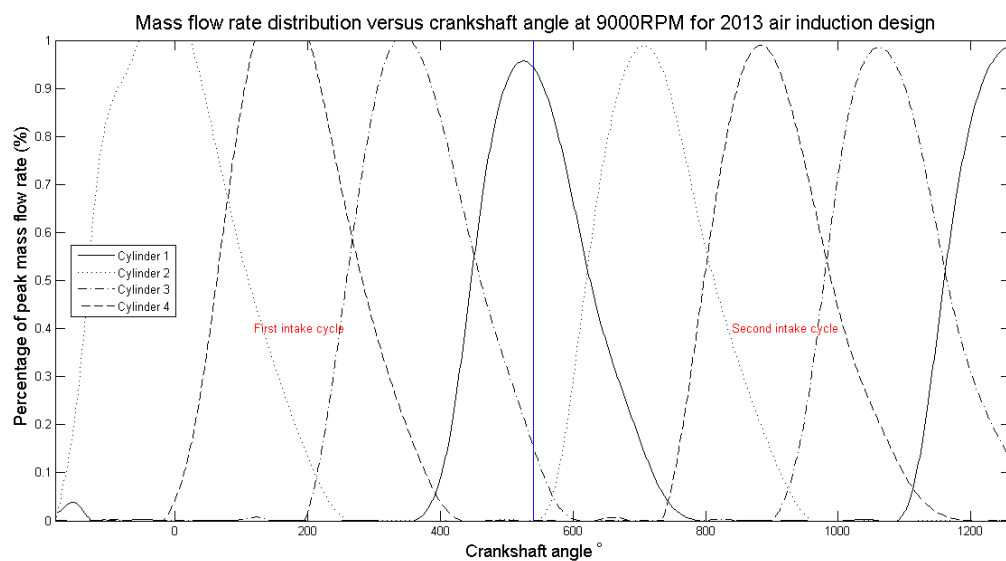


Figure 46: Mass flow rate distribution versus crankshaft angle for 2013 air induction design

Using the mass flow rate distribution figure above, the mass accumulation as a percentage of total mass flow during one intake cycle can be evaluated at each cylinder. For the 2013 air induction design at an engine speed of 9000RPM, cylinder 1 accumulated 24.4%; cylinder 2 accumulated 26.3%; cylinder 3 accumulated 26.6%; and cylinder 4 accumulated 22.6% of the mass over one cycle. Therefore, even though the peaks on the mass flow rate distribution aligned nearly perfectly, the area under the

curves were not equivalent, as there was a significant difference in the amount of total mass accumulation between different cylinders.

Figure 47 shows the mass flow distribution for the 2014 asymmetric air induction design. Focusing on the second intake cycle, it is clear that there are some discrepancies in mass flow peaks, specifically between the outer (1 and 4) and inner (2 and 3) cylinders; this means that each cylinder pair experiences slightly different peak mass flow rates.

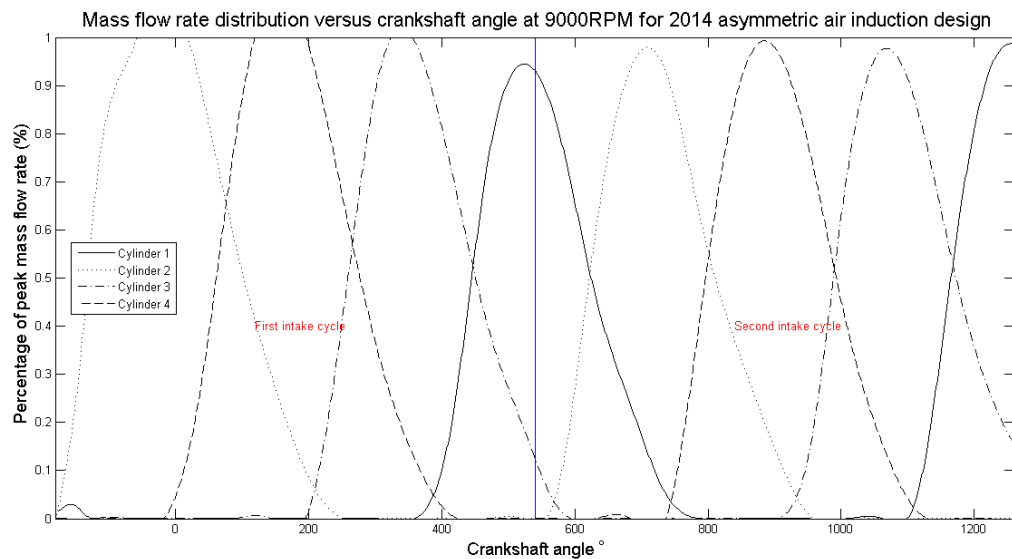


Figure 47: Mass flow rate distribution versus crankshaft angle for 2014 asymmetric air induction design

Using the mass flow rate distribution figure above, the mass accumulation as a percentage of total mass flow during one intake cycle can be evaluated at each cylinder. For the 2014 asymmetric air induction design at an engine speed of 9000RPM, cylinder 1 accumulated 24.3%; cylinder 2 accumulated 25.2%; cylinder 3 accumulated 25.3%; and cylinder 4 accumulated 25.2% of the mass over one cycle. Therefore, even though the

peaks on the mass flow rate distribution are misaligned between groups of cylinders, the area under the curves are nearly equivalent with an almost equal distribution of mass accumulation amongst all four cylinders.

Figure 48 shows the mass flow distribution for the 2014 symmetric air induction design. Focusing on the second intake cycle, it is clear that the peaks are nearly identical, meaning that the peak mass flow rates are evenly distributed amongst the four cylinders.

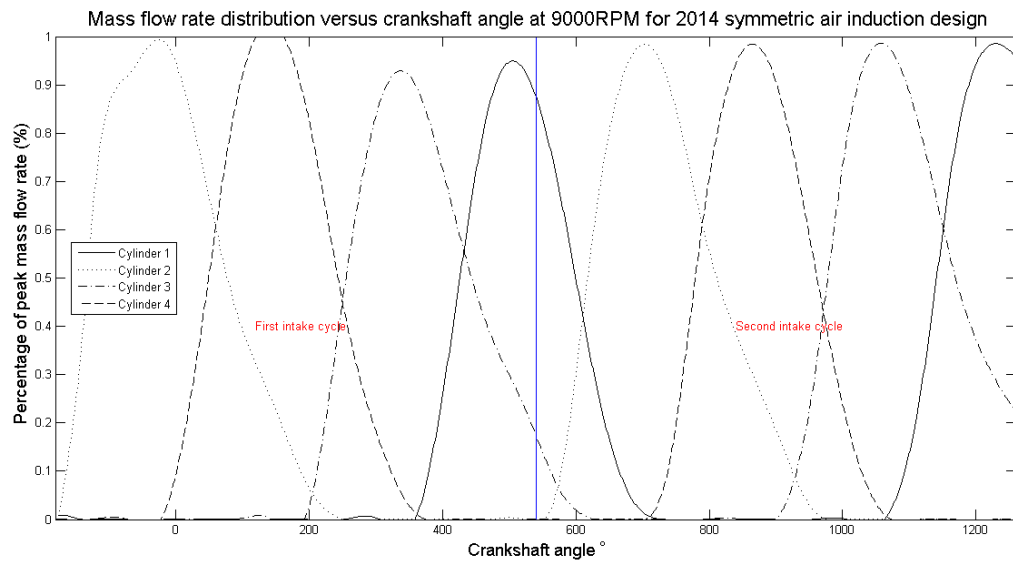


Figure 48: Mass flow rate distribution versus crankshaft angle for 2014 symmetric air induction design

Using the mass flow rate distribution figure above, the mass accumulation as a percentage of total mass flow during one intake cycle can be evaluated at each cylinder. For the 2014 asymmetric air induction design at an engine speed of 9000RPM, cylinder 1 accumulated 24.1%; cylinder 2 accumulated 25.9%; cylinder 3 accumulated 24.9%; and

cylinder 4 accumulated 25.0% of the mass over one cycle. According to these figures, both the peak mass flow rate distribution and mass accumulation per cylinder are nearly equivalent, which alludes to a high performing air induction system design. Table 5 below shows a compilation of the final results depicting the mass accumulation percentages per cylinder for the three air induction designs.

Table 5: Mass accumulation study summary at 9000RPM

Air Induction Design	Mass Accumulation Percentage			
	Cylinder 1	Cylinder 2	Cylinder 3	Cylinder 4
2013 Current	24.42%	26.34%	26.61%	22.62%
2014 Asymmetric	24.29%	25.22%	25.32%	25.17%
2014 Symmetric	24.12%	25.93%	24.93%	25.02%

It is important to take these peak mass flow rate distribution figures and the mass accumulation percentages per cylinder in light of the mass flow rate versus crankshaft angle figure for the entire air induction system design. The mass flow rate analysis showed that the 2014 symmetric air induction design sustained a 19% greater mass flow rate compared to the 2013 design and a 16% greater mass flow rate compared to the 2014 asymmetric design. The results of the peak mass flow rate distribution and accumulation analysis showed that the 2014 symmetric design performed the best, with an almost equivalent peak mass flow rate distribution and total mass accumulation amongst the four cylinders during a single air intake cycle at 9000RPM. While the 2014 asymmetric air induction design proved to feature nearly equivalent mass accumulation

percentages amongst the four cylinders, the peak mass flow rate through the inner and outer cylinders varied, and the 2013 air induction design showed a large discrepancy in mass accumulation between the inner and outer cylinders.

However, it is also important to compare these mass flow rate values to those predicted by both the GT-Power analysis and theoretical analysis. As derived previously, using isentropic flow conditions and having fluid velocities at the throat equal to a Mach number of 1, the theoretical upper bound was determined to be 74.3g/s. This value represents perfect flow conditions, no viscous effects, maximum flow velocity through the throat, and does not include any geometric parameters; it is strictly simplified to a converging-diverging nozzle situation with steady, isentropic flow conditions and is, for all intents and purposes, an unattainable mass flow rate for this application. Then, through the GT-Power optimization process, the best combination given the limitations imposed by the constraints of the Formula-SAE vehicle yielded the 2014 symmetric, small plenum volume air induction design. The GT-Power analysis shows that the proposed 2014 design with parameters for the small volume intake plenum provides a peak mass flow rate of 54.7g/s at 9500RPM, as shown in Figure 49.

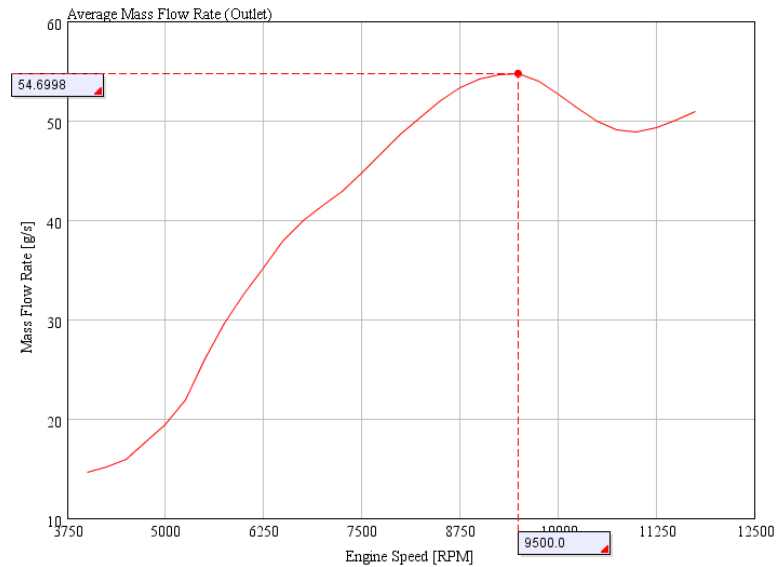


Figure 49: Average mass flow rate versus RPM for 2014 symmetric small plenum design

The GT-Power analysis shows that there is a 35.8% reduction in mass flow rate with the proposed 2014 symmetric design when compared with the theoretical mass flow rate upper bound. This seems to be reasonable since the theoretical calculation did not account for any geometric parameters and assumed perfect flow conditions. The GT-Power analysis, while maintaining a relatively high level of idealization of flow conditions, accounted for the highly unsteady flow environment imposed by the internal combustion engine through camshaft profiles, accounted for engine inefficiencies, and generally models the environment seen by the air induction system much more thoroughly. However, using the Mach number at the 20mm restrictor as seen in the GT-Power simulation (approximately $M=0.52$), Equation 3.1-2 was used to calculate the isentropic mass flow rate given the throat geometry. This ideal mass flow rate equates to

56.9g/s, which is much closer to the mass flow rate predicted to the GT-Power engine simulation; the engine simulation predicted a mass flow rate 3.9% less than the ideal converging-diverging nozzle calculation. However, it is also important to realize that the GT-Power model also has its limitations. While it does account for the unsteady fluid environment, GT-Power assumes a relatively ideal flow throughout the geometric lengths and volumes specified by the model. Pressure losses and viscous effects are kept to a prescribed minimum and the true movement of fluid through a CAD model is not captured accurately due to the two dimensional construction of the GT-Power model.

This is where the SolidWorks Flow Simulation software was able to capture the results of a designed air induction system to meet the functional specifications of the Formula-SAE competition and compare them to both the GT-Power engine simulation and the theoretical calculation for a converging-diverging nozzle. According to the CFD analysis, the mass flow rate at 9000RPM was shown to be approximately 44g/s. According to the GT-Power simulation, the mass flow rate through the 2014 symmetric design is 54.1g/s at 9000RPM, as shown in Figure 50 below, which is not equivalent to its peak mass flow rate stated earlier.

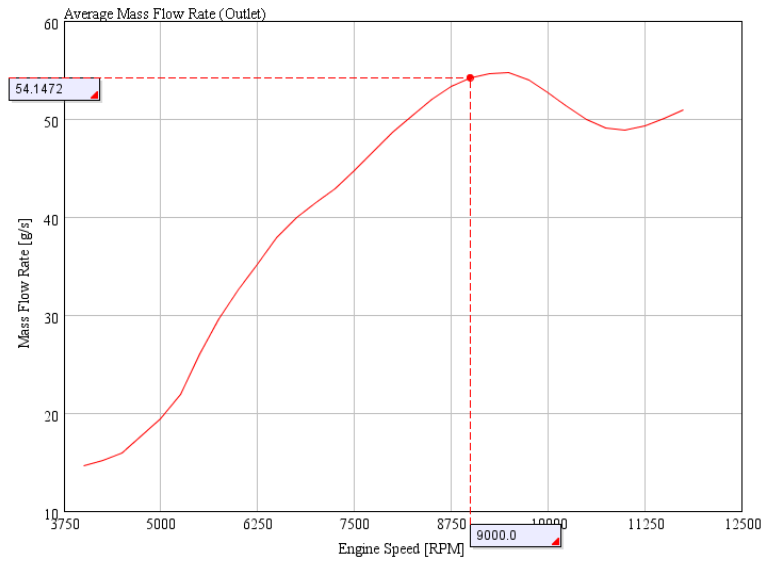


Figure 50: Mass flow rate versus engine speed for 2014 symmetric design

The SolidWorks Flow Simulation CFD analysis shows that the 2014 symmetric design is capable of sustaining a mass flow rate approximately 18.7% lower than the mass flow rate predicted by GT-Power simulation. Although this reduction is significant, there are multiple factors that can account for this discrepancy. One important aspect to keep in mind is the fact that the GT-Power engine simulation configuration does not contain any CAD model for the intake; it is strictly focused on fluid path dimensions rather than how these paths are configured. In other words, the GT-Power simulation assumes an ideal flow configuration, and even though transient fluid interactions are accounted for along with losses through the engine, the true motion of the fluid through the air induction system is not accounted for entirely. Also, another point of consideration is that the boundary conditions used for the SolidWorks Flow Simulation analysis may not be entirely accurate to what is seen on the vehicle.

Since the boundary conditions are pressure based, a small change in the transient pressure boundary conditions would significantly affect the mass flow rate throughout the entire air induction system. The pressure losses examined earlier also allude to the reality of the actual CAD geometry interacting with the internal fluid motion, and these losses contribute to the overall reduction in mass flow rate.

3.3.4 Transient internal flow visualization

A significant benefit to performing the internal flow CFD analysis is the ability to see how the fluid is moving throughout the air induction system given the set of boundary conditions described previously. This section is focused on showing the internal fluid motion through the three different CAD models, specifically focusing on the transition stages for insight as to why the 2014 symmetric design is able to sustain a 19% higher mass flow rate under the same set of boundary conditions. These images were taken at specific instances in time corresponding with a given crankshaft angle at an engine speed of 9000RPM. The focus of the discussion for each of the designs will be around the diffuser flow uniformity, the flow distribution throughout the plenum, and the full utilization of the air induction system volume.

The first CAD model examined is the 2013 design. Figures 51, 52, and 53 below depict three flow scenarios taken at distinct instances in time that provide insight as to the limitations and drawbacks to the 2013 design.

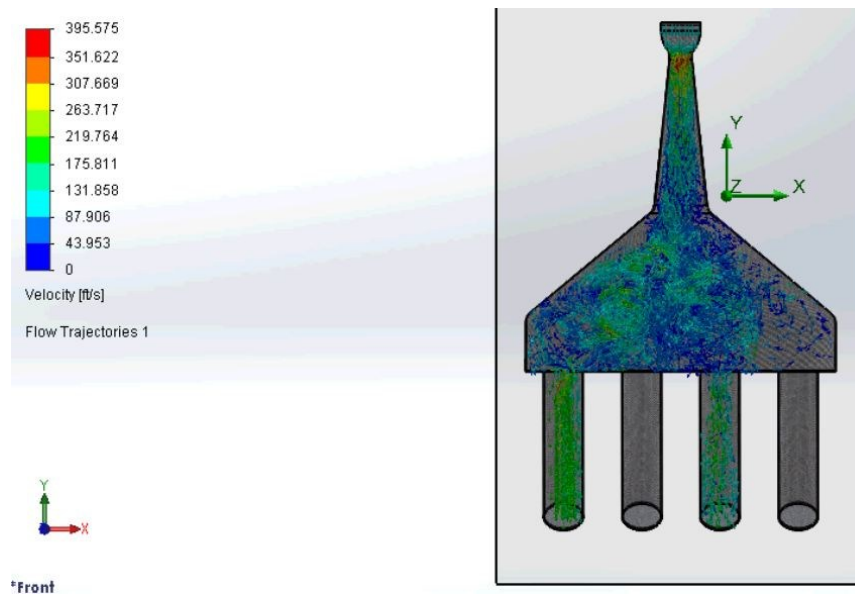


Figure 51: Velocity trajectory configuration. Notice the lack of full utilization of plenum volume, particularly at the sharp junction between the plenum and diffuser

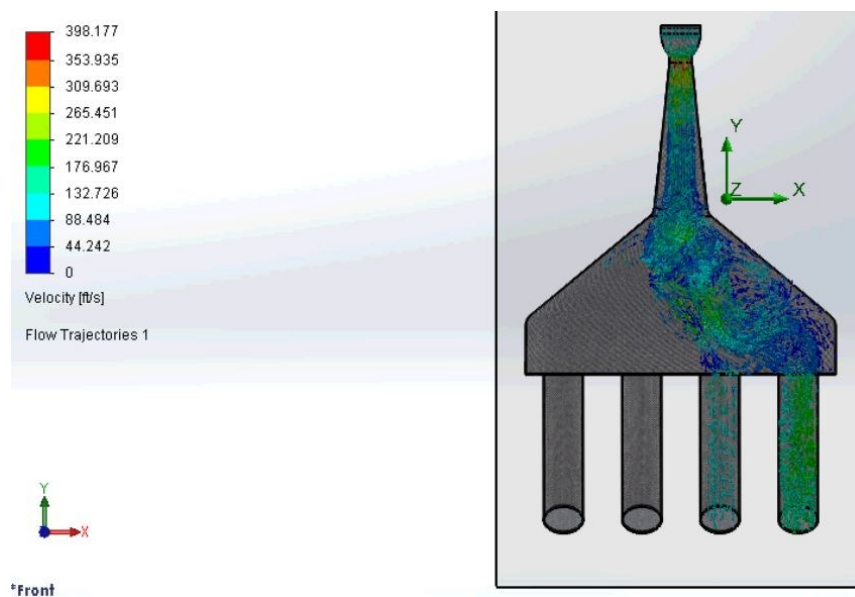


Figure 52: Velocity trajectory configuration. Notice the uneven flow distribution and swirling throughout the plenum

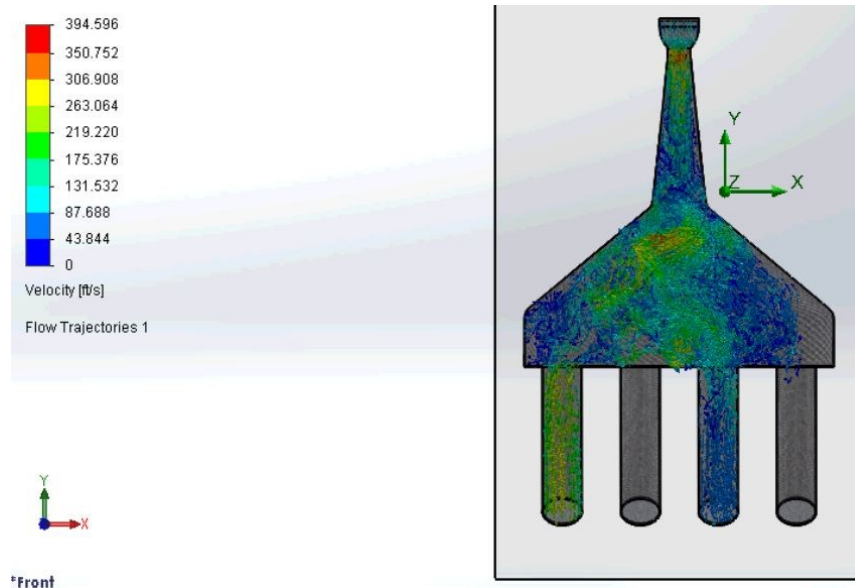


Figure 53: Velocity trajectory configuration. Notice the unevenness of flow throughout the diffuser

The three figures paint a relatively negative picture of the 2013 air induction design, with the worst aspect being the flow distribution and swirling effects in the plenum. While the 1.08L plenum featured in this design is meant to maintain fluid momentum while simultaneously ensuring some level of flow distribution amongst the four cylinders, it is clear that there is a significant amount of swirling and an uneven velocity distribution throughout the plenum. Although there are not significant total pressure losses throughout the air induction system, this unevenness hinders mass flow throughout the entire system; this can be inferred by the velocity values seen at the 20mm restrictor, which is around 385ft/s, corresponding with an average Mach number of approximately 0.34. For reference, the targeted average Mach number according to

the GT-Power analysis is around 0.5. The lower flow velocity through the restrictor indicates that the mass flow rate is limited and not entirely maximized, which has been shown numerically and can be seen through the figures above.

The second CAD model examined is the 2014 asymmetric design featuring the large plenum. Figures 54, 55, and 56 below depict three flow scenarios taken at distinct instances in time that provide insight as to the limitations and drawbacks to the 2014 asymmetric design.

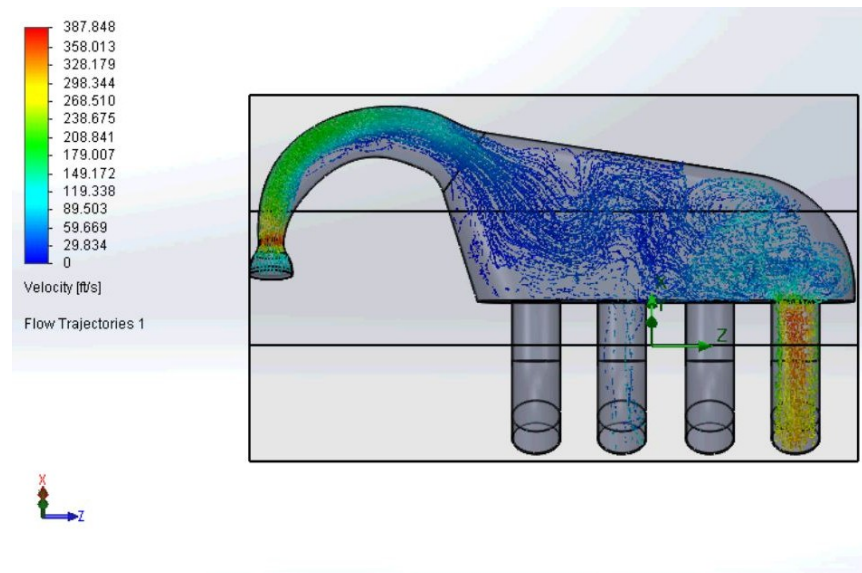


Figure 54: Velocity trajectory configuration. Notice that the air induction volume is used for evenly distributing the air flow amongst the runner inlets while being able to supply the necessary runners when needed

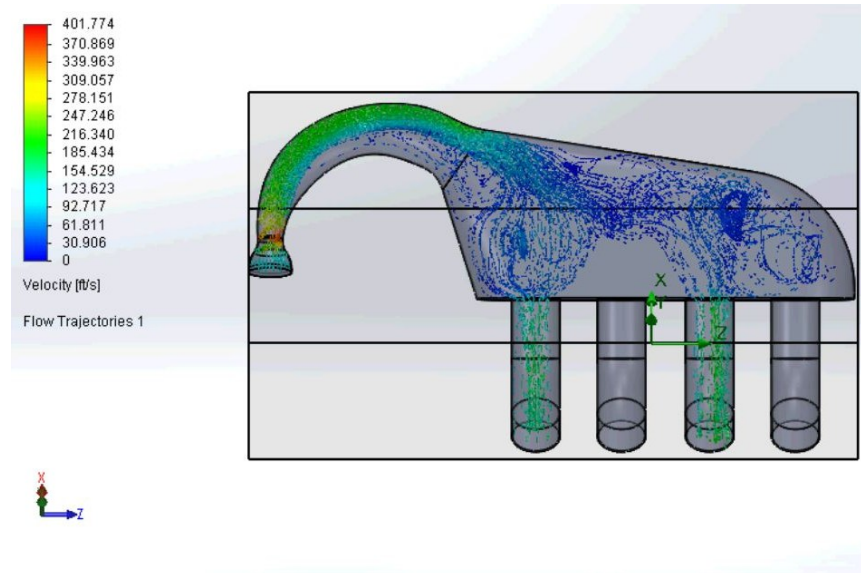


Figure 55: Velocity trajectory configuration. Notice the excessive swirling of the air flow throughout the plenum

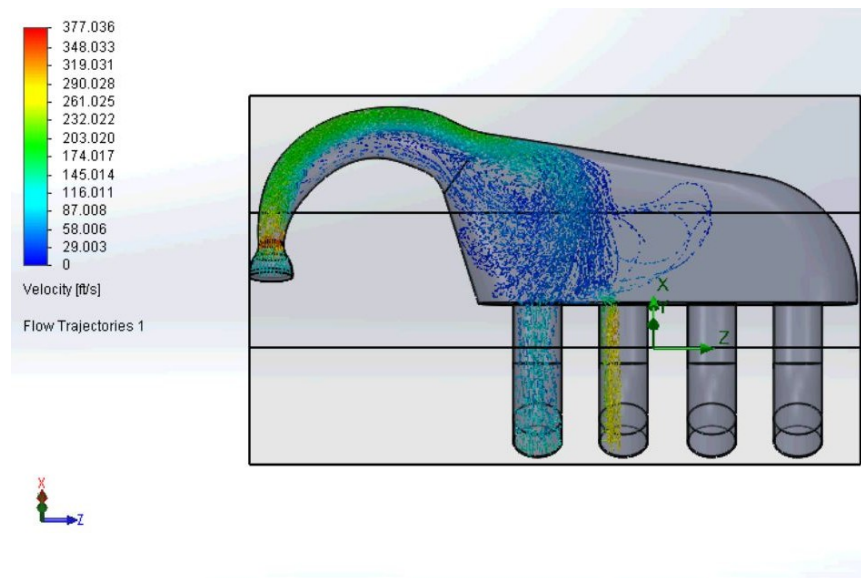


Figure 56: Velocity trajectory configuration. Notice the highly uneven flow distribution through the diffuser as it pushes towards the outer wall, and even has a small amount of back-flow from the plenum

It is clear from the flow trajectories shown in the three figures above that having an asymmetric design, especially with a curved diffuser, is not an effective design for

evenly distributing flow. While the 2.17L plenum does have the benefit of effectively using the air induction volume and enables the flow to be evenly distributed to the necessary runners, it is clear that there still exists an excessive amount of swirling in the plenum. The worst attribute to this design centers around the diffuser design. Although the length of the diffuser is the same length that the GT-Power analysis suggested, the fact that it is curved hinders the mass flow through the entire air induction system. When examining the flow distribution around the exit of diffuser into the plenum, it is clear that the flow is shoved towards the outer wall of the diffuser and maintains its velocity until exiting into the plenum instead of transitioning evenly to a lower velocity inside the diffuser. Also, there appears to be a small, but not insignificant, amount of back flow from the plenum into the diffuser towards the inner wall. Although this design features the smallest total pressure losses throughout the air induction system, this flow unevenness in the diffuser hinders the mass flow rate throughout the entire system; this can be inferred by the velocity values seen at the 20mm restrictor, which is around 400ft/s, corresponding with an average Mach number of approximately 0.36. For reference, the targeted average Mach number according to the GT-Power analysis is around 0.5. The lower flow velocity through the restrictor indicates that the mass flow rate is limited and not entirely maximized, although it is better than the 2013 air induction design; this statement has been shown numerically through the CFD analysis and can be seen through the figures above.

The last CAD model examined is the 2014 symmetric design featuring the small plenum. Figures 57, 58, and 59 below depict three flow scenarios taken at distinct instances in time that provide insight as to why the 2014 symmetric design significantly outperforms the other air induction designs.

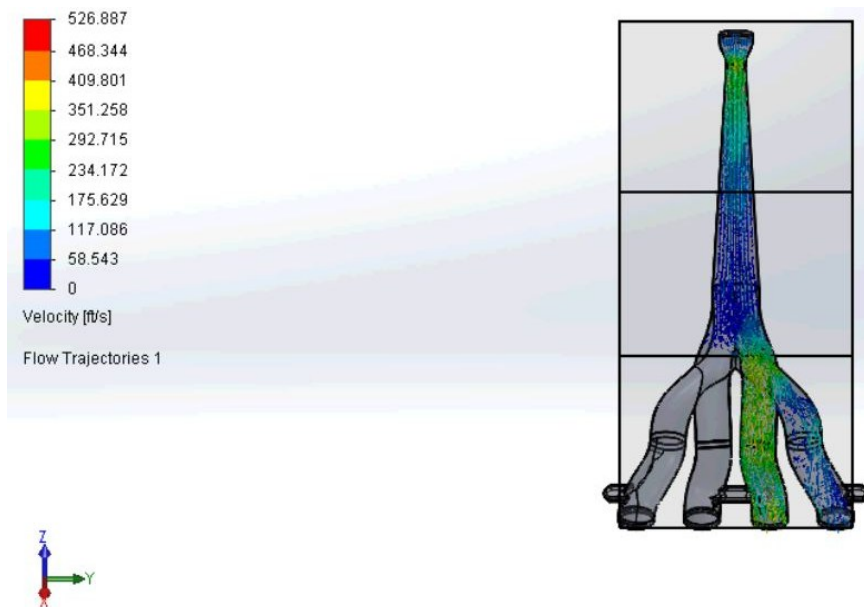


Figure 57: Velocity trajectory configuration. Notice the even flow distribution in the diffuser

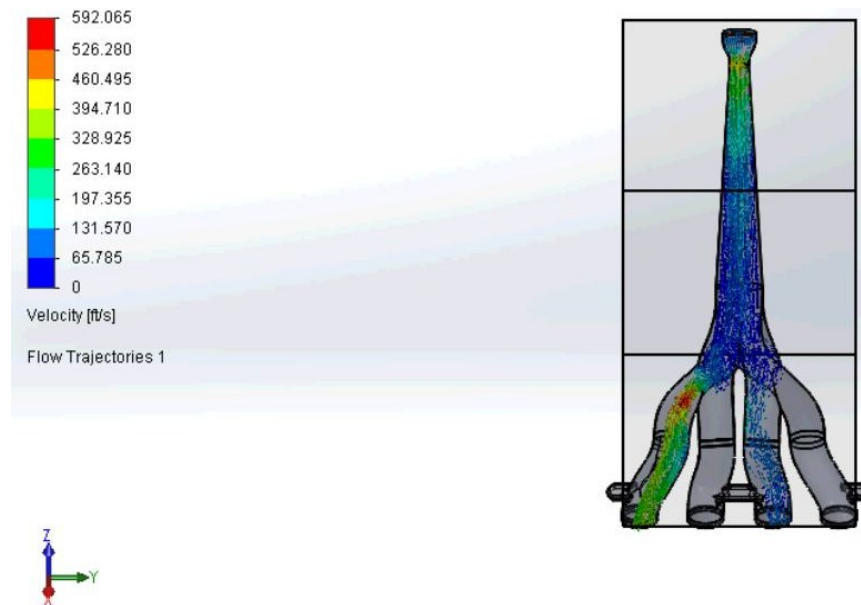


Figure 58: Velocity trajectory configuration. Notice how the plenum is completely filled and is able to efficiently distribute the flow to the necessary runners

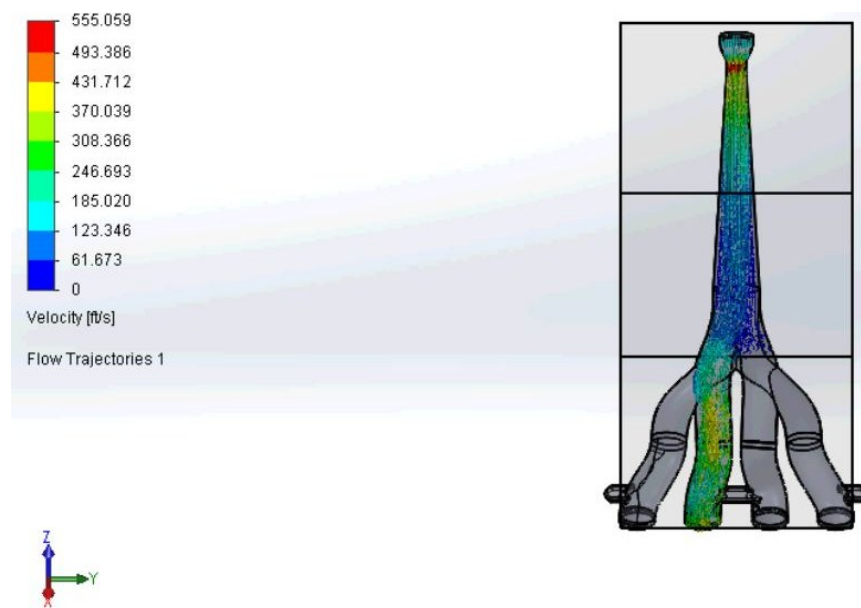


Figure 59: Velocity trajectory configuration. Notice how the fluid velocity is maintained throughout the entire air induction system

It is clear from the flow trajectories shown in the three figures above that having a symmetric design is highly beneficial to maintaining even flow distribution to all four cylinders. The 0.54L plenum effectively maintains flow uniformity while also keeping the design goal of preserving fluid momentum throughout the entire air induction system. There is minimal swirling observed in the flow visualization figures, and the entire air induction system volume is utilized throughout the intake cycle. Because of the small plenum volume, the system is able to respond to the time-varying boundary condition with minimal flow resistance because of the streamlined and direct design.

Although this design features the largest total pressure drop throughout the air induction system due to the elevated velocities, the overall design is able to sustain a much larger mass flow rate; this can be inferred by the velocity values seen at the 20mm restrictor, which is around 555ft/s, corresponding with an average Mach number of approximately 0.49. According to the GT-Power analysis for the 2014 symmetric design, the average Mach number of the fluid passing through the restrictor at 9000RPM is 0.508665 with a maximum average Mach number equal to approximately 0.52, as is shown in Figure 60 below.

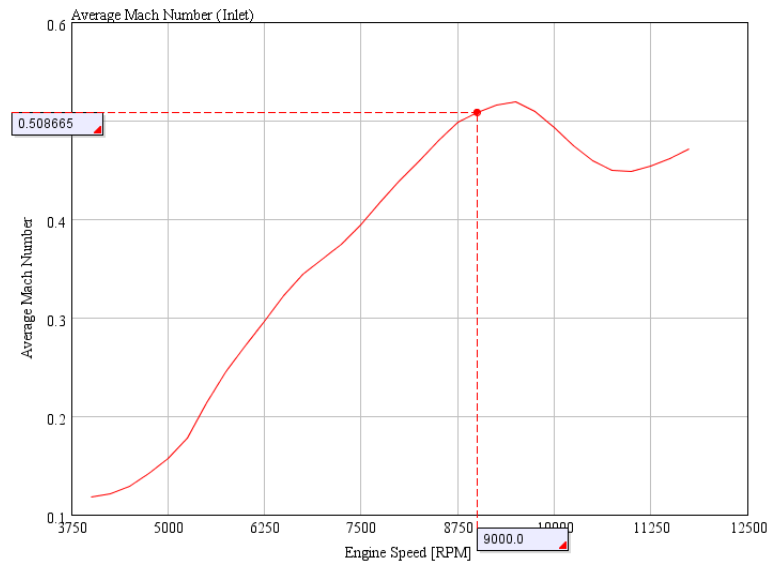


Figure 60: Average Mach number versus engine speed flowing through the restrictor for the 2014 symmetric design

The average Mach number of the flow moving through the restrictor shown in the CFD analysis is 3.0% less than the GT-Power simulation prediction, which means that the 2014 symmetric air induction design almost matches the idealized engine simulation model. However, this small discrepancy accounts for a significant reduction in mass flow rate discussed previously; nevertheless, the 2014 symmetric small plenum volume air induction design clearly outperforms the other air induction designs.

3.4 Prototype development and experimental testing

The final method of analyzing and validating the air induction design is to build a prototype and test it on an engine dynamometer under true race conditions on the Honda CBR600 F4i internal combustion engine. Since the 2014 symmetric design was determined to be the best overall design between the 2014 asymmetric system and the

2013 system, the prototype was constructed based on the SolidWorks CAD model of the 2014 symmetric design. Figure 61 below shows the SolidWorks model for the final air induction prototype.

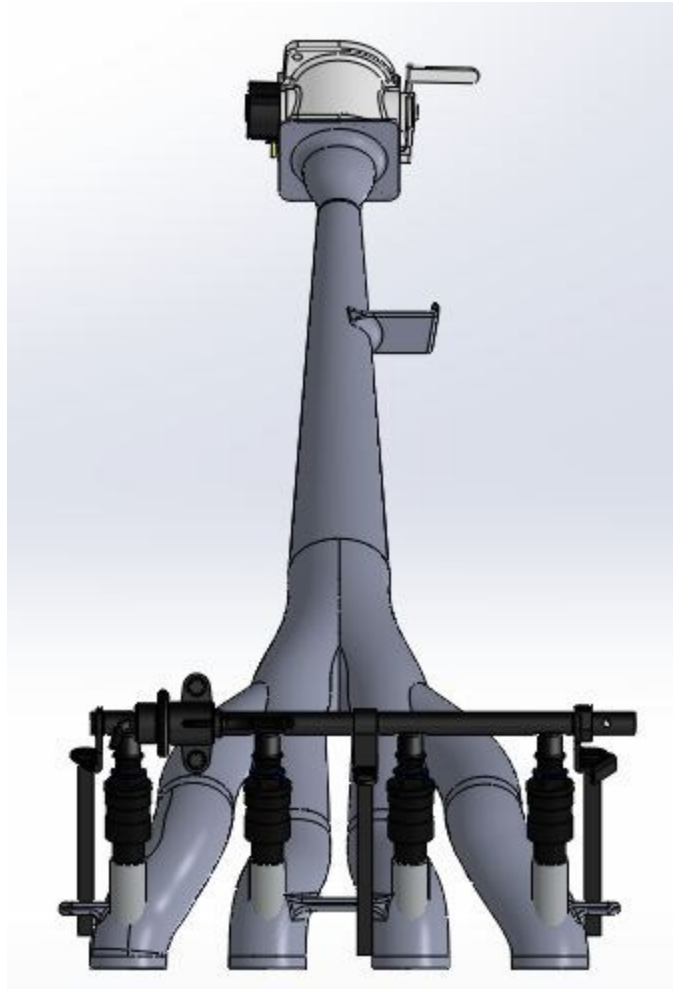


Figure 61: SolidWorks CAD model of 2014 symmetric air induction design

Because of the intricate plenum and runner geometries, typical manufacturing methods were not feasible; instead, the air induction design was segmented into two separate halves and then 3D printed to be assembled afterwards. The model was printed

using ABS plastic in order to maintain structural rigidity while addressing the elevated ambient temperatures from the internal combustion engine. Figure 62 below shows the two rapid prototyped halves.



Figure 62: 3D printed halves of the 2014 air induction design

The two halves were then assembled, and a thin coat of epoxy was applied to the outer surface to ensure structural integrity as well seal the slightly porous layers of ABS plastic. Figure 63 below shows the two halves assembled and lightly sanded, and Figure 64 shows the epoxy coating applied on the top surface.



Figure 63: Assembled halves of 2014 air induction design prototype



Figure 64: Epoxy coating applied to 2014 air induction design prototype

The final design prototype had short steel sleeves installed on the outer surface of the runner outlets to provide structural strength when physically attaching the air induction system to the cylinder head using clamps. The final 2014 symmetric prototype is shown below in Figure 65.



Figure 65: Final prototype of 2014 symmetric air induction system

In order to test the conclusions developed by the GT-Power engine simulations and SolidWorks Flow Simulation CFD analysis, the air induction prototype was tested using an engine dynamometer developed in-house for testing and tuning of the Duke Motorsports Formula SAE competition car. Figure 66 shows the engine dynamometer, which uses an inertial mass system for its derivation of torque and power versus engine speed.



Figure 66: Engine dynamometer used for testing and tuning of powertrain components

In order to compare the performance of the 2014 air induction design, a baseline test for the 2013 design is necessary. Five separate dynamometer sessions were used to document the 2013 air induction design's performance. Figure 67 shows the power versus engine speed plot for all runs of the 2013 air induction design. See Figure 89 in Appendix A for the torque versus engine speed plot for all runs.

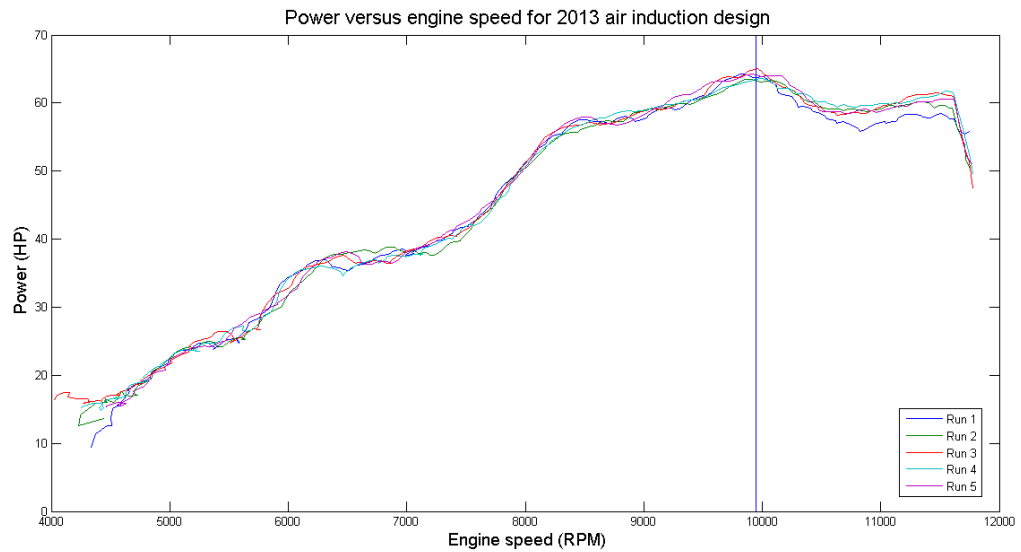


Figure 67: Power versus engine speed dynamometer results for 2013 air induction design

As you can see from the different dynamometer sessions, there are small fluctuations in power and torque values at specific engine speeds; however, the general trend and shape of the curves is nearly identical between separate runs. One potential cause for these small fluctuations, besides being within the noise of the data acquisition system, concerns the specific engine tune at these engine speed values allowing for small fluctuations in performance output to occur. Another important note to make is that the values for the power and torque output are uncorrected values; the dynamometer sessions represent completely raw data using the inertial mass system and do not provide any type of data correction for atmospheric conditions, such as temperature and pressure.

The dynamometer results indicate that the peak horsepower seen by the 2013 air induction system is approximately 64.3HP, which is close to the predicted 68.99HP by the GT-Power engine simulation. Also, there is clearly a peak in power generation shown in the dynamometer data at an engine speed of approximately 9900RPM. While this is 900RPM higher than the GT-Power predicted 9000RPM engine speed for peak power generation, it is clear that the general trend of rapid ramp up to peak power and slowly receding away is present in both the engine simulation and dynamometer data.

The 2014 air induction design prototype was tested on the engine dynamometer using the same engine tuning parameters and is shown installed on the Honda CBR600 F4i in Figure 68 below.



Figure 68: 2014 final intake design installed on engine dynamometer

Using the same parameters to test the 2013 air induction design, the 2014 air induction design was tested during two dynamometer sessions. Figure 69 shows the power versus engine speed curve for the 2014 design for all dynamometer sessions, and Figure 90 in Appendix A shows the torque versus engine speed figure for all sessions.

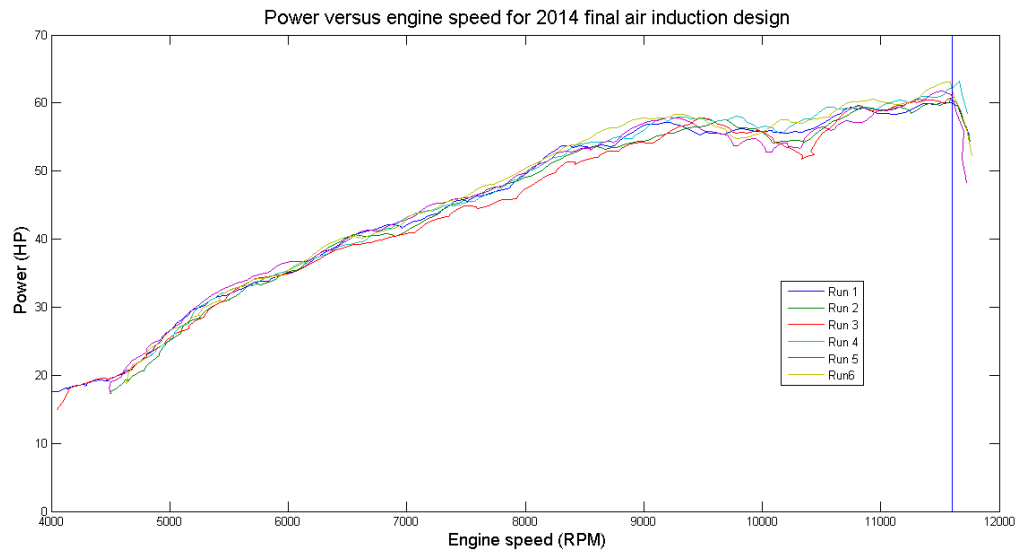


Figure 69: Power versus engine speed dynamometer results for 2014 air induction design

As with the dynamometer testing for the 2013 air induction system, there exist small fluctuations in the curves between runs for both the power and torque figures; however, the general trends remain the same between the runs, and there is a clearly defined behavior in both engine performance parameters versus engine speed. The dynamometer data indicates a peak power generation of 63.6HP at approximately 11500RPM, whereas the GT-Power simulation predicted 72.3HP at 9500RPM. It is clear that the engine speed that this peak power occurs experimentally has shifted in the same direction that was shown using GT-Power, but it is nearly 2000RPM higher than what was predicted by GT-Power. There is also a large discrepancy between the experimental peak power and the predicted peak power. While the peak power output for both the 2013 and 2014 designs are nearly identical at approximately 64HP, GT-Power engine

simulations predicted that the 2014 air induction design would produce 4.75% more peak power than the 2013 design. Figure 70 shows a plot comparing representative power versus engine speed figures for the 2013 and 2014 air induction designs; see Figure 91 in Appendix A for the torque versus engine speed comparison plot.

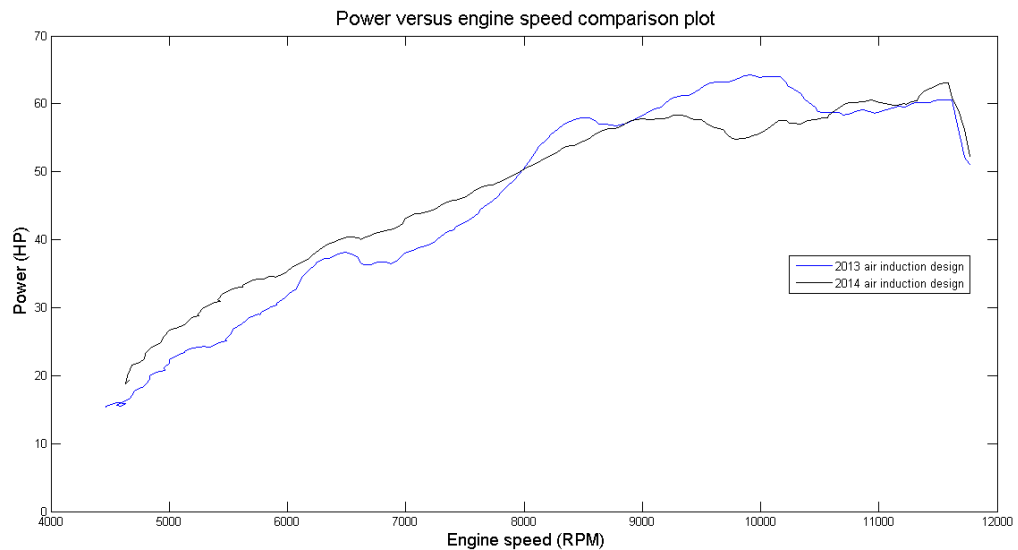


Figure 70: Power versus engine speed dynamometer results comparison for the 2013 and 2014 air induction designs

The comparison plot between the 2013 and 2014 air induction designs clearly shows that the 2014 air induction system has a power versus engine speed curve that is shifted towards the upper engine speed range compared to the 2013 design. As stated previously, the peak power output figures are nearly identical at approximately 64HP, but the engine speed that this power occurs at is separated by 1600RPM between the two designs. However, the general trends predicted by the engine simulation results hold true; the 2013 design peaks in power at an earlier engine speed and then slowly recedes

in power generation, whereas the 2014 design peaks in power at a later engine speed, continuing through the upper end of the engine speed range. Whereas the 2013 design has an effective ramping up and down to power, the 2014 air induction design builds power linearly with respect to engine speed throughout most of the powerband. The 2014 design also produces more power at lower engine speeds compared to the 2013 design; however, if the engine speed range surrounding the peak power output for the 2013 design is inspected (approximately 9900RPM), the 2014 design drastically decreases in power output. This trend was not predicted in GT-Power, and after closely examining the behavior of the engine characteristics, it was noted in the experimental procedure that the air/fuel ratio throughout this engine speed range measured too rich, meaning too much fuel was present during combustion.

At this point in the experimental analysis, it is important to note that the engine tune uploaded onto the engine control unit reflected a tune that was developed and optimized by the Duke Motorsports FSAE team specifically for the 2013 vehicle configuration, which featured the 2013 air induction design. This tune was also used for testing the 2014 air induction design; because of this, the true values and even some of the trends do not necessarily reflect what the 2014 design is capable of outputting. After examining the tune, it is clear to see that the 2013 design has a peak in power output at 9900RPM, which corresponds with an increase in fuel input in order to maintain this power. However, this same fuel input was used in testing the 2014 design, which caused

the air/fuel ratio to measure rich since there is not a peak in power output at this engine speed, therefore causing a drastic decrease in power output.

In order to fairly test the two air induction designs against one another, slight modifications to the engine tune on the engine control unit were made. Specifically, the fuel injector open time in milliseconds, which corresponds with the amount of fuel injected per intake cycle, was altered in order to adjust the air/fuel ratio for a more optimum value for power output; this exact procedure was conducted in the development of the 2013 engine tune featuring the 2013 air induction design. Figure 71 shows the power versus engine speed for the 2014 air induction design featuring two runs on the base tune, two runs on a first iteration tune, and two final runs on a second iteration tune; see Figure 92 in Appendix A for the torque versus engine speed tuning figures.

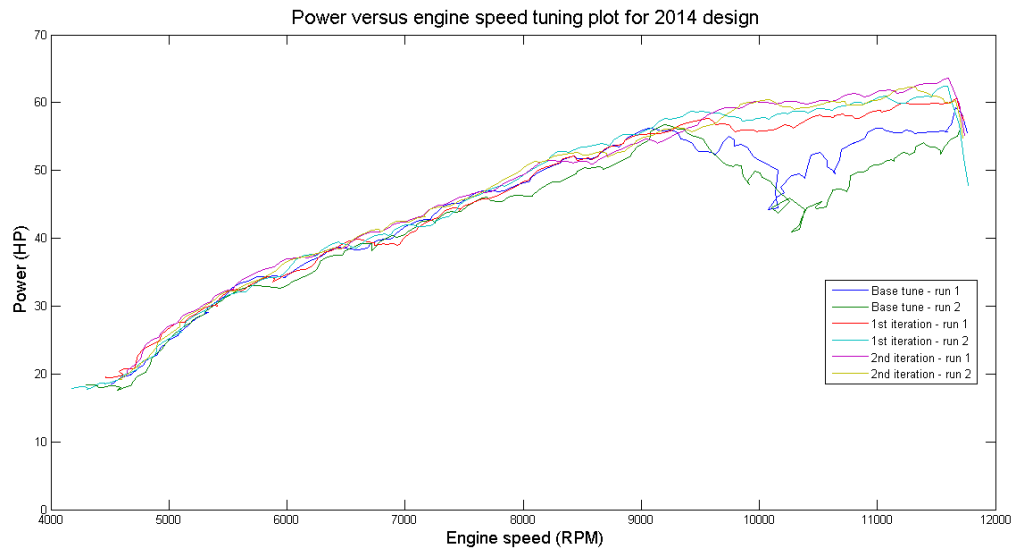


Figure 71: Power versus engine speed dynamometer testing for the 2014 design featuring different ECU tuning

According to the power and torque figures, the tuning conducted for the 2014 air induction design effectively mitigated the drastic decrease in power seen around 9900RPM. Both the power and torque curves reflected this performance benefit at higher engine speed values through redline. Figure 72 shows the drastic change in power output versus engine speed between the initial and final tune on the 2014 design; see Figure 93 in Appendix A for the torque versus engine speed plot.

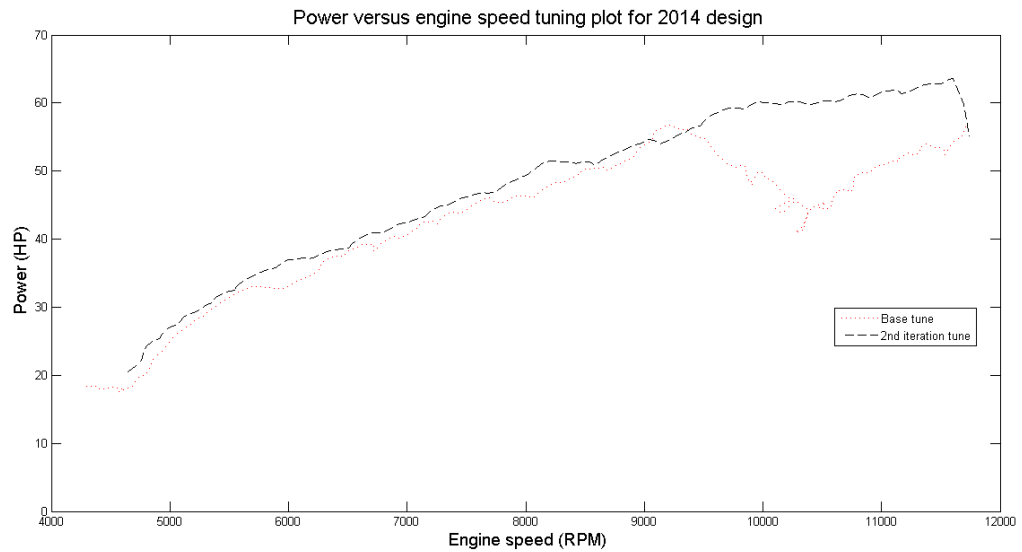


Figure 72: Power versus engine speed for the 2014 design documenting the effect of engine tuning

For a more accurate representation of the trends in performance between the 2013 and 2014 designs, it is necessary to compare the tuned 2014 setup with the 2013 design. Figure 73 compares the experimental power versus engine speed results for the 2013 air induction design and the tuned 2014 air induction design, and Figure 74 compares the experimental torque versus engine speed results for the 2013 and tuned 2014 designs.

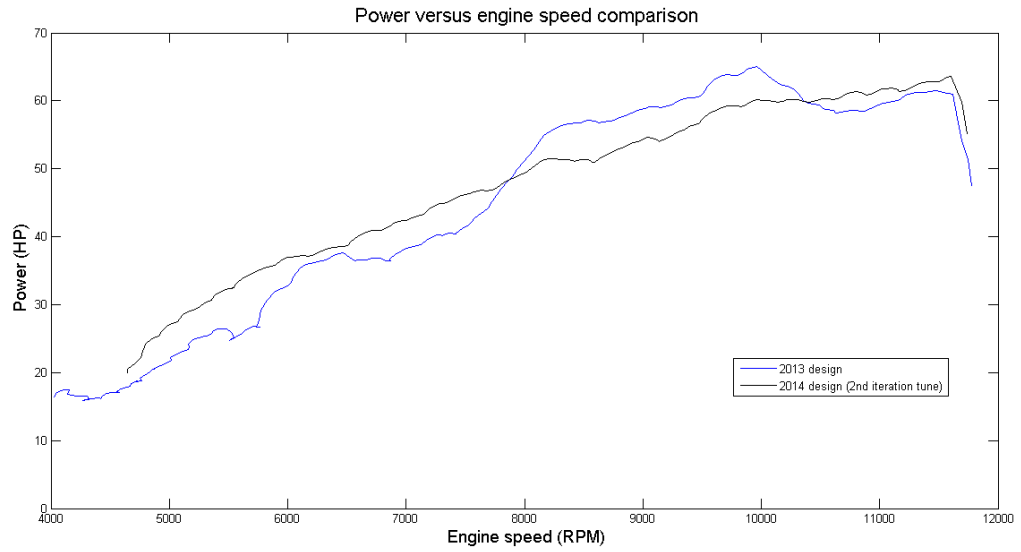


Figure 73: Power versus engine speed dynamometer results comparison for the 2013 and tuned 2014 air induction designs

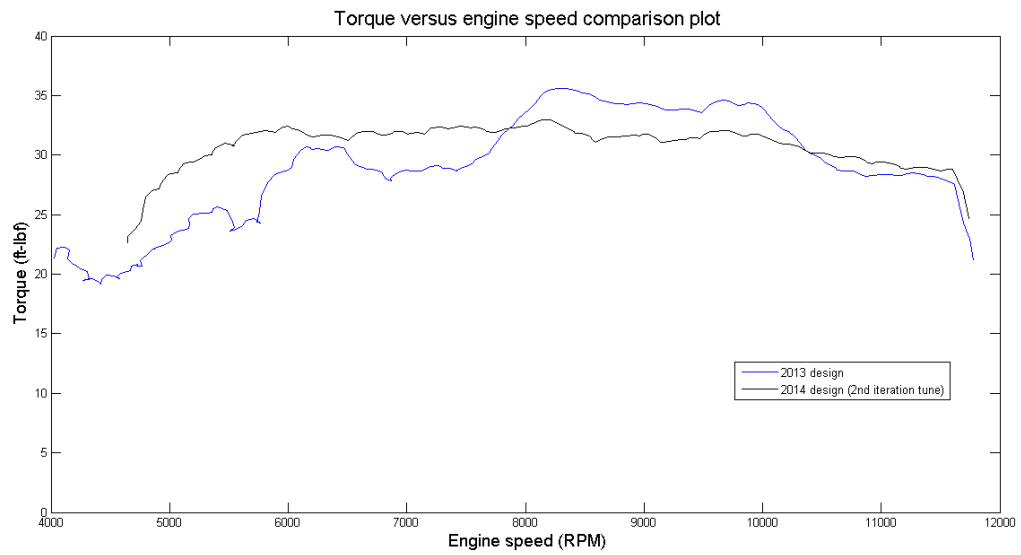


Figure 74: Torque versus engine speed dynamometer results comparison for the 2013 and tuned 2014 air induction designs

The comparison plot between the 2013 and tuned 2014 air induction designs shows that the peak output values have not changed; the 2013 design produces 64.3HP at 9900RPM and 36ft-lb at 8300RPM, and the 2014 tuned design produces 64.0HP at 11000RPM and 33ft-lb at 8100RPM. However, the biggest change is that the 2014 design now does not decrease in power throughout the entire operating engine speed range; the 2014 design allows for linear power generation with respect to engine speed, which also emerges as a flat torque curve seen in Figure 74. While the output figures and corresponding engine speed values do not align with those predicted by the GT-Power engine simulations, the trends developed through the simulations can be seen through the experimental data. Also, while the peak values for power and torque output do not distinguish the 2014 design from the 2013 design, there are other parameters that are interesting to compare.

In racing applications, it is sometimes considered more important to have a larger average performance characteristic than strictly a large peak performance figure. This assertion depends on the type of racing application, but for road course and autocross racing, the vehicle is performing at a wide range of engine speeds and therefore needs more focus on a greater overall performance. For the Formula SAE competition, there is a strong focus for autocross racing performance, and Figure 75 shows an engine speed histogram throughout the course of one racing event at a previous competition. This histogram shows that, while there is a small range of engine

speeds that the majority of the race is spent at, there is a need for the engine to perform throughout virtually the entire engine speed range, heavily focused on the 6000-11000RPM range.

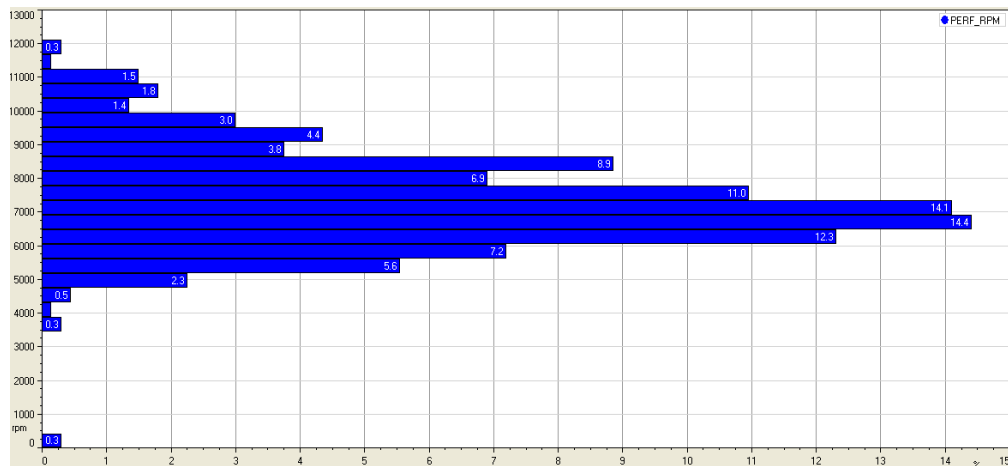


Figure 75: Engine speed histogram for a competition autocross event

After looking at the engine speed histogram, it is clear that there needs to be a balance between peak performance and average performance over a large range of engine speeds. The 2013 air induction design features an average power output of 44.5HP and an average torque output of 28.8ft-lb throughout the entire engine speed range; the 2014 air induction design features an average power output of 47.9HP and an average torque output of 30.7ft-lb throughout the entire engine speed range, representing a 7.6% increase in average power and a 6.6% increase in average torque. While the peak performance figures showed that the 2013 design produced slightly higher power and torque numbers, the average performance figures clearly demonstrate

that the 2014 design outperforms the 2013 design throughout the entire engine speed range.

Due to the fact that the peak power and torque output numbers are close in magnitude between the 2013 design and the 2014 design, an easy way of visualizing the breadth of the powerband is to compare the normalized performance characteristics of each air induction design. Figure 76 shows the normalized power versus engine speed curves for the 2013 and 2014 air induction designs, and Figure 77 shows the normalized torque versus engine speed curves.

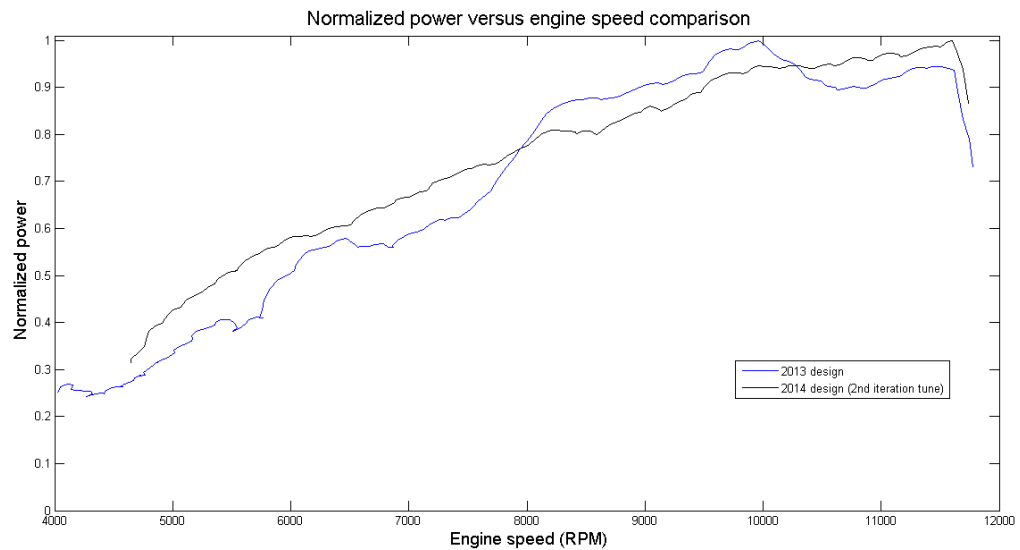


Figure 76: Normalized power versus engine speed dynamometer results

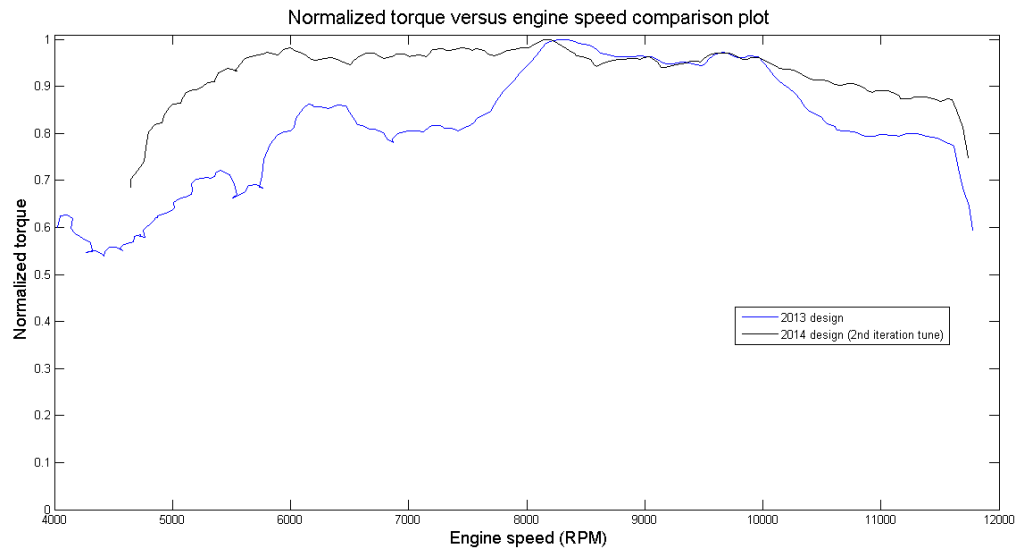


Figure 77: Normalized torque versus engine speed dynamometer results

While the shape of both the raw data and normalized performance curves are identical, it is beneficial to normalize the curves based on the peak power and torque output in order to have a plot showing the percentage of maximum power and torque generation versus engine speed. This allows for an understanding of not only the trends in power and torque generation, but also an understanding of the ability for the design to supply the engine with a broad powerband for the specific racing application. Beginning with the 2013 air induction design, the power versus engine speed plot shows that the 2013 design is capable of sustaining 95% of the engine's peak power output (sustaining 61HP) for approximately 14% of the total engine speed range, and 95% of the engine's peak torque output (sustaining 34ft-lb) for approximately 20% of the total engine speed range. The 2014 air induction is capable of sustaining 95% of the engine's peak power output (sustaining 60.4HP) for approximately 19.5% of the total engine

speed range, and 95% of the engine's peak torque output (sustaining 31.3ft-lb) for approximately 63% of the total engine speed range. Furthermore, these results can be expanded for sustaining 90% of peak power and torque; the 2013 design sustains 90% peak power (57.9HP) for 36.6% of the total engine speed range, and 90% peak torque (32.4ft-lb) for 31.5% of the total engine speed range, whereas the 2014 design sustains 90% peak power (57.2HP) for 30.9% of the total engine speed range, and 90% peak torque (29.7ft-lb) for 81.5% of the total engine speed range. This analysis shows that the 2014 air induction design is capable of providing the broadest powerband, which equates to sustaining 95% of peak torque output for more than 3000RPM longer than the 2013 design.

Overall, the experimental tests conducted on the engine dynamometer validated the general trends of power and torque generation versus engine speed for both the 2013 and 2014 symmetric air induction designs, especially with the normalized comparison curves. However, there is a need to understand why there exists such a large discrepancy between the predicted power and torque values for the GT-Power engine simulation and the dynamometer experimental sessions for the 2014 air induction design. Further investigation is needed to determine the cause of the inconsistency and to see if the predicted mass flow rates and performance characteristic figures are, in fact realistic expectations, or if there is a limitation to the 2014 air induction design that was overlooked in its development.

4. Conclusion

The goal of this investigation was to define the most dominant parameters in an air induction system for a restricted, internal combustion race engine in order to maximize power output, and then to design an air induction system that would comply with the Formula SAE rules for application to the Duke University Motorsports Formula SAE competition car. Using theoretical calculations, GT-Power engine simulations with varying parameters, SolidWorks CAD modeling program and Flow Simulation CFD software, and finally engine dynamometer experimental testing, a final air induction design was established and verified. The final design features a predicted 19% increase in maximum sustained mass flow rate that is evenly distributed across all four cylinders, a predicted 4.8% increase in peak horsepower, and perhaps the most important factor being that the air induction system is able to broaden the overall powerband by sustaining 95% of the peak torque output for 1000RPMs longer than the 2013 air induction design. The final 2014 air induction design was built and tested using an engine dynamometer against the 2013 air induction design. The experimental results validated the performance trends predicted by the GT-Power engine simulations. The peak values recorded for power and torque versus engine speed did not indicate any increase for the 2014 air induction system compared to the 2013 air induction design; the peak power and torque figures remained virtually the same between the two designs. However, the experimental data indicated that the 2014 air induction design featured a

flat torque curve capable of sustaining 95% of peak torque for 63% of the total engine speed range, equating to having a 3000RPM broader powerband than the 2013 design. This also corresponded with the 2014 design featuring a linear power generation curve versus engine speed that continually developed power until redline, sustaining an increase of 7.6% for average power generation over the engine speed range compared to the 2013 design.

While there still is a need for engine tune refinement, the normalized experimental results attempted to mitigate any experimental inconsistencies between dynamometer sessions to provide a more equalized comparison. These results converge on an overarching conclusion that an air induction system for restricted race engines does not benefit from having a “plenum volume”; in other words, air induction designs should be focused on maintaining fluid momentum throughout its internal geometry rather than trying to place a large plenum volume in series with the restrictor and the runners to return the flow to a pressure close to atmospheric. This investigation sheds light onto a different realm of air induction design that is typically not considered, especially not with current Formula-SAE race design teams. Overall the combination of theory, computational engine simulation, computational fluid mechanics analysis, and experimental testing prove to be a strong and holistic investigation for shifting the design paradigm of an air induction system for restricted race engines.

5. Suggestions for future work

As with all research endeavors, future work is one of the most important aspects leading to the legacy left by the investigation. The GT-Power engine simulation is capable of running the engine simulation with full 3D models of the air induction system, internal combustion engine, and exhaust system, which would allow for a much more comprehensive understanding and evaluation of the different designs. Using this simulation, a full optimization study could be performed with constraints applied to certain lengths and volumes in order to comply with the rules of the specific racing application. This approach would produce more accurate power versus engine speed and torque versus engine speed figures for comparison purposes, as well document a full optimization of the air induction internal geometry.

The same type of optimization could be applied using the SolidWorks Flow Simulation software using CFD analysis. The time varying boundary condition developed in this investigation was extremely beneficial in establishing a means of visualizing and calculating flow parameters for a scenario virtually equivalent to what is experienced inside the air induction system installed on an internal combustion engine. However, these boundary conditions can be further utilized to form design criteria to ensure that equal mass flow rates and pressures occur throughout the entire range of engine speeds.

Finally, experimental results are always beneficial to any investigation, especially one involving such a complex fluid environment as a restricted internal combustion race engine. A proposed method of coordinating experimental testing with analytical and computational simulations would be to perform the same type of single parameter testing as conducted in this investigation, but to then also perform the same testing experimentally by configuring multiple adjustable prototypes that can be evaluated on the engine dynamometer. While this is particularly tedious and the main reason it was not pursued for this investigation, the ultimate goal would be to eventually derive a set of non-dimensional parameters that could be applied to not only restricted race engines, but to virtually any internal combustion engine.

Appendix A: Torque versus engine speed figures

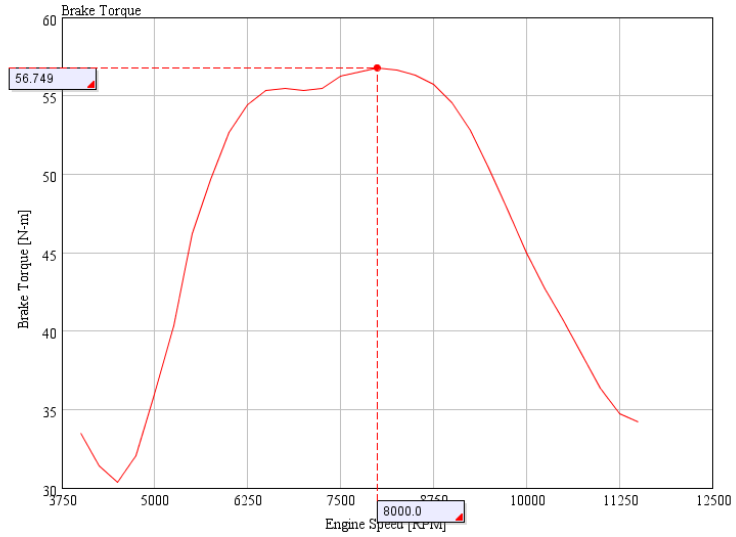


Figure 78: Torque versus engine speed for 12.3° diffuser angle

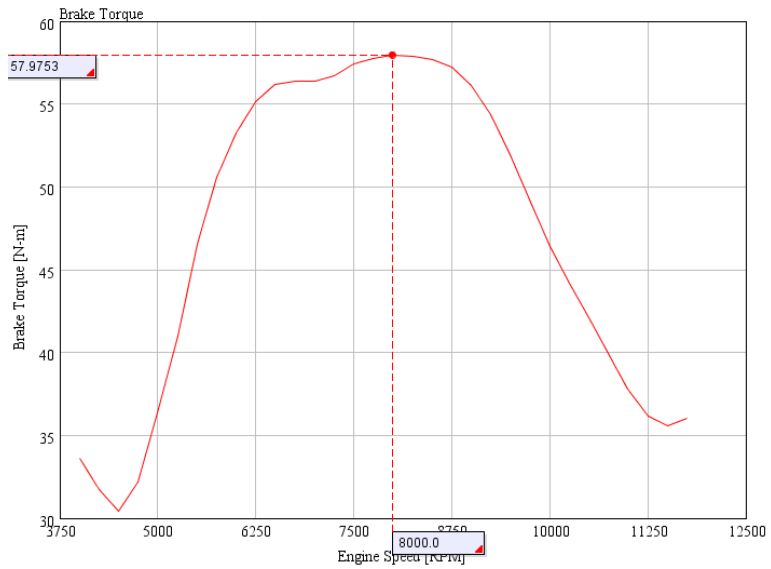


Figure 79: Torque versus engine speed for 9.2° diffuser angle

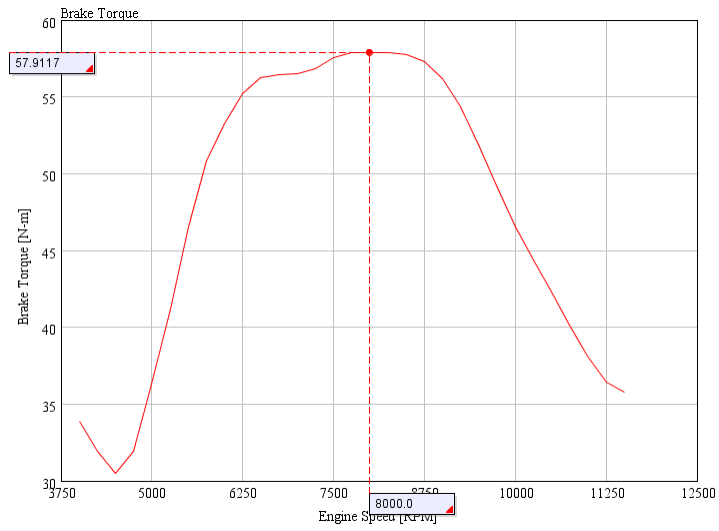


Figure 80: Torque versus engine speed for 6.0° diffuser angle

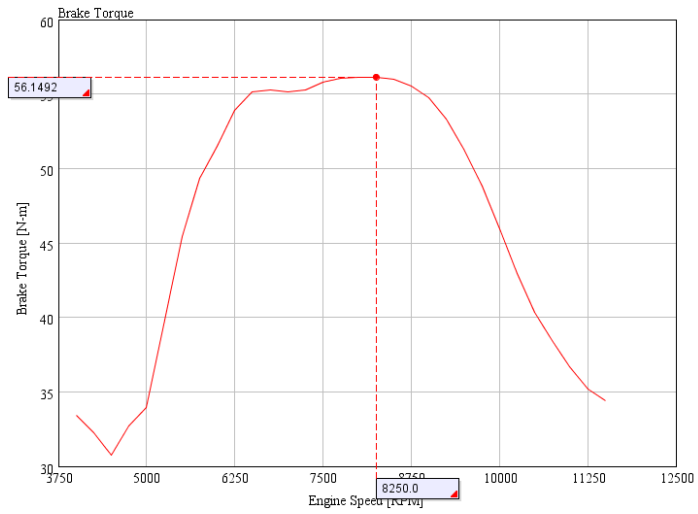


Figure 81: Torque versus engine speed for 0.54L plenum

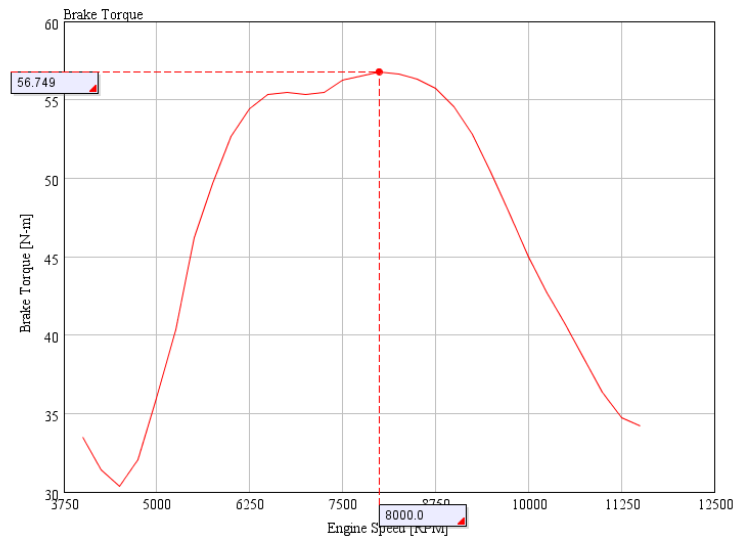


Figure 82: Torque versus engine speed for 1.08L plenum

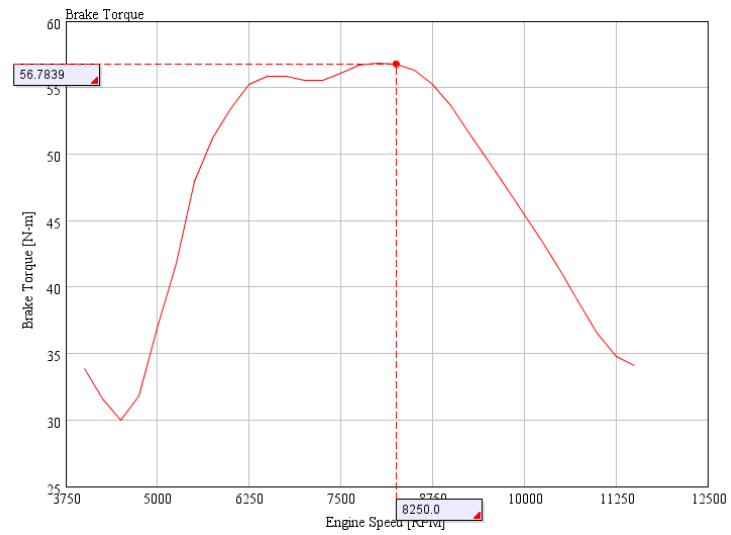


Figure 83: Torque versus engine speed for 2.17L plenum

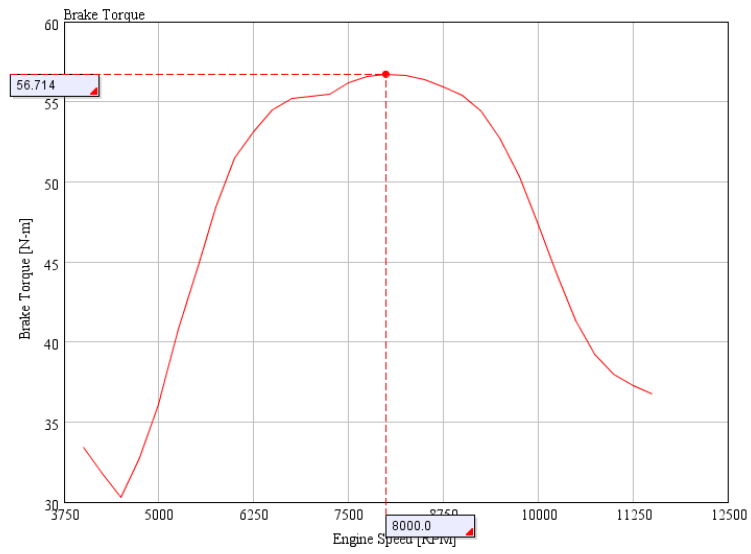


Figure 84: Torque versus engine speed for 5" runner length

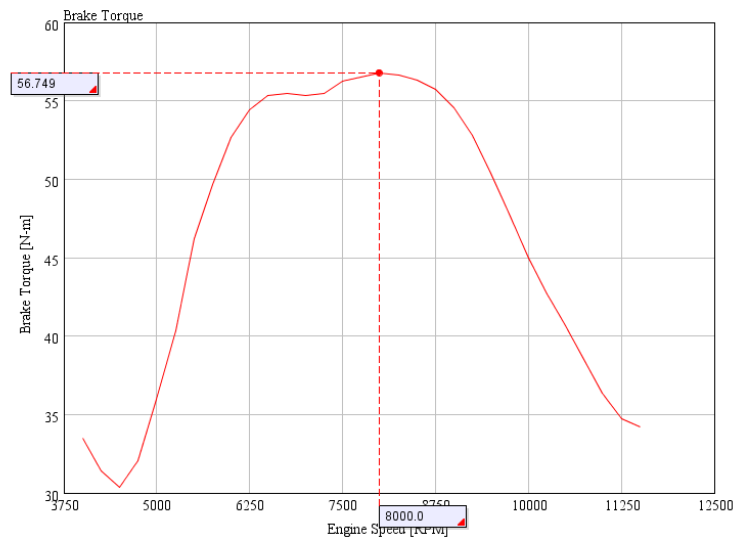


Figure 85: Torque versus engine speed for 6" runner length

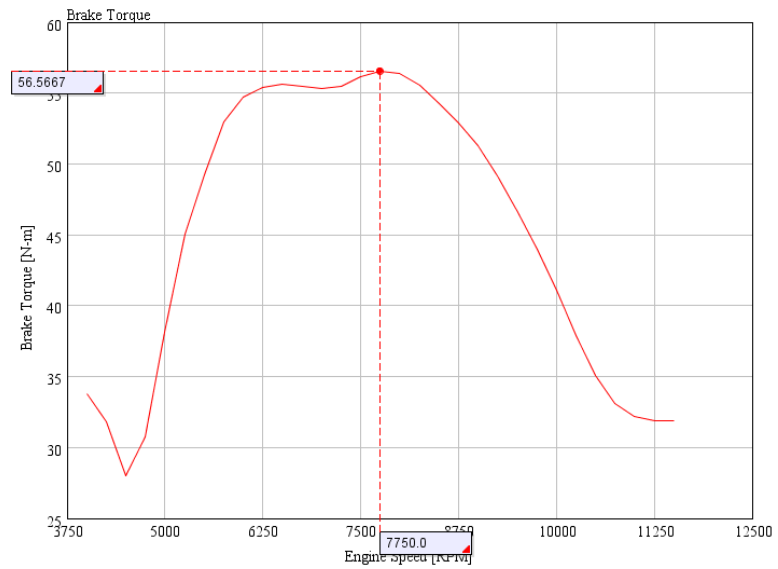


Figure 86 Torque versus engine speed for 8" runner length

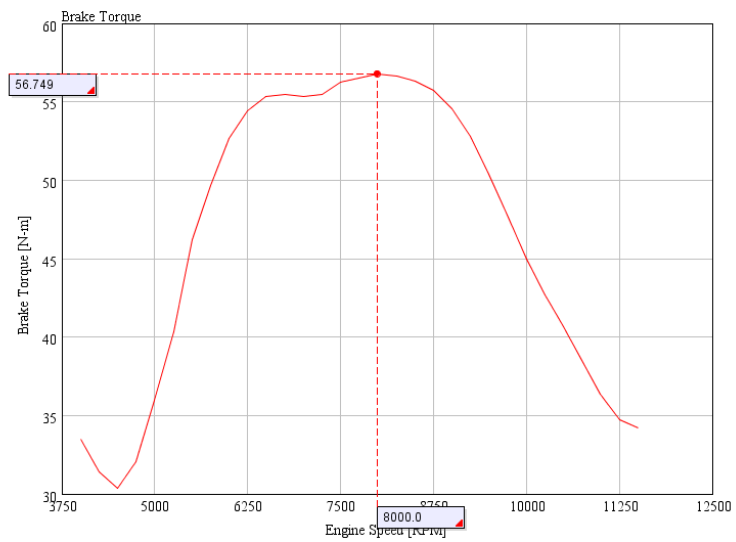


Figure 87: Torque versus engine speed for 2013 air induction design

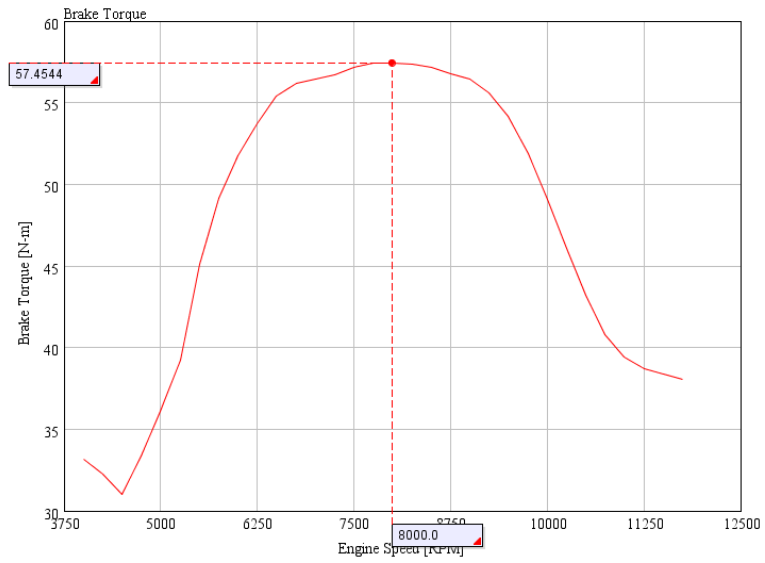


Figure 88: Torque versus engine speed for optimized 2014 air induction design

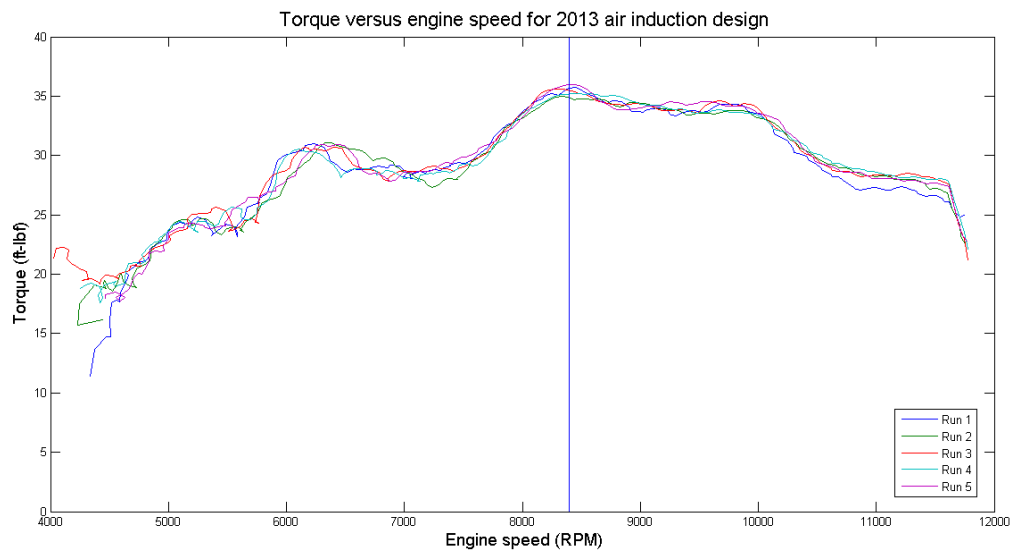


Figure 89: Torque versus engine speed dynamometer results for 2013 air induction design

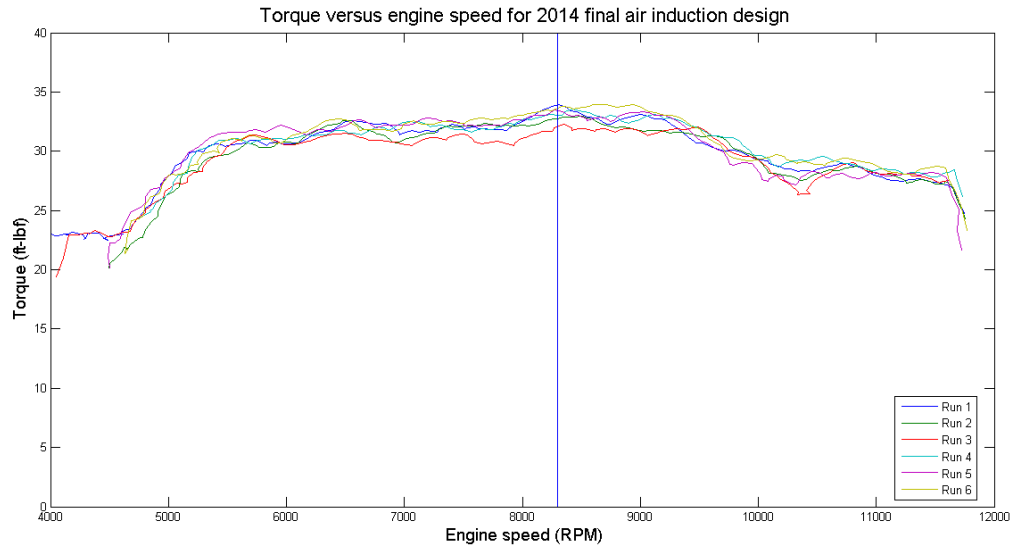


Figure 90: Torque versus engine speed dynamometer results for 2014 air induction design

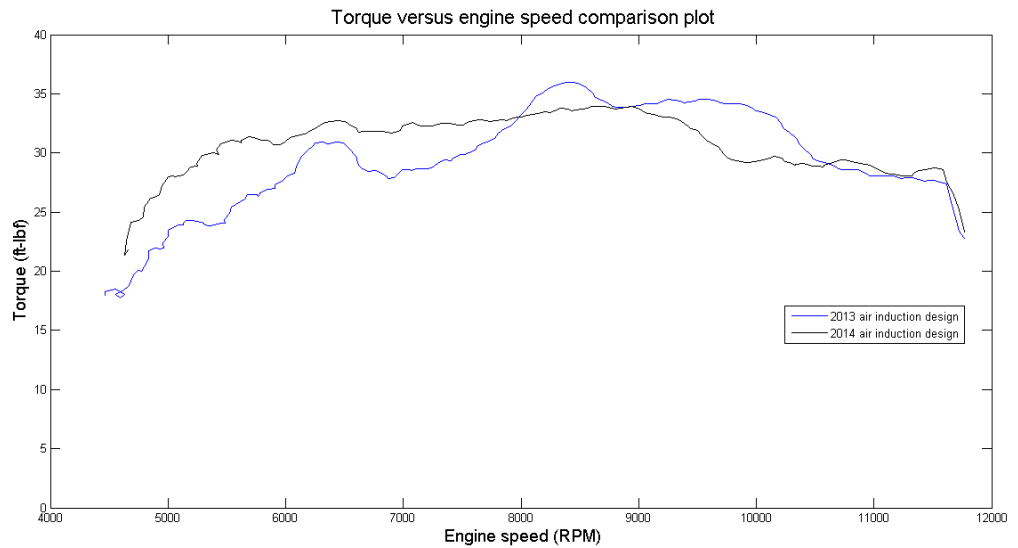


Figure 91: Torque versus engine speed dynamometer results comparison for the 2013 and 2014 air induction designs

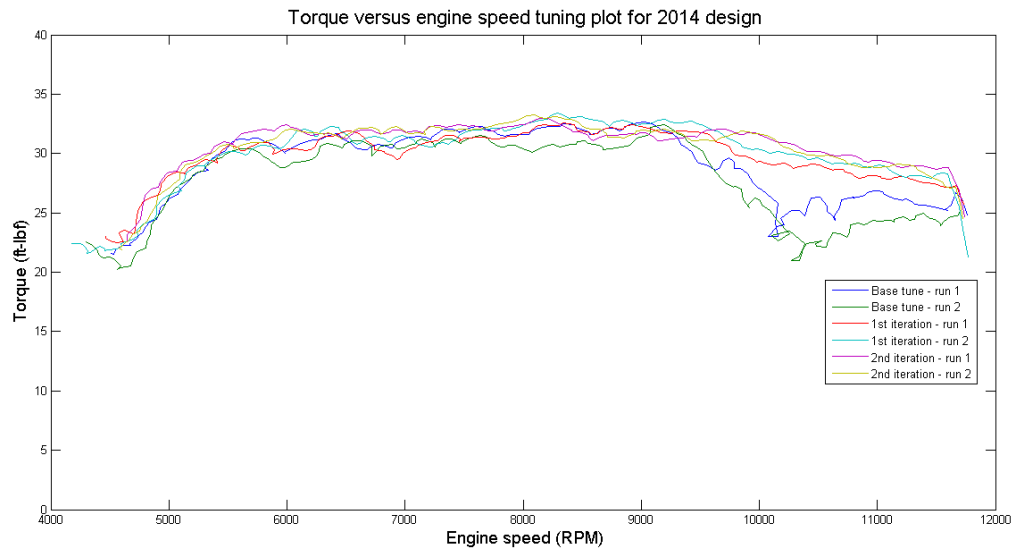


Figure 92: Torque versus engine speed dynamometer testing for the 2014 design featuring different ECU tuning

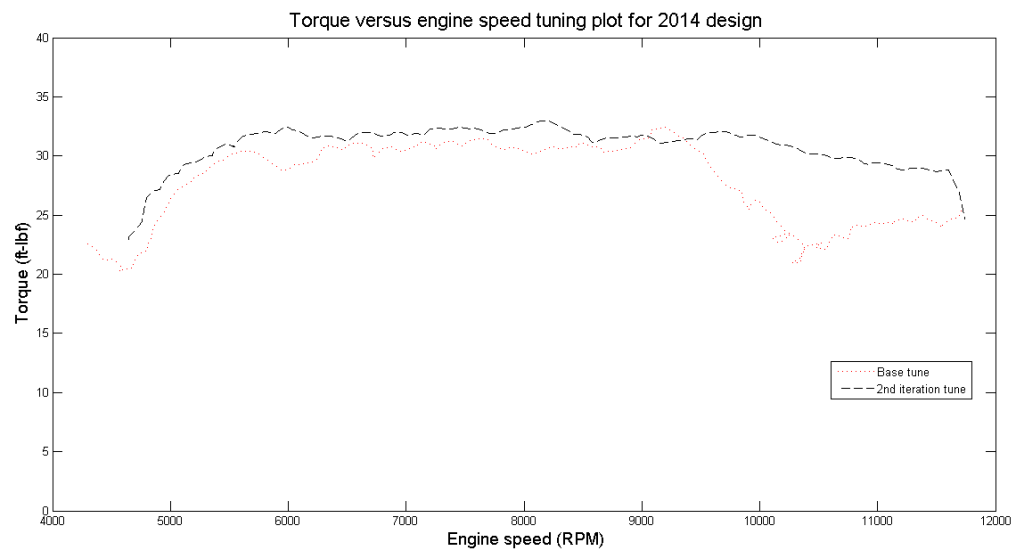


Figure 93: Torque versus engine speed for the 2014 design documenting the effect of engine tuning

References

- Ceviz, M. (2007). Intake plenum volume and its influence on the engine performance, cyclic variability and emissions. *Energy Conversion and Management*, 961-966.
- Davies, P. O. (1996). Piston engine intake and exhaust system design. *Journal of Sound and Vibration*, 667-712.
- (Figure 15-13). 4 stroke gasoline engine (internal combustion). Pearson Prentice Hall, Inc.
- Fridolin, K. (2013). *CFD for air induction systems with OpenFOAM*. Gothenburg: Chalmers University of Technology.
- Gamma Technologies. (2006). *GT-Power User's Manual*. Westmont: GT-Suite Version 6.2.
- Harrison, M., & Dunkley, A. (2004). The acoustics of racing engine intake systems. *Journal of Sound and Vibration*, 959-984.
- Harrison, M., & Stanec, P. (2004). Measuring wave dynamics in IC engine intake systems. *Journal of Sound and Vibration*, 389-408.
- Harrison, M., & Stanev, P. (2004). A linear acoustic model for intake wave dynamics in IC engines. *Journal of Sound and Vibration*, 361-387.
- Harrison, M., & Stanev, P. (2004). A linear acoustic model for intake wave dynamics in IC engines. *Journal of Sound and Vibration*, 361-387.
- Honda Motor Company. (2001). *Service Manual CBR600F4i*.
- Kmec, J. F., Kassebaum, D. A., & Noerenberg, R. L. (2009). *First-time experience with engine simulation software in an internal combustion engines course*. West Lafayette: College of Technology, Purdue University.
- Kopeliovich, D. (2012). *Bearings in internal combustion engines*. SubsTech: http://www.substech.com/dokuwiki/doku.php?id=bearings_in_internal_combustion_engines.
- Masi, M., Toffolo, A., & Antonello, M. (2010). Experimental analysis of a motorbike high speed racing engine. *Applied Energy*, 1641-1650.
- Quattrochi, D. (2006). The internal combustion engine (Otto cycle). *Thermodynamics and Propulsion*, <http://web.mit.edu/16.unified/www/SPRING/propulsion/notes/node25.html>.

SAE International. (2014). 2014 Formula SAE Rules. IC1.4-IC1.6.

Yang, X., Liao, C., & Liu, J. (2012). Harmonic analysis and optimization of the intake system of a gasoline engine using GT-power. *Energy Procedia*, 756-762.